The Mechanics of Wound Closure for Laparoscopic Surgery

Mathew Lyons, BA BAI PGDip, MIEI, Sch.

A thesis submitted to the University of Dublin, Trinity College, in part fulfilment of the requirements of the degree of

Doctor of Philosophy

June 2014

Supervisor

Dr. Ciaran K. Simms

Internal Examiner

Dr. Daniel J. Kelly

External Examiner

Dr. David Mitton

"Do what you do so well that they will want to see it again and bring their friends"

Walt Disney

Declaration

I, Mathew Lyons, declare that this thesis has not been submitted as an exercise for a degree at this or any other university and it is entirely my own work.

I agree to deposit this thesis in the University's open access institutional repository or allow the library to do so on my behalf, subject to Irish Copyright Legislation and Trinity College Library conditions of use and acknowledgement.

Signed:

Date:

Abstract

The increase in popularity of laparoscopic surgery over the past 25 years has led to a greater importance of reducing the incidence of complications associated with the surgery. Development of a hernia at a trocar port site is a serious complication with a 1-3% incidence that often results in additional surgery for the patient. There is evidence that the occurrence of a hernia is related to the quality of the wound closure, with an absence of closure being a significant risk factor for the development of a hernia. There is also evidence that a mesh-based, tension-free repair of herniae results in fewer complications than suture repair but there has been limited study on the nature of closure failure or methods to improve it.

Methodical design of a novel closure method, using a tension-free mesh approach that will reduce the incidence of hernia formation requires a fundamental understanding of the abdominal environment and requires facilities to test concepts and prototypes.

To achieve this, an experimental rig representing the abdomen has been developed that incorporates an ability to generate intra-abdominal pressure. This rig can hold either real porcine small intestine or a surrogate material and a real procine abdominal wall or a surrogate. Simulating an intra-abdominal pressure in the rig causes the intestine to extrude through the abdominal wall, similar to the formation of a hernia following laparoscopic surgery.

A surrogate small intestine material has been developed by examining the extrusion properties of porcine small intestine and a number of potential surrogate materials. Reconstituted powdered potato was selected as the most suitable surrogate material that accurately replicates the extrusion properties of small intestine and can be used in the surrogate abdomen rig.

A fundamental mathematical and analytical understanding of the mechanics and physiology of hernia formation has also been developed and provides a clear understanding of the root cause of the problem of trocar site herniae and of intra-abdominal pressure.

There is limited literature on the structural properties of the abdominal wall, particularly the rectus sheath, which has been shown to be implicated in ventral incisional herniae. A detailed analysis of the uniaxial and biaxial structural properties of the rectus sheath is presented. It was found that the response of porcine rectus sheath to uniaxial loading is similar to human rectus sheath, permitting the use of a porcine model in herniae investigations. Comprehensive stress-stretch plots are also presented which could allow future development of a surrogate abdominal wall for surgical device testing.

The surrogate abdomen rig was partially validated against data from a small observational study of surgical patients. The rig was found to perform well, with hernia generation at pressures similar to those realised physiologically and RPP again proving to be a suitable surrogate for real small intestine. Additionally, a quadratic relationship was established between the pressure required to initiate a hernia and the diameter of the defect.

This quadratic relationship was further developed in an examination of mesh overlap requirements for defect closure. With limited literature on the ideal mesh overlap, and current practice likely to be over-estimating the mesh size required, the surrogate abdomen model was employed in a preliminary study to develop a mesh and defect size relationship. Similar to the findings of the rig validation study, it was found that the relationship between mesh diameter, defect diameter and hernia generation pressure is quadratic, explained by the relationship between pressure, force and area. A mathematical formula developed to predict the required mesh size was found to under-perform due to the complexity of the interaction with tacks used to secure the mesh, however a novel empirical model recommended a mesh twice the hole diameter plus an additional 25mm.

In conclusion, a detailed understanding of the intra-abdominal pressure environment has been developed through fundamental analysis of the physiological processes and tissues involved. This understanding has been used to develop a novel surrogate abdomen environment in which new abdominal surgery devices and techniques can be tested with the aim of reducing the incidence of post-operative complications.

Acknowledgements

First, and foremost, I would like to thank my supervisor Dr. Ciaran Simms. The first academic research project that I undertook was under Ciaran's supervision in the summer of 2010, and I have thoroughly enjoyed working with and learning from him over the past four years. His dedication and interest has been unwavering and I look forward to continuing to work with him in the future. Similarly, Prof. Des Winter has also been an inspiration throughout this project, and his support has been invaluable. His enthusiasm and interest in the project was boundless and he was always available to offer suggestions and advice on the technical aspects from his point of view as a surgeon. I look forward to being a colleague of his in the future, and hope we can continue our relationship with further research projects.

I would like to sincerely thank all of the technical and workshop staff in the department, particularly Mick for his help with rig construction and Peter for the assistance with the Zwick machine. This project would not have been possible without their expertise and I am grateful for their patience with my constant queries.

I have to pay tribute to everyone who I shared an office with over the course of my study: Fionn, Hanifeh, Katey, Feng, Stephen Whelan, Stephen Yates, Michael Takaza, Michael Gibbons, Rudi, Gerard, Diarmuid, Richard, Melika and Guibing. The relaxed atmosphere, endless tea and time spent not working made the time fly!

My family and friends have always been by my side and supportive of all that I do. They are always happy to lend an ear when I am frustrated and be by my side during my successes, regardless of how small. Grace's help with proofreading has been fantastic, always identifying the smallest of errors and areas for improvement. Similarly, my mum probably knows as much as me about my work, having read countless revisions and drafts.

Finally, I would like to thank my fiancée, Aoife. I don't think it is possible to put in words how much I appreciate you always being there, through absolutely everything.

Table of Contents

Declaration i
Abstract iii
Acknowledgements v
Table of Contents vii
List of Figures xi
Chapter 2 xi
Chapter 3 xi
Chapter 5 xi
Chapter 6 xii
Chapter 7 xii
Chapter 8 xii
Chapter 9 xiv
Chapter 10 xiv
List of Tables xvii
Chapter 3 xvii
Chapter 5 xvii
Chapter 7 xvii
Chapter 8 xvii
Chapter 9 xvii
Chapter 10 xviii
Glossary xix
Publications xxi
Journal Publications xxi
Conference Abstracts xxi
1. Introduction 1
2. Background 5
2.1. Introduction 5
2.2. Anatomy of the Abdominal Wall 5
2.2.1. Muscles 6
2.2.2. Rectus Sheath 8
2.2.3. Other Layers 9
2.3. Intestines 10
2.3.1. Overview 10
2.3.2. The Small Intestine 10
2.3.3. The Large Intestine 11
2.4. Hernia 11
2.4.1. Inguinal Hernia 11
2.4.2. Incisional Hernia 12
2.5. Intra-Abdominal Pressure 13

2.5.1. Abdominal Straining and the Valsalva Manoeuvre 13
2.5.2. Coughing 14
2.5.2.1. Inspiration 14
2.5.2.2. Compression 15
2.5.2.3. Expiration 15
2.6. Laparoscopic Surgery 15
2.6.1. Technique 15
2.6.1.1. Umbilical Port 16
2.6.1.2. Medial◊ Port Below the Arcuate Line 16
2.6.1.3. Medial Port Above the Arcuate Line 16
2.6.1.4. Lateral Port 17
2.6.1.5. After Port Insertion 17
2.7. Conclusion 17

3. Literature Review 19
3.1. Introduction 19
3.2. Intra-Abdominal Pressure 19
3.3. Tissue Properties 24
3.3.1. The Abdominal Wall 24
3.3.2. The Small Intestine 30
3.4. Herniae 32
3.5. Meshes 35
3.5.1. Mesh Techniques 35
3.5.2. Mesh Fixation 36
3.5.3. Mesh Overlap 37
3.5.4. Mesh Complications 39
3.5.4.1. Mesh Adhesion 39
3.5.4.2. Other Complications 40
3.6. Conclusion 41

4. Project Approach 43

5. Intra-Abdominal Pressure 45
5.1. Introduction 45
5.2. Generation of Intra-Abdominal Pressure 45
5.3. Approximation of the Volume of the Abdominal Cavity 46
5.3.1. Thin Walled Pressure Vessel Formulation 48
5.4. Discussion 48
5.4.1. Effects of Pressure on the Anatomy 48
5.4.1.1. Activation of the Abdominal Muscles 49
5.4.1.2. No Activation of the Abdominal Muscles 50
5.4.2. Limitations of the Assumptions 51
5.5. Conclusions 51

6. Surrogate Abdomen Rig Design 53
6.1. Introduction 53
6.2. Concept 53
6.3. Design 54
6.4. Operation 56
6.5. Conclusion 57

7. Small Intestine 59
7.1. Introduction 59
7.2. Methods 60
7.2.1. Custom Testing Rig Development 60
7.2.2. Materials Tested 61
7.2.3. Test Conditions 63
7.2.4. Yield Strength Evaluation 63
7.3. Results 64
7.3.1. Graphical Comparison Between Cleaned and Non-Cleaned Small Intestine 64
7.3.2. Graphical Comparison Between Cleaned Small Intestine and Surrogate Materials 65
7.3.3. Force-Extrusion Relationships 66
7.4. Discussion 70
7.4.1. Yield Strength 71
7.4.2. Variability 72
7.5. Conclusions 72

8. Rectus Sheath 75
8.1. Introduction 75
8.2. Methods 76
8.2.1. Uniaxial Tests 76
8.2.1.1. Sample Preparation 76
8.2.1.2. Testing 77
8.2.1.3. Results Analysis 78
8.2.2. Biaxial Tests 79
8.2.2.1. Sample Preparation 79
8.2.2.2. Testing 80
8.2.2.3. Results Analysis 81
8.2.3. Statistical Methods 81
8.2.4. Computational Modelling 82
8.3. Results 83
8.3.1. Uniaxial 83
8.3.2. Biaxial 86
8.3.3. Computational Modelling 87
8.4. Validation of Strain Measurement Techniques 89
8.5. Discussion 90
8.5.1. Uniaxial 91
8.5.1.1. Comparison with other authors 91
8.5.2. Biaxial 93
8.5.3. Statistical Tests 95
8.5.4. Computational Modelling 96
8.6. Conclusions 98

9. Surrogate Abdomen Evaluation 99
9.1. Introduction 99
9.2. Observational Study in Surgery 99
9.2.1. Methods 99
9.2.1.1. Statistical Methods 101
9.2.2. Results 101

9.2.3. Discussion 103
9.3. Rig Validation 103
9.3.1. Methods 104
9.3.1.1. Porcine Tissue 104
9.3.1.2. Surrogate Small Intestine 105
9.3.2. Results 105
9.3.3. Discussion 107
9.4. Conclusions 109
10. Mesh Overlap 111
10.1. Introduction 111
10.2. Analytical Approach 112
10.2.1. Parameter Estimation 114
10.3. Clinical Recommendation 117
10.4. Experimental Methods 118
10.5. Results 119
10.6. Discussion 121
10.7. Conclusion 126
11. Discussion 127
11.1. Small Intestine 129
11.2. Rectus Sheath 131
11.3. Surrogate Abdomen Rig 134
11.4. Mesh Overlap 136
12. Conclusions 139
13. Further Work 141
References 143

List of Figures

Chapter 2

Figure 2.1 – Cavities of the body, from [21]. 6
Figure 2.2 – Muscles of the abdominal wall, from [22]. 6
Figure 2.3 – Direction of muscle fibres for: (a) the external oblique, (b) the internal oblique and *rectus abdominis* and (c) the *transversus abdominis*, adapted from [22].....7
Figure 2.4 – Anatomy of the abdominal wall above the arcuate line, with the rectus sheath lying anterior and posterior to the *rectus abdominis* muscle, from [24]. 9
Figure 2.5 – Anatomy of the abdominal wall below the arcuate line with the rectus sheath lying only anterior to the *rectus abdominis* muscle, from [24].....10
Figure 2.6 – Trocar ports inserted for a laparoscopic surgical procedure. 16

Chapter 3

Figure 3.1 – Stress-stretch response of rabbit abdominal muscle composite layer, from [60]. 27
Figure 3.2 – Various results of stress-stretch data for the *trasversalis fascia*, adapted from [58, 59, 61]. 29
Figure 3.3 – Various results of stress-stretch data for the *linea alba*, adapted from [64, 65, 71]. 30
Figure 3.4 – Various results of stress-stretch data for the rectus sheath, adapted from [66, 68, 69]. 30
Figure 3.5 – Sample piece of polypropylene mesh manufactured by PFM Medical (Köln, Germany). 35

Chapter 5

Figure 5.1 – Dimensions of the abdominal cavity, from [142]. 47
Figure 5.2 – Layers of the abdominal wall, adapted from [148]. 50

Chapter 6

Figure 6.1 – Surrogate abdomen rig with a Perspex box to hold the balloon and small intestine and a curved lid to replicate the curvature of the abdominal wall.....54
Figure 6.2 – Nutmeg grater. 55
Figure 6.3 – Compressed air pipe network. 56

Chapter 7

Figure 7.1 – Line drawing of the extrusion rig. 61
Figure 7.2 – Photograph of the extrusion rig. 61
Figure 7.3 – Graphical comparison of cleaned and non-cleaned small intestine. The object marked with "§" is tissue paper to protect the machine from the biological samples. 65
Figure 7.4 – Still captures from videos of extrusion tests at a crosshead displacement of 7.5mm. Object marked with "§" is tissue paper to protect the machine from the perisible samples. 66
Figure 7.5 – Force-displacement curves for intestine, RPP and dough at 7.5mm/min showing average force-displacement curves +/- one standard deviation. 67
Figure 7.6 – Force-displacement curves for intestine, RPP and dough at 15mm/min showing average force-displacement curves +/- one standard deviation. 67
Figure 7.7 – Force-displacement curves for intestine, RPP and dough at 30mm/min showing average force-displacement curves +/- one standard deviation. 68
Figure 7.8 – Average force-displacement curves for small intestine at the three extrusion rates +/- one standard deviation. 69
Figure 7.9 – Average force-displacement curves for RPP at the three extrusion rates +/- one standard deviation. 69
Figure 7.10 – Average force-displacement curves for dough at the three extrusion rates +/- one standard deviation. 70

Chapter 8

Figure 8.1 – Posterior◊ view of a porcine belly showing the fibre and cross-fibre directions. 77
Figure 8.2 – (a) Gripping jig and (b) gripped sample in the Zwick machine. 78
Figure 8.3 – One edge of the gripping jig with hooks. 80

Figure 8.4 – Complete biaxial gripping jig. 80
Figure 8.5 – Equi-force biaxial testing rig. 81
Figure 8.6 – Sample under equi-force biaxial tension. 81
Figure 8.7 – Vertical stretch in the individual regions of a cross-fibre direction sample plotted against time. 84
Figure 8.8 – Horizontal stretch in the individual regions of a cross-fibre direction sample plotted against time. 84
Figure 8.9 – Vertical stretch in the individual regions of a fibre direction sample plotted against time. 85
Figure 8.10 – Horizontal stretch in the individual regions of a fibre direction sample plotted against time. 85
Figure 8.11 – Stress-stretch plots for fibre and cross-fibre direction samples. 86
Figure 8.12 – Typical fibre direction sample raw displacement as recorded by DIC code. 86
Figure 8.13 – Typical cross-fibre direction sample raw displacement as recorded by DIC code. 86
Figure 8.14 – Biaxial stress-stretch plots for all samples. 87
Figure 8.15 – Fit of FeBio stress-stretch results to experimental results in the cross-fibre direction. 88
Figure 8.16 – Typical fit of FeBio stress-stretch results to experimental stress-stretch results in the fibre direction. 88
Figure 8.17 – Fit of biaxial FeBio stress-stretch results to experimental biaxial stress-stretch results. 89
Figure 8.18 – Validation of the dot tracking method. The initial position of the dots is shown in red, the final position is shown in blue. The ratio of the distance between the final points to distance between the initial points gives the stretch. 90
Figure 8.19 – Comparison between the current study and the results of Martins et al. [66] and Rath et al. [68]. 92
Figure 8.20 – Comparison between the current study and the results of Ben Abdelounis et al. [69]. 93
Figure 8.21 – Predicted strains from Hooke's Law analysis in fibre and cross-fibre directions for a range of Poisson's Ratios and Young's Moduli. 95

Figure 8.22 – Hypothesis for the bulging of the tissue in the fibre direction tests. In (a) to (b), the tissue is clamped in the grips, causing it to spread horizontally under the grips. (c) As the tissue is stretched, the force of the fibres trying to straighten outweighs the force of the matrix trying to contract. (d) When the fibres are straight, the tissue can contract as normal. 97

Figure 8.23 – FeBio stress-stretch plots for a gripped and a non-gripped cross-fibre direction sample. 97

Figure 8.24 – FeBio stress-stretch plots for a gripped and a non-gripped fibre direction sample. 98

Chapter 9

Figure 9.1 – Perioperative mean IAP and standard deviation. 102

Figure 9.2 – Blunt Tip Trocar inserted into the abdominal wall in the surrogate abdomen rig. 105

Figure 9.3 – Recorded hernia pressures for RPP and small intestine at a range of hole sizes with error bars (± one standard deviation) and quadratic fits for both materials. 106

Figure 9.4 – Probability of hernia formation through an open 10mm defect predicted using a logistical regression and a ramp function. The horizontal axis also shows typical activities that generate such pressures, from [41]. In the experiments, these pressures were applied as static pressures which over-estimates their influence in hernia generation and provides for a factor of safety in this prediction. 107

Chapter 10

Figure 10.1 – Mesh placement to cover a circular hole deforming spherically due to an applied pressure. 112

Figure 10.2 – A 3-dimensional representation of a mesh covering a defect with a cross-section showing pressure (P), tack pull-out force ($Fpull$) and circumferential area ($\boldsymbol{Acir}$). 113

Figure 10.3 – Number of tacks that must fail for the defect closure to fail. In (a), only one tack must fail as the mesh is small and only secured by four tacks. However, in (b), up to five tacks may need to fail before the defect closure will fail and expose the hole (shown in green). 117

Figure 10.4 – Abdominal wall containing a defect closed with a tacked mesh. 118

Figure 10.5 – Relationship between mesh diameter and hernia onset pressure for each hole size from 10 to 50mm. 120
Figure 10.6 – Relationship between hole diameter and hernia onset pressure for each mesh size....120
Figure 10.7 – Surface plot showing the relationship between hole diameter, mesh diameter and hernia onset pressure. 121
Figure 10.8 – Comparison of mesh size calculations including the empirical (Equation 10.10) and complex (Equation 10.9) mathematical models derived in Section 10.2....123
Figure 10.9 – Comparison of the complex mathematical model (Equation 10.9) and some modifications to the model based on the results of the experimental data. 124

List of Tables

Chapter 3

Table 3.1 – Intra-abdominal pressure for various manoeuvres as reported by Cobb et al. [41]. 21
Table 3.2 – Various reports of the incidence of trocar site herniae following laparoscopic surgery. 34

Chapter 5

Table 5.1 – Dimensions of the abdominal cavity, from [142] and [143]. 46

Chapter 7

Table 7.1 – List of materials tested. 61
Table 7.2 – Regular dough ingredients. 62
Table 7.3 – Oatmeal dough ingredients. 62
Table 7.4 – Average extrusion forces and material yield strengths for dough, RPP and small intestine at the three extrusion rates presented as mean (standard deviation). 68

Chapter 8

Table 8.1 – FeBio material model parameters. 87
Table 8.2 – Average goodness of fit of computational data to experimental data for all samples. 87
Table 8.3 – Results of the validation of the dot tracking method. 90
Table 8.4 – Results of the validation of the DIC method. 90
Table 8.5 – Values used for various material properties for Hooke's Law analysis. 95

Chapter 9

Table 9.1 – Summary of patient demographics for all seven patients. 101
Table 9.2 – Summary of IAP recordings in Pascals [Pa]. 102
Table 9.3 – Recorded pressures at hernia formation for both RPP and intestines at various hole sizes. 106

Chapter 10

Table 10.1 – Pull-out forces per tack showing mean and minimum, from [100, 163]. 115

Table 10.2 – Summary of constants for Equation 10.9 115

Table 10.3 – Number of tacks required to be pulled out to cause failure of the defect closure. 116

Glossary

Words marked with a superscript lozenge (◊) in the text are explained in the glossary below.

Term	Definition
Anastomosis	The connection of two streams, usually hollow organs.
Anterior	Relating to or situated towards the front of the body.
Aponeurosis	Flat, broad tendinous structure that large flat muscles insert into.
Arcuate Line	Specifically, the Arcuate Line of Douglas, is an imaginary line that marks the lower limit of the posterior rectus sheath. It occurs approximately 5cm inferior to the umbilicus.
Body Mass Index (BMI)	Body mass index is a measurement of a person's mass, normalised by their height. It is calculated by dividing the mass by the square of the height.
Caudal	Towards the tail (i.e. coccyx of the spine).
Caecum	A pouch considered to be the beginning of the large intestine.
Cholecystectomy	Surgical removal of the gallbladder, a small organ attached to the liver that stores bile for use in digestion.
Contra-	Opposite.
Coronal Plane	The coronal plane is any vertical plane from left to right dividing the body into ventral and dorsal sections.
Cranial	Related to the skull or in the direction of the skull.
Dehiscence	The bursting open of a surgically closed wound.
Dorsal	Pertaining to the back.
Extra-	Outside of.
Fascia	A sheet of fibrous connective tissue enveloping or separating any soft structures of the body.
Fibrin Glue	A formulation used to create a fibrin clot to stick body tissues to other tissues or foreign bodies.
Formalin	A solution of formaldehyde often used to preserve or "fix" biological specimens.
Glottis	A valve like mechanism controlling the release of air from the trachea.
Hernia	Protrusion of an organ, or part of an organ, through the wall of a cavity that normally contains it.
Hypogastric	Relating to the lower abdominal region.
Hypoxia	The failure of the body to adequately oxygenate a given tissue.
Iliac Crest	Anterior, superior border of the wing of the ilium, or pelvis. It is the bone located in the lower right and left quadrants of the abdomen.
Inferior	Located closer to the bottom of the feet than another.
Infra-	Below. See inferior.
Inguinal	Relating to the region of the groin.
Intra-	Inside of.
Intubate	Insertion of a tube into the trachea of a patient to facilitate mechanical ventilation.
Ipsi-	Same.

Laparoscopy	A minimally invasive surgical procedure using small, keyhole sized ports, a fibre optic camera and long thin instruments.
Laparotomy	Surgical procedure usually involving a large craniocaudal incision in the abdominal wall along the *linea alba*.
Lateral	Relating to or situated towards the side.
Lithotomy Position	Position in which the patient is supine with their feet held higher than their hips in stirrups and their perenium is at the edge of the examination table.
Mechanoreceptors	Sensory receptors of the nervous system that respond to mechanical stimuli including pressure and distortion.
Medial	Relating to or situated towards the midline.
Mesentery	A double layer of peritoneum that surrounds the intestines, attaches them to the posterior wall of the abdomen and supplies them with blood vessels and nerves.
Midclavicular Line	An imaginary vertical line passing through the middle of the left or right clavicle used as a point of reference.
Morbidity	A diseased state or symptom.
Obese	Being grossly overweight, typically with a BMI greater than 30kg/m^2.
Parietal	Relating to the walls of a cavity (opp. visceral).
Pathophysiology	The disordered physiological processes associated with disease or injury.
Peristalsis	A radially symmetrical contraction of smooth muscles which propagate in a wave down a muscular tube. It is used in the digestive tract to propel food.
Peritoneum	Smooth, serous membrane lining the abdominal cavity and abdominal viscera.
Port	See trocar.
Posterior	Relating to or situated towards the back of the body.
Pubic Symphysis	The midline cartilaginous joint connecting the left and right rami of the pelvis.
Radio Pill	A small, pill-like device containing a radio transmitter that is swallowed by a patient. During its passage through the body it transmits information to a receiver outside the body.
Sagittal Plane	The sagittal plane is any vertical plane from ventral to dorsal dividing the body into right and left sections.
Serous Membrane	A smooth, thin layer of cells that secrete a lubricating liquid.
Superior	Located closer to the top of the head than another.
Supra-	Above. See superior.
Transverse Plane	The transverse plane is any horizontal plane dividing the body into superior and inferior sections.
Trocar	A surgical instrument with a cutting point encased in a tube used for gaining access in laparoscopic surgery, also referred to as a port.
Umbilicus	Scar on the abdominal wall at the site of attachment of the umbilical cord.
Vagal Reflex	Stimulation of the vagus nerve which controls the reduction of blood pressure, heart rate and general "rest and digest" conditions.
Ventral	Referring to the front.
Vesical	Referring to the urinary bladder.
Viscera	Soft internal organs of the body.
Xyphoid Process	Small, cartilaginous extension of the inferior portion of the sternum.

Publications

Journal Publications

Lyons, M., Winter, D.C., Simms, C.K., Extrusion properties of porcine intestines and surrogate materials for ventral hernia modelling. Journal of the Mechanical Behavior of Biomedical Materials (2012), http://dx.doi.org/10.1016/j.jmbbm.2012.10.01

Lyons, M., Winter, D.C., Simms, C.K., Mechanical characterisation of porcine rectus sheath under uniaxial and biaxial tension. Journal of Biomechanics (2014). http://dx.doi.org/10.1016/j.jbiomech.2014.03.009

Lyons, M., Mohan, H., Winter, D.C., Simms, C.K., A biomechanical abdomen model applied to study mesh overlap requirements. British Journal of Surgery. In Review.

Conference Abstracts

Lyons M., Devane, L., Winter, D.C., Tierney, P., Simms, C.K. Towards a Wound Closure Device for Laparoscopic Surgery. Bioengineering in Ireland. Belfast. 2012.

Lyons M., Winter D.C., Simms C.K., A Physical Surrogate Model of the Abdomen for Hernia Modelling. Bioengineering in Ireland. Dublin. 2013.

Lyons M, Winter D.C., Simms C.K., Structural Properties of Porcine Rectus Sheath. European Society of Biomechanics. Patras. 2013.

Lyons M., Winter D.C., Simms C.K., Uniaxial and Biaxial Tensile Tests on Porcine Rectus Sheath. Bioengineering in Ireland. Limerick. 2014.

Lyons M., Winter D.C., Simms C.K., Uniaxial and Biaxial Response of Porcine Rectus Sheath. World Congress of Biomechanics. Boston. 2014.

1. Introduction

Laparoscopic surgery is an increasingly popular, minimally-invasive surgical technique performed through keyhole-sized ports◊[1] in the abdominal wall. The first reported laparoscopy took place in 1981 [1] when Kurt Semm, a surgeon in Kiel, Germany conducted an appendectomy using gynaecological instruments. Since this surgery, the technique has rapidly increased in popularity with over two million patients currently undergoing laparoscopic procedures in the United States alone each year [2].

However, as with all surgeries, laparoscopic procedures are not without their complications. While there are significant advantages over open surgery, including reduced trauma, lower risk of infection, shorter hospital stays and dramatically improved cosmetic results [3], there remain a number of issues with the laparoscopic technique. Operating on the abdominal wall, either in a minimally invasive fashion or with open surgery, generates defects in the abdominal wall. These defects reduce the ability of the abdominal wall to constrain the abdominal contents. It is not uncommon for an incisional hernia◊ to develop post-operatively, where a structure normally contained by the abdominal wall protrudes out through one or more of its layers [4]. Laparoscopy reduces the incidence of this complication from 20% [4] to between 1-3% [5, 6], but does not eliminate it. With two million surgeries in the U.S. each year, this equates to 20,000 – 60,000 incisional herniae after laparoscopic surgery among this population alone. The complication typically requires a revision surgery which raises costs and prolongs hospital stays (thus increasing the probability of infection) and also puts the patient at risk of developing another incisional hernia at the site of the newly created defects from the revision surgery.

While complete eradication of the problem is probably impossible, reduction of the incidence is an achievable and worthwhile goal. A number of confounding factors exist that increase the likelihood of a patient developing an incisional hernia. The main factor is

[1] Words marked with a superscript lozenge (◊) in the text are explained in the glossary on page xvii.

inadequate closure of the defects post-operatively [7-9], however it has also been shown that high Body Mass Index◊ (BMI) is a risk factor [10]. Obesity, therefore, can be a complicating factor since a large layer of fat will impede access to the deeper layers of the abdominal wall for suturing, resulting in poor closure of the defect.

While it is clear that a novel solution to wound closure is required to reduce complications, particularly in obese◊ patients, there has been little work to date to develop such a solution. There have been significant developments in hernia repair, with a move from suture repair to a tension-free mesh-based repair, which has dramatically reduced the incidence of recurrence of herniae [11]. It is possible that an adaptation of this solution might be applicable to post-operative wound closure for laparoscopic surgery, as has been suggested previously [12]. To solve the problem, however, it is necessary to start from the root cause – what causes herniae to occur where defects exist in the abdominal wall?

By developing a fundamental understanding of the abdominal environment and identifying the physiological process that result in raised intra-abdominal pressure which subsequently forces viscera◊ out through defects in the abdominal wall, a novel closure solution can be more accurately designed.

An essential criterion for the design of any new medical device is adequate, accurate and repeatable testing to ensure that it can perform in a variety of environments in a predictable and effective manner to accomplish its goal. To this end, a test rig is required that allows for replication of the abdominal environment in a laboratory setting without many of the ethical issues surrounding the use of animals, and without the time restrictions or variability associated with using real, *ex vivo* tissue. There is no commercially available or research based surrogate abdomen that achieves these goals and allows for simulation of a hernia and testing of closure methods. Furthermore, there is little data on the mechanical and structural properties of the tissues of the abdomen, and thus no accurately developed surrogate that replicates the key structural and mechanical properties.

Lastly, there is very little data on the ideal mesh overlap ratio for variously sized defects. Many authors have reported on the efficacy of a constant, 50mm mesh overlap for all defects [13-18], but there have been very few laboratory studies or trials to corroborate this [19, 20]. It would seem intuitive that the optimum mesh size for a particular defect would

be related to the size of the defect, but currently only one study exists which examined this relationship [20] and there is little evidence that defect size is actively considered during procedures.

The aim of this thesis is, therefore, to develop an understanding of the mechanics of wound closure for laparoscopic surgery by developing a physical model of the human abdomen for device testing and to use this model to investigate mesh overlap requirements for effective repair of abdominal wall defects.

2. Background

2.1. Introduction

This chapter presents a background to the content of this thesis. It will focus on five core areas: the abdominal wall, the intestines, herniae◊, intra-abdominal pressure and laparoscopic surgery and will provide the reader with context and understanding of the pertinent theory underlying this PhD.

Section 2.2 outlines the anatomy of the abdominal wall which is composed of an array of interconnected muscles and fibrous layers.

Section 2.3 provides a brief overview of the small and large intestines, which, combined, are the largest organ within the abdominal cavity.

Section 2.4 details the process of hernia formation and the various types of hernia that can arise from the contents of the abdominal cavity.

Section 2.5 describes intra-abdominal pressure and the physiology of its generation as well as providing a brief outline of the physiological processes of coughing.

Finally, Section 2.6 provides a brief explanation of the general techniques of laparoscopic surgery and trocar◊ port◊ insertion.

2.2. Anatomy of the Abdominal Wall

The abdomen is one of the few large cavities of the human body (Figure 2.1). It is bounded anteriorly◊ and laterally◊ by the abdominal wall, posteriorly◊ by the spinal column and associated dorsal◊ muscles, superiorly◊ by the diaphragm and inferiorly◊ by the pelvis. The abdominal wall is a complex array of overlapping muscles, fascial◊ layers and other tissues designed to protect the contents of the abdominal cavity, whilst facilitating a broad range of motion and assisting with breathing and other bodily functions. Muscles in the abdominal wall appear in pairs, symmetrically about the midline of the body. The *linea alba* (white line) runs down the centre of the abdominal wall from the xyphoid process◊ at the

base of the sternum, through the umbilicus◊, to the pubic symphysis◊. It is a fibrous structure, composed mainly of collagenous connective tissue and serves as the line of symmetry for the abdominal wall. Emanating from it are the four pairs of abdominal muscles: the pillar-like *rectus abdominis* muscles, the external oblique muscles, the internal oblique muscles and the *transversus abdominis* muscles (Figure 2.2).

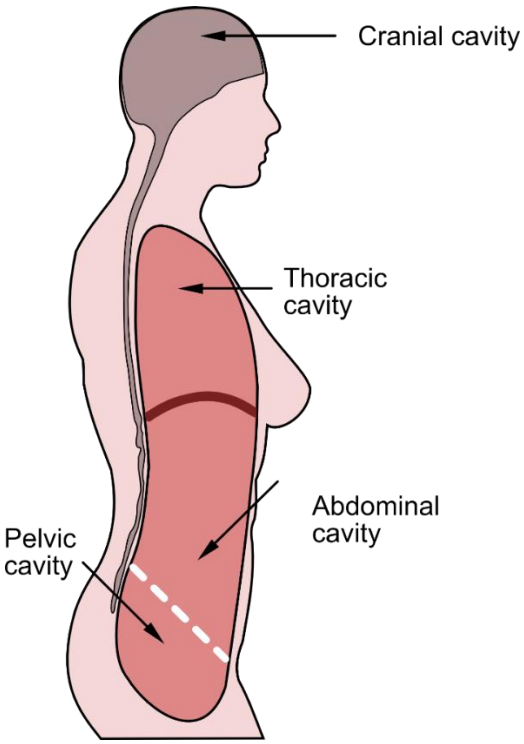

Figure 2.1 – Cavities of the body, from [21].

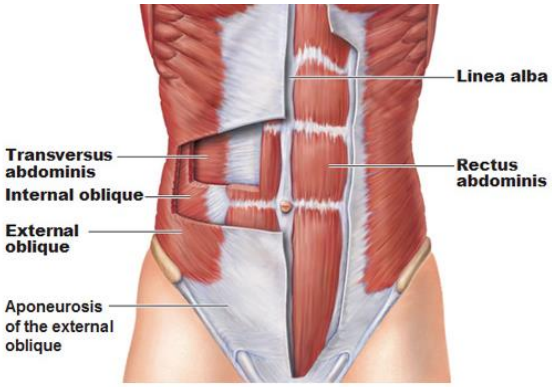

Figure 2.2 – Muscles of the abdominal wall, from [22].

Deep to the muscle layers are two fibrous layers that are theoretically separate but practically quite difficult to distinguish. The more superficial of the two is the *transversalis fascia*. Deep to this layer is the peritoneum◊, which is a serous◊ membrane covering the majority of the intra-abdominal viscera◊.

2.2.1. Muscles

The *rectus abdominis* is the most medial muscle layer of the abdominal wall. This pair of muscles, one each side of the *linea alba*, is commonly known to give a distinctive "six pack" when well-toned (Figure 2.3b). These muscles are responsible for flexion of the spine.

Laterally, the most superficial muscle is the external oblique. The fibres in these muscles run approximately at a 45° angle to the transverse plane◊ beginning at the inferior, lateral

portion of the 5th to 12th ribs and extending in the direction of the contralateral◊ iliac crest◊ (Figure 2.3a). The muscle inserts into an aponeurosis◊ midclavicularly◊ (Figure 2.4) and this aponeurosis becomes the anterior portion of the rectus sheath, passing anterior to the *rectus abdominis* before joining with the *linea alba*. Activation of the external oblique pulls the chest downwards and compresses the abdominal cavity which increases intra-abdominal pressure during an abdominal straining manoeuvre. The muscles contribute to flexion and rotation of the spine. Activation of one external oblique and one internal oblique on the same side causes lateral flexion.

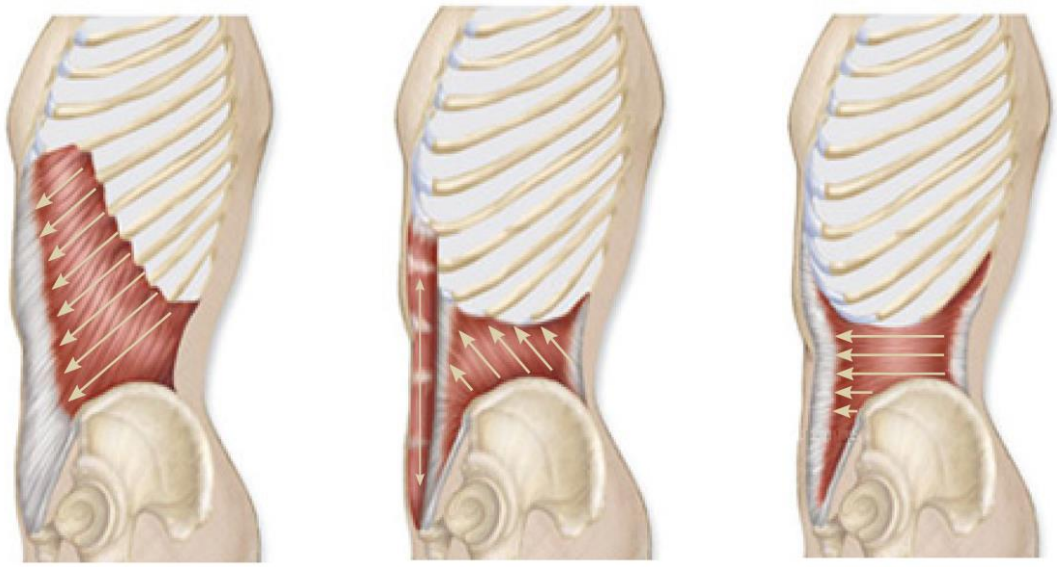

(a) (b) (c)

Figure 2.3 – Direction of muscle fibres for: (a) the external oblique, (b) the internal oblique and *rectus abdominis* and (c) the *transversus abdominis*, adapted from [22].

The internal oblique is deep to the external oblique. Its fibres run at 45° to the transverse plane, in the opposite direction to the fibres of the external oblique, beginning at the iliac crest and travelling medio-superiorly towards the *linea alba* and the contralateral costal margin (Figure 2.3b). Again, the muscle inserts into an aponeurosis midclavicularly. Above the arcuate line◊ (superior three quarters of the abdominal wall), this aponeurosis splits to pass both anteriorly and posteriorly to the *rectus abdominis*, but below the arcuate line it passes only anteriorly to the *rectus abdominis* before joining with the *linea alba* (Figures 2.4 and 2.5). The actions of the internal oblique are similar to the external oblique. It aids rotation and forward flexion of the spine and, in conjunction with the ipsilateral◊ external oblique muscle, permits lateral flexion of the spine.

The deepest of the abdominal muscles is the *transversus abdominis*. It is located laterally and its fibres follow a transverse direction, roughly aligned with the transverse plane of the body (Figure 2.3c). The muscle begins between the ribs and the iliac crest, along the mid-axillary line, and inserts anteriorly into its own aponeurosis which becomes the rectus sheath. The superior three quarters of the aponeurosis lies posterior to the *rectus abdominis* while the inferior quarter, below the arcuate line, lies anterior to the *rectus abdominis* (Figures 2.4 and 2.5). Activation of the *transversus abdominis* compresses the ribs and the abdominal viscera and increases intra-abdominal pressure. As a result, the *transversus abdominis* is the primary muscle used to retain the abdominal contents [4].

The actions of the internal and external oblique muscles, along with the *transversus abdominis* muscles aid with continence, child birth and laboured breathing. During exhalation in laboured or heavy breathing, these three muscles increase the intra-abdominal pressure, forcing the viscera upwards into the diaphragm which compresses the lungs and expels the air.

2.2.2. Rectus Sheath

The rectus sheath and aponeuroses of the abdominal muscles compose an inter-muscular fibrous layer. As mentioned above, the lateral abdominal muscles insert into their respective aponeuroses midclavicularly. The anatomy of these aponeuroses changes above and below the arcuate line. This line is defined as the point at which the anatomy of the aponeuroses changes. It is located in the hypogastric◊ region of the abdomen, approximately 2-3cm inferior to the umbilicus. Above the arcuate line the *rectus abdominis* muscle is encapsulated by the anterior and posterior rectus sheaths. The anterior rectus sheath is composed of the aponeurosis of the external oblique muscle and a portion of the aponeurosis of the internal oblique muscle. The posterior sheath is composed of the rest of the aponeurosis of the internal oblique muscle and the aponeurosis of the *transversus abdominis* muscle. Below the arcuate line, there is no posterior rectus sheath. The r*ectus abdominis* is covered anteriorly by a sheath composed of the aponeuroses of each of the three pairs of lateral abdominal muscles (Figures 2.4 and 2.5)

2.2.3. Other Layers

Two fibrous layers lie beneath the muscles. The *transversalis fascia* is the more superficial of these two layers. It is a thin, membranous structure that is dense in the inguinal◊ region and thinner in the region of the diaphragm. It is a 'true fascia' as defined by Schleip et al. [23] as it has a dense, irregular structure. The *transversalis fascia* is continuous with the fasciae of the iliac, pelvic and diaphragm regions.

The peritoneum is the deeper of these fibrous layers. It is a smooth, serous membrane consisting of a connective tissue layer and a thin layer of cells that secrete a fluid to allow friction-free sliding of the abdominal wall over the abdominal viscera. As a membranous, collagenous structure, the peritoneum can also technically be defined as a fascia as per the definitions of Schleip et al. [23]. Not all structures within the abdominal cavity are within the peritoneal cavity. The bladder, kidneys, uterus, and portions of the pancreas and colon are extraperitoneal◊. The peritoneum consists of two layers; an outer parietal◊ peritoneum that attaches to the abdominal wall and an inner visceral peritoneum that attaches to the intraperitoneal viscera. The serous fluid secreted by the peritoneal cells fills the space between these two layers, known as the peritoneal cavity.

The anatomical structure of the abdominal wall is shown graphically in Figure 2.4 (superior to the arcuate line) and Figure 2.5 (inferior to the arcuate line).

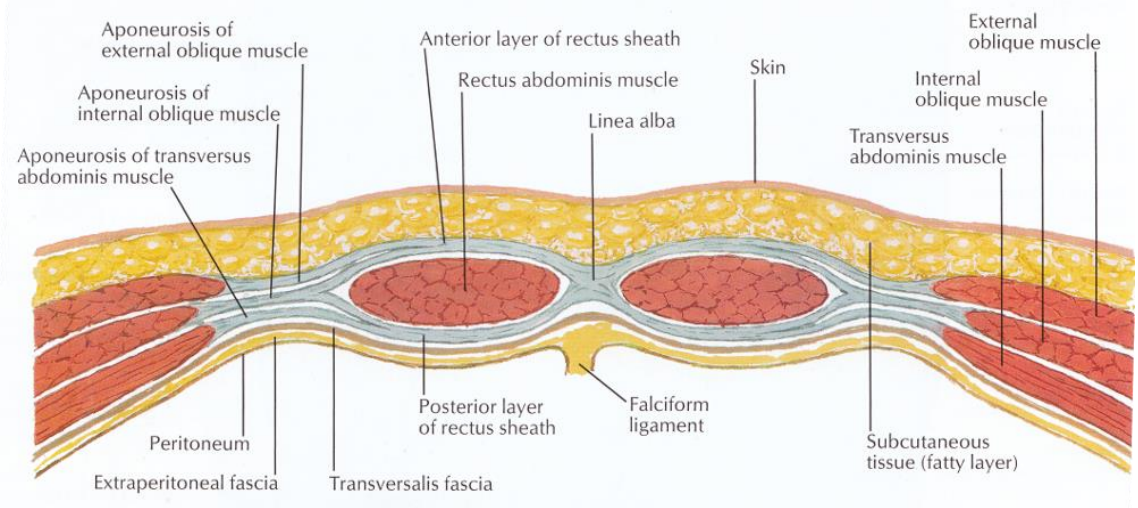

Figure 2.4 – Anatomy of the abdominal wall above the arcuate line, with the rectus sheath lying anterior and posterior to the *rectus abdominis* muscle, from [24].

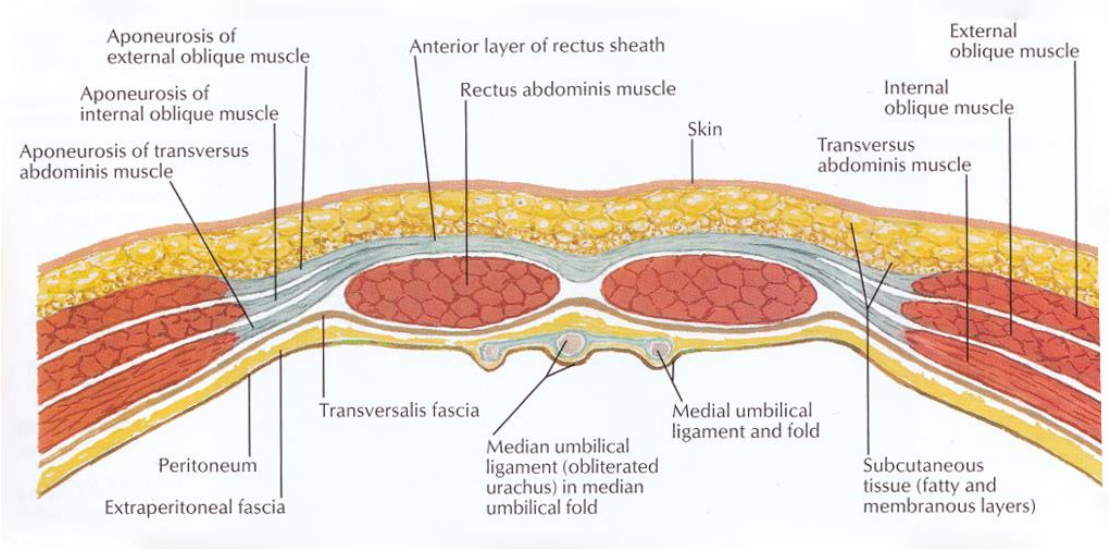

Figure 2.5 – Anatomy of the abdominal wall below the arcuate line with the rectus sheath lying only anterior to the *rectus abdominis* muscle, from [24].

2.3. Intestines

2.3.1. Overview

The intestines are hollow organs of the gastrointestinal tract, and part of the digestive system. They are typically distinguished as large and small, although there are also further segregations within each organ. The organs extend from the distal end of the stomach to the anus and are responsible for the digestion and absorption of nutrients from ingested food.

2.3.2. The Small Intestine

The small intestine originates from the distal end of the stomach, specifically the pylorus of the stomach, and ends at the caecum◊ at the anastomosis◊ with the large intestine. The organ is approximately 6m in length and 2.5cm in diameter [25] and is segregated into three sections: the duodenum, the jejunum and the ileum. Chemical digestion typically occurs in the duodenum, while absorption of carbohydrates and proteins takes place in the jejunum, and absorption of vitamin B12 and bile salts happens in the ileum. The small intestine occupies a large portion of the abdominal cavity and it is a relatively fluid organ, held in place by mesenteries◊. As with other tracts of the digestive system (e.g. the oesophagus), the small intestine is a muscular organ. Within its structure it has both circumferentially

and longitudinally orientated muscle fibres that contract in waves to "push" the contents along its length in a process called peristalsis◊.

Due to the small diameter of the organ and its fluid nature, the small intestine is frequently implicated in herniae (Section 2.4), often leading to obstruction, blocking the passage of food through its length, with consequences ranging from transient pain, vomiting and nausea to death.

2.3.3. The Large Intestine

The proximal end of the large intestine begins at the distal end of the small intestine. The anastomosis between the two organs is typically located in the right lower quadrant of the abdomen. The organ is approximately 1.5m long and 6cm in diameter. Its wall structure is somewhat different to the small intestine and its function is simply to remove water and remaining vitamins from food before compacting and storing waste pending egestion. Due to its large diameter, location and limited mobility, the large intestine is less frequently implicated in herniae.

2.4. Hernia

A hernia is the protrusion of an organ, or part of an organ, through the wall of a cavity that normally contains it [26]. In the abdominal cavity, the ventral◊, lateral and dorsal abdominal wall is the largest structure containing the contents of the abdomen. The cavity is also bounded superiorly by the diaphragm and inferiorly by the pelvis. The most common type of hernia is a hiatus hernia [26] which is caused by the stomach moving up through the diaphragm via the oesophageal hiatus. Herniation of the rest of the abdominal contents through the diaphragm is uncommon, mainly because a large portion of the diaphragm is in direct contact with the liver. Other types of herniae include inguinal herniae, umbilical herniae and incisional herniae.

2.4.1. Inguinal Hernia

An inguinal hernia is the protrusion of some of the contents of the abdominal cavity through the inguinal canal. The inguinal canal is a passage in the anterior abdominal wall that conveys structures from the pelvis into the abdominal cavity. As this passage is

effectively a natural defect in the abdominal wall, it is not uncommon for structures of the abdomen, typically the small intestine, to protrude through it [27]. Inguinal herniae are more common in men than women due to the larger size of the male inguinal canal [27]. The only definitive treatment for this injury is surgery, however 'watchful waiting' may also be recommended [28].

2.4.2. Incisional Hernia

Incisional herniae result from the protrusion of some of the contents of the abdomen through a defect, typically in the abdominal wall, caused by an incision. The incidence of incisional herniae after a laparotomy, or other open surgery, can be as high as 20% [4, 29-31]. The weakened structure of the abdominal wall, as a result of the incision and manipulation, is less able to contain the contents of the abdomen, especially under load from high intra-abdominal pressure. If an incisional hernia occurs after a laparotomy and is repaired with a tension repair, it has up to a 50% chance of recurring [4]. A tension repair exists when the edges of the defect that facilitated the hernia are re-approximated and stitched together. A more modern practice for repair of these herniae is the installation of a prosthetic mesh over the defect. This is known as a tension-free repair and has a much lower likelihood of recurrence [4].

Similar to the development of an incisional hernia after open surgery, it is also possible for an incisional hernia to occur after a laparoscopic surgical procedure. The defects created in the abdominal wall by the trocar ports, particularly ports greater than 5mm in diameter, weaken the structure of the abdominal wall and create a possibility for small intestine, or other structures, to protrude through [5, 8, 9, 31-33]. Defects created by the use of larger trocars are more likely to develop herniae, particularly if there is manipulation of the port site to remove excised tissue from inside the abdomen. Due to the fact that it is a naturally pre-existing scar, the umbilicus is frequently used as the site for a large trocar. The umbilicus is located on the midline, and thus has no abdominal wall muscles behind it for protection. The frequent use of large ports and its lack of muscular protection leave it more prone to herniae than other port sites [34].

Age, smoking, the use of steroids and having diabetes or other co-morbidities diminish the ability of the body to heal wounds, thus this population is at a greater risk of developing

an incisional hernia after either open or laparoscopic surgery [35-37]. Obese◊ patients are also at a greater risk of developing an incisional hernia; this may be for a number of reasons including the more frequent presence of co-morbidities, but also as a result of increased intra-abdominal pressure due to their weight [36-38].

2.5. Intra-Abdominal Pressure

Intra-abdominal pressure (IAP) is a natural pressure within the abdominal cavity that exists because the abdominal cavity is a sealed compartment bordered by muscles, the most mobile of which is the diaphragm. At rest, the abdomen has a positive pressure above atmospheric pressure of 1-1.5kPa [39-41]. In ill patients, this can rise to 2-2.5kPa [42], with higher pressures resulting in organ dysfunction if sustained. During strenuous exercise, IAP can rise to 20kPa, but this will not be sustained for long periods and will, most likely, not occur in patients recovering from surgery. The maximum pressures realised in these patients will most likely be due to coughing, which, according to Cobb et al. [41], results in an IAP of 11kPa.

The abdomen is not a simple engineering pressure vessel. It consists of a complex array of organs, fluids, air pockets and blood/lymph vessels. The solid organs and the fluids are effectively incompressible. However, blood and other fluids can be expelled via the network of vessels connecting the abdominal cavity to other parts of the body. Organs such as the liver, spleen and kidneys hold significant amounts of blood, and applying pressure to these organs will squeeze the blood out in much the same fashion as squeezing a sponge. The blood will drain through the vasculature and out of the abdomen. Simplistic analysis of the intra-abdominal pressure situation is therefore difficult, however Section 5 attempts to quantify the physiology of IAP generation, mathematical pressure calculations and geometry to give a broad understanding of the *in vivo* mechanisms of pressure generation.

2.5.1. Abdominal Straining and the Valsalva Manoeuvre

The Valsalva manoeuvre is the activation of a specific combination of muscles to raise both intra-abdominal and intra-thoracic pressure in order to inflate the middle ear [43]. This is frequently done to equilibrate the pressure in the middle ear with atmospheric pressure in

one's current environment. The manoeuvre is named after the Italian physician, Antonio Maria Valsalva who had significant interest in the anatomy and physiology of the ear [43].

The Valsalva manoeuvre is distinctly different from, although often confused and used interchangeably with, abdominal straining. Abdominal straining also involves the generation of intra-abdominal and intra-thoracic pressures, although the goal of these pressures is to aid in defaecation, child birth or other bodily functions. Talasz et al. [43] discuss the difference between the two manoeuvres in detail, but the essential difference is that abdominal straining involves a larger inspiration followed by attempted forced expiration against a closed glottis with associated contraction of the abdominal muscles and eccentric contraction and relaxation of the pelvic floor muscles to improve defaecation. The Valsalva manoeuvre, on the other hand, involves attempted forced expiration against a closed mouth and nostrils, contraction of the abdominal muscles and contraction of the pelvic floor muscles to inhibit urine leakage.

While both manoeuvres result in increased IAP, the more common manoeuvre is abdominal straining as it is invoked during coughing, straining, lifting and even sitting up using the abdominal muscles.

2.5.2. Coughing

A cough is a sudden reflex which helps to clear foreign objects, secretions or other irritants from the large breathing passages by forceful expulsion of air from the lungs. During a cough, the intra-abdominal pressure reportedly rises to 11kPa [41]. The mechanics of a cough were explained by Leith et al. [44]. A cough consists of three stages: inspiration, compression and expiration.

2.5.2.1. Inspiration

The inspired volume varies with anticipated forcefulness of the cough. In some cases inspiration will be supressed so as to minimize the penetration of the foreign body into the airway. Inspiration occurs by expanding the volume of the chest through contraction of the diaphragm, and the intercostal muscles. The diaphragm moves inferiorly and the intercostal muscles cause the ribcage to move superiorly and anteriorly. This expansion of

the volume of the thoracic cavity creates a negative pressure relative to the atmosphere drawing air in through an open mouth and/or nostrils.

2.5.2.2. Compression

After inspiration, the glottis is closed and the expiratory muscles of the abdomen activate, as do the costal muscles, causing a decrease in the lung volume and thus an increase in pressure. Abdominal pressure is raised due to the already contracted diaphragm and is further elevated by the increase in thoracic pressure.

2.5.2.3. Expiration

The glottis is opened and the diaphragm relaxes. The pressure within the abdomen forces the diaphragm upwards and forcefully exhales the air from the lungs. The high thoracic/pleural pressure also aids in the expiration and is expected to force the unwanted object or substance out of the airway.

2.6. Laparoscopic Surgery

Laparoscopic surgery is an increasingly popular, minimally invasive operative technique performed through small, keyhole-sized ports in the abdominal wall. It was first performed in 1987 [45] and has rapidly increased in popularity with more than two million operations in the United States alone each year [2]. Despite its popularity, there are still some complications associated with the procedure, including the development of a hernia at the incision site. There are many reasons cited for this, although it is expected that the true cause is a combination of factors compounding to develop the complication in a small number of cases. Reported incidence of port site hernia is 1-3% [5, 6, 32, 46]. A commonly cited potential cause of these herniae is the inadequate closure of the layers of the abdominal wall [31, 33].

2.6.1. Technique

Laparoscopic surgery involves the insertion of ports through the abdominal wall to gain access to the abdominal cavity. Typically one port will be used for the laparoscope and two other ports will be used for instruments and removal of tissues. Ports range in diameter

from 5-15mm and typically the largest port is placed at the umbilicus to minimise scaring (Figure 2.6).

To insert a port by the Hasson method [47], a small incision is made in the skin and subcutaneous fat at the desired location for the port.

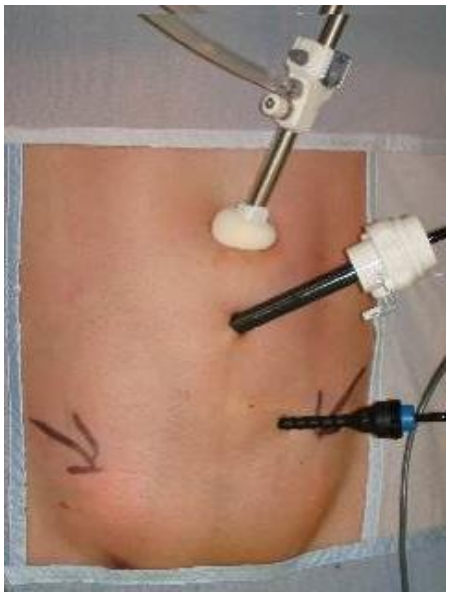

Figure 2.6 – Trocar ports inserted for a laparoscopic surgical procedure.

2.6.1.1. Umbilical Port

The port is placed inside the skin incision and pushed with a steady force and with an oscillating twisting motion until it reaches the abdominal cavity.

2.6.1.2. Medial◊ Port Below the Arcuate Line

The anterior layer of the rectus sheath is incised and the *rectus abdominis* muscle is reflected. The trocar is then pushed through the *transversalis fascia* and peritoneum.

2.6.1.3. Medial Port Above the Arcuate Line

The anterior layer of the rectus sheath is incised and the *rectus abdominis* muscle is reflected. The trocar is then pushed through the posterior layer of the recuts sheath, the *transversalis fascia* and the peritoneum.

2.6.1.4. Lateral Port

Muscles are reflected and intermuscular fascia is incised either to the level of the deepest aponeurosis or to the *transversalis fascia*. The trocar is then pushed into the abdominal cavity.

2.6.1.5. After Port Insertion

After insertion of the first port, the abdominal cavity is insufflated with CO_2 gas up to a pressure of approximately 2kPa [48]. A laparoscope is inserted through the trocar and subsequent ports are inserted under direct visualisation from within the abdominal cavity to minimise the risk of damaging viscera during port insertion.

2.7. Conclusion

The anatomy of the abdominal wall is complex, with a number of layers of various tissues interacting to protect the contents of the abdominal cavity and to facilitate a number of manoeuvres and physiological functions. Defects in the abdominal wall, regardless of the cause, can result in the development of a hernia. Intra-abdominal pressure is a key factor in creating a hernia at an abdominal wall defect and surgery is often required to repair the hernia and prevent further complications.

Current closure of abdominal wall defects after surgery is not optimised for preventing the development of a port site hernia (Section 3.4). This thesis takes the first steps in developing a closure solution to reduce the incidence of post-operative hernia development.

3. Literature Review

3.1. Introduction

This chapter will give a broad overview of the literature in the field of post-operative incisional herniae◊ and properties of the abdominal wall and viscera◊. Certain specific abbreviations and terminology will be used in this section that have previously been explained in the background section (Section 2). Obscure abbreviations will be annotated and briefly explained in a footnote, with specific reference to the relevant theory section.

The literature review will focus on four main areas: intra-abdominal pressure, abdominal tissue properties, incisional herniae and mesh closure mechanisms.

Section 3.2 focuses on the importance of understanding intra-abdominal pressure, factors pertaining to its generation and its general physiology.

Section 3.3 examines existing literature on the mechanical and structural properties of both the abdominal wall and the small intestine, and debate the relevance of the available data to the current study.

Section 3.4 examines the extensive literature on herniae, examining their prevalence, particularly after laparoscopic surgery, the details of incisional herniae and the debate on closure methods and their importance.

Finally, Section 3.5 examines the use of meshes for hernia repair and the possibility of using a similar method for the closure of laparoscopic trocar◊ wounds. The efficacy of meshes will be examined along with some discussion on the advantages of mesh repair over traditional suture repair.

3.2. Intra-Abdominal Pressure

Intra-abdominal pressure (IAP) (Section 2.5) is a natural pressure within the abdominal cavity that exists because the abdominal cavity is a sealed compartment bordered by muscles; the most mobile of which is the diaphragm. As discussed in Section 2.5.2.1, in

normal circumstances inhalation occurs due to the diaphragm contracting and moving inferiorly◊. This causes the abdomen to distend slightly which maintains a broadly constant resting IAP. If the abdomen is constrained from distending, usually via contraction of the abdominal muscles, the IAP will rise. There are a number of techniques to measure IAP, all of which involve inserting a device into the abdominal cavity. Methods include measurement via intra-gastric pressure as done by Campbell et al. [40], measurement via a urinary catheter which will obtain pressure within the bladder, as done by Sanchez et al., Cobb et al., and Sugerman et al. [39, 41, 49], and measurement via a swallowed radio pill◊, which records intra-gastric or intra-intestinal pressure, as used by Marras et al. [50]. Malbrain et al. [51] conducted an extensive review of the main IAP measurement techniques and concluded that there is no "gold standard" method of measuring IAP, despite the widespread use of the bladder technique as such. It is concluded, however, that the bladder technique does provide a good estimation of IAP, as do continuous gastric techniques. Thus, for the purposes of this review, the method of measuring IAP will not be considered for discussion as all methods are considered equally accurate. Additionally, a wide variety of units of pressure are used in the literature. For clarity and convenience, all pressures will be converted to Pascals, the base SI unit for pressure, and reported as such.

Campbell et al. [40] investigated the variation in IAP with breathing in nine healthy young male adults. Pressure was recorded on an Ediswan ink-writer. This very early study into the effect of breathing on IAP reveals that during normal, quiet breathing at rest there is little or no activation of the abdominal muscles and a variation in IAP of only about 980Pa. It was discovered that as breathing becomes more laboured and the patient becomes more distressed with the onset of hypoxia◊, muscular activity increases and IAP variation is noticeable as a result. In normal breathing, and even at the beginning of laboured breathing, IAP is usually greatest at the end of inhalation. This is corroborated intuitively, if one considers the movement of the diaphragm downwards and the ability of the abdomen to distend. In very laboured breathing, however, the activation of the abdominal muscles is such that the IAP at the end of expiration is actually higher than at the end of inspiration. This confirms that activation of the abdominal muscles can have a significant effect on IAP. Marras et al. [50] and Cobb et al. [41] confirm this in their studies investigating the variation in IAP during certain activities.

Marras et al. [50] investigated IAP during heavy lifting by recording intra-intestinal pressure in 114 healthy subjects by means of an ingested radio pill. It was found that when more than 54Nm of trunk torque was applied, the IAP rose significantly. It is also reported that IAP increases monotonically as a function of trunk velocity. It is the internal and external oblique muscles (Section 2.2.1) that generate trunk torque, thus it must be activation of these muscles that causes increased IAP during lifting and exercise.

Manoeuvre	Range [kPa]	Mean [kPa]
Supine	-0.13 – 0.8	0.2
Bench Press	0.27 – 4.5	1.0
Bend at Waist	0.8 – 4	1.9
Sitting	0.13 – 2.8	2.2
Standing	2 – 3.6	2.7
Bend at Knees	1.87 – 4	2.7
Arm Curl	2.27 – 4.93	3.4
Abdominal Crunch	0.93 – 6.27	3.6
Abdominal Straining Manoeuvre	2.67 – 8.53	5.3
Standing Abdominal Straining Manoeuvre	4.27 – 15.2	8.7
Stairs	5.33 – 14.67	9.2
Cough	5.33 – 16.93	10.9
Standing Cough	8.53 – 18.8	14.3
Jumping	5.73 – 33.6	22.8

Table 3.1 – Intra-abdominal pressure for various manoeuvres as reported by Cobb et al. [41].

Cobb et al. [41] also investigated IAP in healthy, non-obese◊, young adults to determine normal IAP during a range of activities. It was found that activities requiring activation of the abdominal muscles, such as abdominal crunches, climbing stairs, coughing and performing an abdominal straining manoeuvre[2] (incorrectly referred to as a Valsalva manoeuvre), resulted in higher IAP. The most significant IAP rise was found when the subject was asked to jump. The full list of reported IAPs is summarised in Table 3.1.

[2] An abdominal straining manoeuvre is a moderately forceful exhalation attempt against a closed glottis (Section 2.5.1).

Most pertinent to hospitalised patients is IAP rise due to coughing. Cobb et al. reported a pressure range of 5.33kPa – 16.93kPa for coughing, although they do not report how many coughs the patient was asked to perform. The values agree somewhat with those reported by Campbell et al. [40], though Campbell et al. noted that IAP during coughing seemed to exceed the maximum recordable value in their system, although the magnitude of the IAP in these cases is not estimated (the system could only record pressures up to 5kPa).

Similar to, though less in-depth than Cobb et al., Iqbal et al. [52] investigated IAP changes in coughing, vomiting, retching and bench-press weightlifting. Ten healthy, young subjects were asked to cough forcefully, lift weights and had vomiting induced medically. Average IAP during coughing was 4.67kPa, which is significantly lower than that reported by Cobb et al. Retching and vomiting was found to generate higher IAPs of 9kPa and 11kPa respectively. Unsurprisingly, bench-pressing while supine did not significantly increase IAP as IAP not needed to maintain posture or assist with spinal loading when supine [53].

Iqbal et al. [52] recorded all pressures using both a urinary catheter and a nasogastric tube technique. Similar to the findings of Malbrain et al. [51], it was found that there was no difference between the pressures recorded by these methods.

It is reported by many authors that IAP is well correlated with BMI◊ and an increasing BMI◊ resulted in increased IAP [39, 41, 49, 54]. Cobb et al. reported statistically significant correlations between BMI and IAP for coughing while sitting and standing. Sanchez et al. [39] reported a statistically significant positive relationship between BMI and IAP, and interestingly also cited recent abdominal surgery among the risk factors for increased IAP. Similarly, Sugerman et al. [49] found that obese patients had a resting IAP almost three times higher than non-obese patients, with a correlation coefficient of 0.45; in a large, multi-centre study covering 13 intensive care units in six countries, Malbrain et al. [42] corroborated this finding. Lambert et al. [38] made a similar finding, but positively correlated a high IAP with sagittal◊ abdominal diameter and not with BMI or body weight. It is also reported that the mean resting IAP of the obesity group was 1.18kPa, compared with a control group mean IAP of 0kPa. The sample size of the control group for this study was particularly small compared to the obesity group however, with only four patients included in the control compared to 45 in the obesity group.

The increased risk of high IAP in obese patients is of particular concern when considered alongside the findings of Sanz-Lopez et al. [31] who reported that obesity is a factor in impeding access to trocar site wounds for post-operative closure. It is possible that this may result in poor closure of the wound or, in some cases, the wound being left open. As discussed in Section 2.4, inadequate or absent closure of a defect is a risk factor in developing a port◊-site hernia. This is further corroborated by de Vries et al. [55] who reported a correlation between BMI, IAP and the presence of herniae. Furthermore, Bowrey et al. [6] reported that patients who developed a trocar site hernia post-operatively had a higher BMI, which has been shown above to be correlated with high IAP.

IAP can vary significantly from person to person [41, 50, 54] and, considering simple mechanics, the pressure within a confined space is related to the stress in the walls containing the pressure. Thus, patients with higher IAP will have a higher stress in their abdominal wall, which is already weakened by surgery. Most patients will rest post-operatively, thus strenuous exercise, heavy lifting and jumping (all associated with increased IAP, as above) will not be a problem. However, coughing, vomiting climbing stairs and performing abdominal crunches (which may happen as patients sit up in bed) are of concern. In the presence of any respiratory co-morbidities, such as COPD[3] or pneumonia, the increased IAP during coughing is particularly worrying. Interestingly, it is reported that smokers are more prone to incisional hernia due to poor healing [35]. Smoking is also a significant risk factor for COPD and other respiratory diseases [56] which can result in a chronic cough, substantially increasing their risk of hernia development.

Given the added importance of the integrity of the abdominal wall for abdominal surgery patients, the role of IAP in their recovery and possible post-operative complications is important and must be carefully considered when managing the patient from wound closure to recovery. Adequate wound closure, particularly in high risk patients (high BMI, smoking, etc.) should reduce the incidence of trocar site herniation.

[3] Chronic Obstructive Pulmonary Disease is a chronic progressive lung disease often characterised by a chronic chough.

3.3. Tissue Properties

As with most biological tissue, the mechanical properties of tissues relevant to this study are inherently non-linear, anisotropic and viscoelastic. These phenomena make them more difficult to classify and more difficult to replicate with surrogate engineering materials for experimental purposes. Relevant tissues for this study include the *linea alba*, the rectus sheath, the *transversalis fascia*◊ and the small intestine. The *linea alba*, rectus sheath and *transversalis fascia* are part of the abdominal wall that must be closed post-operatively. Inadequate closure of these layers is reported to cause greater incidence of post-operative herniation [7]. The small intestine is most frequently implicated in these herniae [7].

3.3.1. The Abdominal Wall

Mechanical properties of the *linea alba*, rectus sheath and *transversalis fascia* are poorly reported. Due to the lack of detail it is not possible to generate a mechanically similar engineering material that can be used for experimental purposes. Song et al. [57] measured the elasticity of the abdominal wall during laparoscopic surgery when the abdominal cavity is inflated with carbon dioxide (see Section 2.6). The authors inferred the stress in the abdominal wall from this insufflation pressure using Laplace's Law[4] for a thin walled pressure vessel and measured the strain in the abdominal wall by tracking the movement of markers placed on the abdomen using a computer software package. The thin walled pressure vessel assumption applies for thickness to radius ratios of 1:10 or greater. Song et al. reported an average abdominal wall thickness of 30mm, however an average transverse◊ radius of the abdomen of 200mm is reported. Technically this means that the thin walled assumption is not valid, although the experiments do give some insight into the mechanical properties of the abdominal wall. The aim of the study by Song et al. was to quantify the elasticity of the abdominal wall for more accurate simulation of insufflation for training purposes. It is difficult to accept the reported results as the Young's Modulus of the abdominal wall, however, as the abdominal wall is composed of a number of layers, each

[4] Laplace's Law can be used to describe the stress in a thin walled pressure vessel. The circumferential, or "hoop" stress is given by $\sigma_c = \frac{pr}{t}$ and the longitudinal stress is given by $\sigma_l = \frac{pr}{2t}$ where p is the pressure, r is the radius of the vessel and t is the wall thickness.

with inherently different structures and thus very different mechanical properties. There are between three and four layers of muscle (depending on the region of the abdominal wall observed), numerous layers of connective tissue, fat and skin making up the abdominal wall. Given the simplicity of the method, the results were considered and compared to results of more traditional mechanical tests of the separate layers of the abdominal wall. The graphical comparison can be seen in Figure 3.3 on page 30.

Kureshi et al. [58] examined the properties of the *transversalis fascia* with a goal of determining differences in properties between herniated and non-herniated *transversalis fascia*. Herniated *transversalis fascia* specimens were harvested from patients undergoing hernia repair, while non-herniated specimens were harvested from organ donors with no history of herniae. The tissue was tested in a simple uniaxial tensile test and the stress-strain response was calculated. This method is more fundamental than that of Song et al. [57].

During lateral◊ laparoscopic port insertion the *transversalis fascia* is incised with a scalpel or punctured by the trocar. As a result, the *transversalis fascia* must be closed post-operatively. Knowledge of the stiffness of the layers needing closure is important to ensure a similar stiffness match between the natural tissue and the method of closure. When compared to the results of Song et al. [57], Kureshi found that the *transversalis fascia* was much more compliant, however Kureshi also found that the *transversalis fascia* could strain up to 100% before failure. This seems surprising and is contrary to the results of Kirilova et al. [59] who conducted similar tests and found that *transversalis fascia* reached a maximum stress at 20-40% strain before beginning to slowly fail. Some authors would consider the onset of failure after the maximum stress as the end of the test, however Kirilova et al. continued stretching the specimen at 15mm/s until complete rupture. The secant modulus of elasticity is reported for strains of 5% and 10%. Given the linear stress-strain relationships up to at least 20%, the secant moduli can be accepted as the stiffness of the tissue. Interestingly, the reported stiffness is much higher than the stiffness reported by Song et al. [57], although there is variation in the Kirilova et al. results of up to 300%. Maximum stiffness reported by Song et al. is 0.05MPa, while the maximum stiffness reported by Kirilova et al. is 15.12MPa. The discrepancies between the two authors are most likely due to the very different testing methods as well as the influence of the extra layers of the abdominal wall in the Song et al. cases. Additionally, Song et al. only calculated stiffness using CO_2 insufflation during

surgery, thus they were limited in the magnitude of loading that could be applied to a living patient. It is likely that the tests were within the toe region of the stress-strain curve for the abdominal wall. This can be verified by examining the mechanical testing of rabbit abdominal muscles by Hernandez et al. [60] that show a clear toe region dominating for stretches less than 1.1 (Figure 3.1). Kirilova et al. reported significant variation in the results, even between specimens harvested from similar locations in the same donor which is attributed to natural variation in tissue. There is a lack of data to confirm or deny this claim, however similar variation is not reported by Kureshi et al. or by Minns and Tinckler [61]. Minns and Tinckler conducted similar tests to Kureshi et al. and found that less energy is required to rupture previously damaged tissue. Reported maximum failure stress is approximately 3MPa. Young's Modulus is not reported, and difficult to infer due to the shape of the stress-strain curves.

Linea alba (Section 2.1) incorporates the rectus sheath and the *transversalis fascia* along the midline of the abdominal wall. It has been studied somewhat more extensively than *transversalis fascia*. Korenkov et al. [62] studied the effect of anatomical features (fibre thickness, direction, etc.) on the tensile strength of *linea alba* of formalin◊-fixed cadavers. Tensile strength is reported in kiloponds[5] and sample dimensions were provided. It is difficult to determine an exact range of ultimate strength values as there is no identification of the sample sizes for specific values of force, but rather ranges for both values. A mean ultimate strength can be derived using the mean force and mean area as 4.33MPa. This is stronger than the values reported by authors testing *transversalis fascia*, as would be expected, due to the formalin embalming and the denser nature of the *linea alba* tissue.

Hollinsky et al. [63] examined the difference in strength between scar tissue and normal tissue at the *linea alba*, based on reports that scar tissue is more likely to rupture and cause incisional hernia. It was discovered that scar tissue is indeed weaker than unscarred *linea alba*, by a factor of approximately 30% in the fibre direction and 25% in the cross-fibre direction, with an average failure stress of intact *linea alba* of 9.2MPa in the fibre direction.

[5] A kilopond, or kilogram-force is a unit of weight equal to 9.81N.

This supports the findings of Minns and Tinckler [61] and Kureshi [58], who found that damaged *transversalis fascia* was weaker than undamaged *transversalis fascia*.

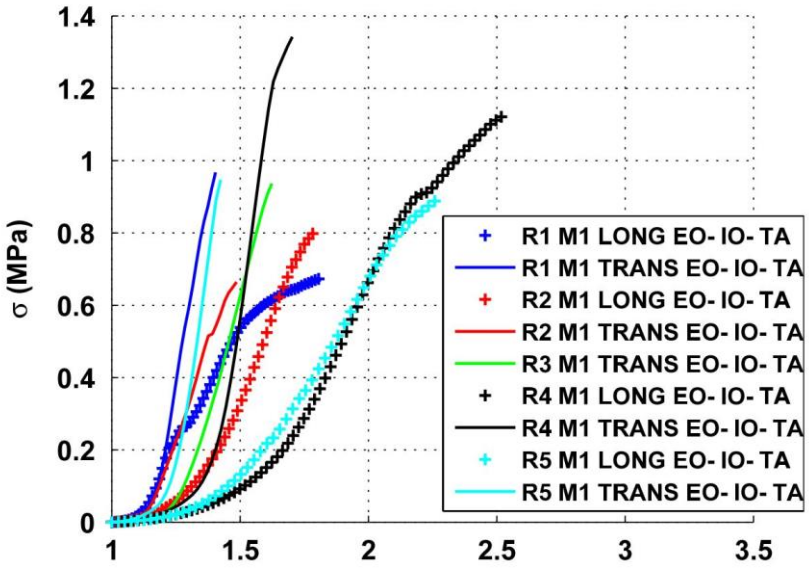

Figure 3.1 – Stress-stretch response of rabbit abdominal muscle composite layer, from [60].

Forstemann et al. [64] examined the mechanical response of *linea alba* under tensile loading in a very similar manner to Hollinsky et al., and reported maximum stresses before failure of 7.5MPa in the fibre direction or 1.1MPa in the cross-fibre direction. These results complement the findings of Hollinsky et al. and Graβel et al. [65], who also investigated the tensile mechanical properties of fresh-frozen human *linea alba* but reported stress in units of N/cm without reporting an average thickness of the tissue. Using the results of Korenkov et al., who reported a *linea alba* thickness of approximately 2mm, a maximum test stress of 12MPa can be calculated from the Graβel et al. data. The authors ended the tests at this stress level and reported that the tissue is more compliant in the cross-fibre direction than in the fibre direction. Ultimate tensile stress or strain values are not provided.

There is overall agreement about tensile strength of *linea alba*, and all authors reported that it is stiffer than *transversalis fascia*. It is not possible to fully characterise the tissue from this data, however, and further work is required to obtain a clear picture of the behaviour of this tissue under load.

The rectus sheath is a fibrous layer enveloping the *rectus abdominis* muscle. It was examined by Martins et al. [66] with the aim of developing a constitutive model. Specimens extracted from cadavers were tested in uniaxial tension in the fibre and cross-fibre directions. A wide

range of stress-strain curves were generated from the various samples. Maximum stress in the fibre direction was 12MPa and the maximum stretch was 1.71. This stretch is very high, suggesting the tissue almost doubled in length before failure, and raises questions about the possibility of slippage during the tests. Stretch was analysed using machine grip displacement rather than by optical methods which have been shown to be superior [67]. A statistically significant difference was noted between the ultimate tensile strength of rectus sheath for those with a BMI greater than 25kg/m^2 compared with a BMI of less than 25kg/m^2, however the questions about tissue slippage overshadow this result. In contrast to the 70% elongation reported by Martins et al., Rath et al. [68] reported maximum average elongation of only 36% in a similar study also conducted on fresh cadaver tissue. Maximum breaking stress of the tissue is reported as 7.6MPa, however it is not clear if this is also the ultimate tensile strength of the tissue. Only failure stress and strain values are reported by these authors, so it is not possible to compare the stress-strain profile with other results. More recently, Ben Abdelounis [69] studied human rectus sheath, also in tensile loading. A small number of cadavers were dissected and the tissue was only tested in the cross-fibre direction. To counter the problem of slippage at the grips, the authors drew dots on the sample which they tracked by analysing video footage on a computer. Stress and strain results were lower than both Rath et al. and Martins at al. with failure stress at only 0.6MPa and failure strain at 16%.

Nilsson et al. [70] also conducted a study on rectus sheath, however the authors included the rectus abdominal muscle in the tests. Breaking strength and elastic stiffness are reported in Newtons and cross-sectional area is not provided, thus comparison with other literature is not possible.

Overall, it is particularly difficult to quantify the strength of the abdominal wall. Firstly, this is because of the various layers from which it is composed, each of which appears to have different strengths, and, secondly, because of the significant variation in the reported strength values of these individual layers. Variation in testing procedures and methods between laboratories is probably the cause of some discrepancies between authors, but the variation between samples from a single donor is more difficult to explain and is usually attributed to natural variations within the tissue. It is also important to critically analyse only the key tissues implicated in the problem of incisional herniae. To identify these tissues

a mechanical analysis of the abdominal environment is needed, which has not been previously reported.

It is important when making comparisons between various studies that the same layers of the abdomen are compared. Figures 3.2 to 3.4 compare the results of tensile tests by various authors on *transversalis fascia* (Figure 3.2), *linea alba* (Figure 3.3) and rectus sheath (Figure 3.4). It should be noted that, notwithstanding the test to test variations, there are, in general, significant differences in strength, structure and composition between the three tissues. Detailed comparison of data reported by authors examining rectus sheath is not possible. Martins et al. [66] and Ben Abdelounis et al. [69] were the only authors to provide stress-stretch data. Rath et al. [68] only provide a breaking stress and strain, thus the shape of the curve is not known, and Nilsson et al. [70] also present just the breaking stress and strain, stress is reported in Newtons and there is no mention of cross-sectional area, thus Figure 3.4 shows a representative plot of these results for illustrative purposes only.

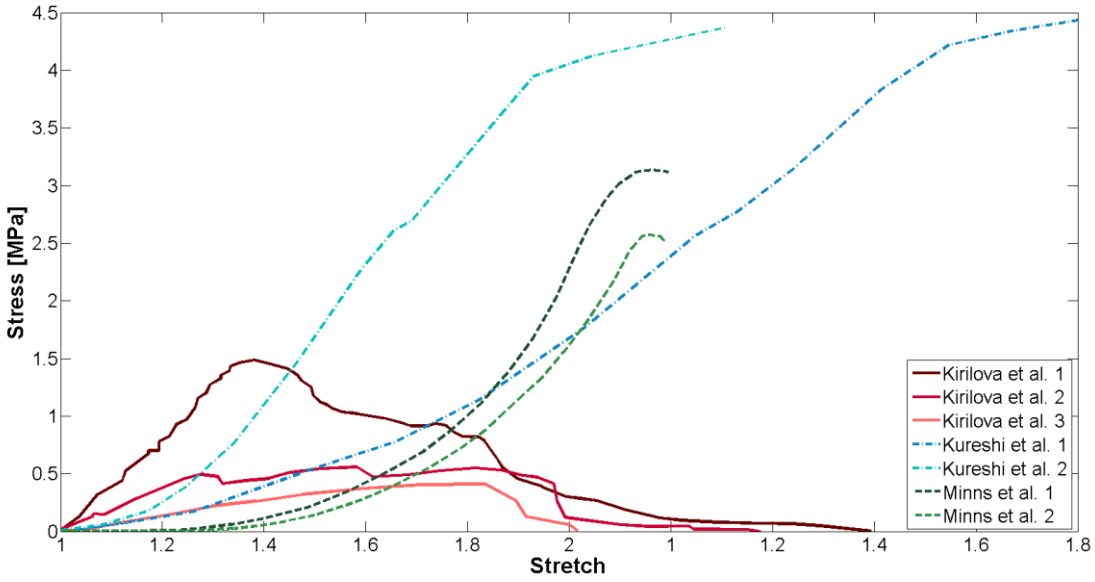

Figure 3.2 – Various results of stress-stretch data for the *trasversalis fascia*, adapted from [58, 59, 61].

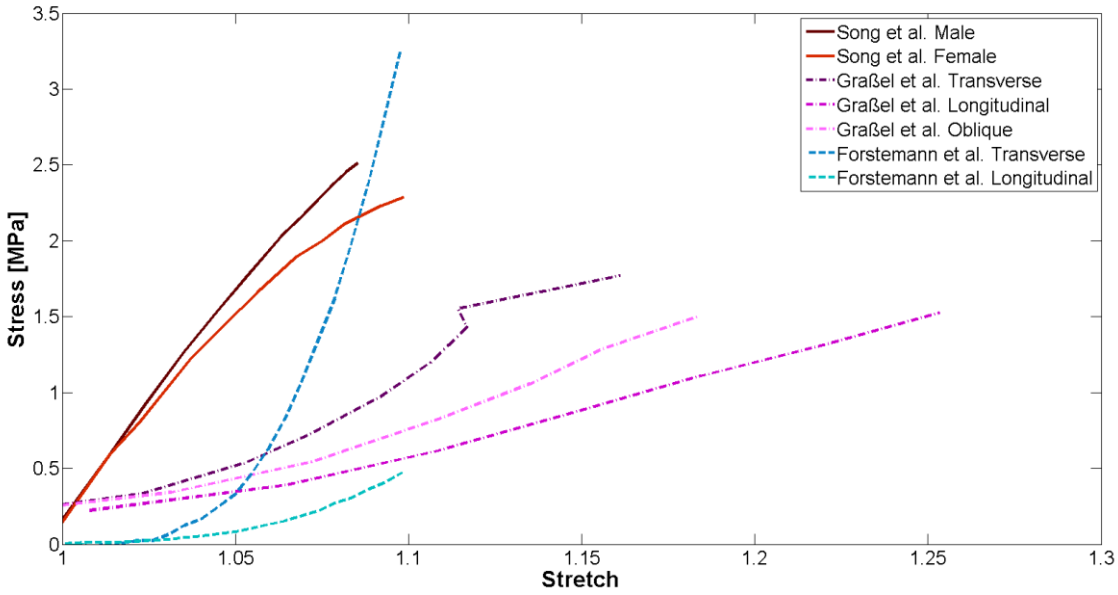

Figure 3.3 – Various results of stress-stretch data for the *linea alba*, adapted from [64, 65, 71].

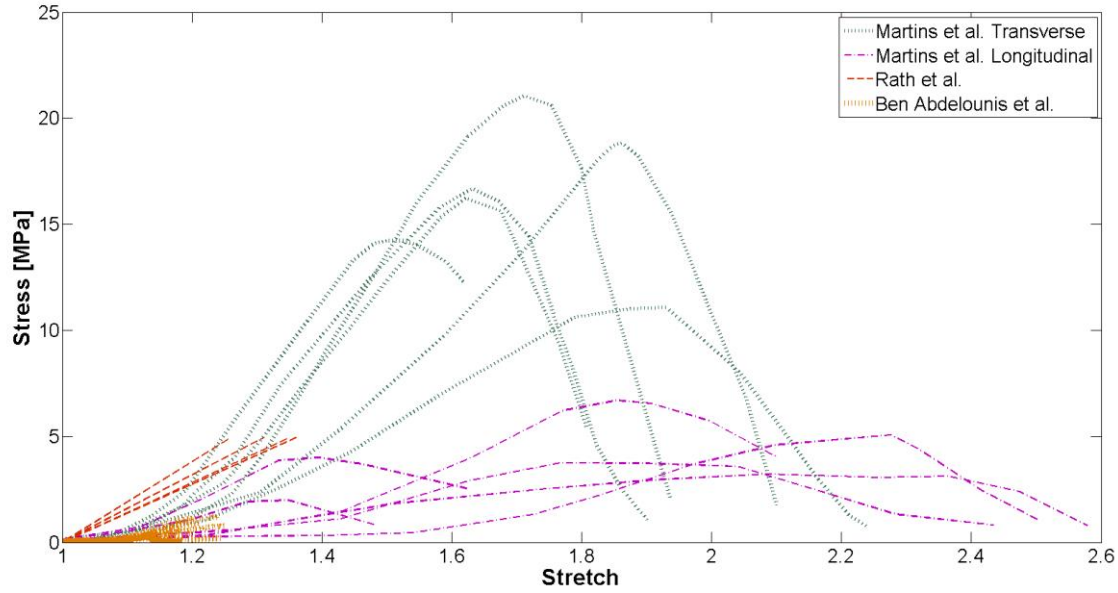

Figure 3.4 – Various results of stress-stretch data for the rectus sheath, adapted from [66, 68, 69].

3.3.2. The Small Intestine

The small intestine (Section 2.3.2) is frequently implicated in herniae, caused when it protrudes through the abdominal wall or the inguinal◊ canal (Section 2.4.1). The mechanical properties of human intestine have not been widely studied from a biomaterials perspective. The majority of studies relate to the distensibility of the organ (e.g. [72, 73]), while some authors have reported on the tensile strength of the organ [74] and others have examined the properties of the intestines of other mammals [75].

Understanding the distensibility of the organ is of particular importance as intestines are hollow tubes, through which food passes at various stages of digestion. Gregersen et al. [73] conducted an extensive review into the mathematics and understanding of the distension of the small intestine. The authors assert that pressure-volume relationships, derived by simply inflating a section of intestine and measuring the distension, do not give useful results as there is no direct measurement of luminal cross-sectional area, thus erroneous calculations of tissue properties result. The properties that could be deduced have the potential to provide understanding of fluid mechanics, peristaltic reflexes and kinematics of mechanoreceptors◊ among other useful items. The authors also claim that a better understanding of viscoelastic properties could lead to important discoveries relating to gastrointestinal diseases that are associated with growth and remodelling of the tissues. A comprehensive overview of the mathematics of pressure-volume relations within the small intestine is provided, which includes an in-depth modelling of the viscoelasticity of the tissue under such pressure conditions. Consideration is also given to the effect of clinical interventions, particularly the use of inflatable balloons, which will cause distension of the tissue.

Bellini et al. [72] conducted a similar study into the distensibility of the organ, but approached it from an experimental perspective. Planar biaxial tensile tests were conducted on pieces of porcine intestine to evaluate the planar stress-strain behaviour of the tissue. A Fung constitutive model that accurately replicated the behaviour of the intestine was then developed and was built into a 3-dimensional computer model. This model was then used to analyse the distension of the intestine during the passage of an endoscopy pill. This system was used to analyse the stress-strain effects on the intestine by the endoscopy pill. The use of detailed experimental testing involving measurement of key tissue dimensions is in agreement with the recommendations of Gregersen et al. [73], which call for correctly detailed examination of distensibility.

These discoveries and recommendations, however, do not examine the behaviour of the tissue *in vivo*, particularly under the action of intra-abdominal pressure. It is possible that the action of abdominal pressure or other movement of the abdomen could have a bearing on the findings. Additionally, the study by Bellini et al. [72] does not take into account possible abnormalities with the small intestine, or incarcerations, such as herniae.

The understanding of the mechanisms and the abdominal pressures required to initiate a hernia, and the state of the intestine during a hernia have not been studied. From an engineering perspective, a hernia is effectively the extrusion of the small intestine, or other structure, through a defect. There is no available data on the extrusion properties of the small intestine, nor how they behave in compression. The poor availability of data for these simple mechanical properties shows the limit of the investigations into the behaviour of the small intestine *in vivo*.

3.4. Herniae

A hernia is the protrusion of an organ, or part of an organ, through the wall of a cavity that normally contains it [26]. In the abdominal cavity, the ventral◊, lateral and dorsal◊ abdominal wall is the largest structure containing the contents of the abdomen. The cavity is also bounded superiorly◊ by the diaphragm and inferiorly by the pelvis. The most common type of internal hernia is a hiatus hernia [26], which is caused by the stomach slipping up through the diaphragm via the oesophageal hiatus. Herniation of the rest of the abdominal contents through the diaphragm is uncommon, mainly because a large portion of the diaphragm is in direct contact with the liver. Other types of herniae include inguinal herniae, umbilical◊ herniae and incisional herniae. Incisional herniae occur when part of the abdominal contents protrudes through an abdominal surgical scar, usually the result of a laparotomy and less frequently resulting from laparoscopy (Section 2.6). In a review of the socioeconomic aspects of hernia repair, Rutkow [76] reports that 360,000 ventral hernia repairs were conducted in the United States alone in 2003, with over 100,000 of these being incisional herniae, indicating the prevalence of incisional hernia. Luijendijk [77] further reports that one in five laparotomy patients will develop an incisional hernia and this could occur up to five years or more after the original laparotomy [29]. Interestingly, repair of these incisional herniae is often unsuccessful, with failure rates of up to 50% [77] if standard suture repairs are used. This concurs with the findings of Hollinsky et al. [63] who found that scar tissue is inherently weaker and thus will be more prone to rupture. Luijendijk et al. reported that more modern, tension-free repair techniques, such as the placement of a mesh, significantly reduce the reoccurrence of incisional herniae by approximately half.

Despite the minimal trauma caused by laparoscopic abdominal surgical techniques in comparison to laparotomies, incisional herniae are still prevalent post-laparoscopically, with reported rates of 1-3% [5, 6, 31, 32, 34, 37, 46, 78-84], as summarised in Table 3.2. While this may appear low, with over two million laparoscopic surgeries taking place in the U.S. alone each year [2], this represents over 60,000 cases of incisional hernia. If this is extrapolated to the whole world, it is evident that cases of incisional hernia pose a significant cost to health-care systems. Tonouchi et al. [7] conducted an extensive literature review into trocar site herniae. Seven reports were examined, referring to 59 cases of abdominal surgery. Of these cases, the incidence of trocar site hernia ranged from 0.65% to 2.8%, which correlates well with the findings of many authors (e.g. [32, 46]). Thirty individual case reports of trocar site herniae were also examined. Of these, 14 reported that the defect from the trocar site was left open, eight reported that it was closed and eight do not report. Tonouchi et al. believe this is a clear indication that leaving a fascial defect open is correlated with trocar site herniae. Kadar et al. [5] confirm this assertion in a review of incisional herniae in 10mm and 12mm trocar ports. An incidence of 0.23% and 3.1% was discovered for 10mm and 12mm ports respectively. They found that herniae are significantly more common if the fascial defect is left open, but also reported that three of five herniae identified at 12mm trocar site occurred after attempted closure of the trocar defect. Tonouchi et al. claim that insufficient closure of trocar defects may contribute to the development of some incisional herniae. Comajuncosas et al. [32] conducted a similar review of the literature and discovered an incidence of between 0.18% and 2.8%. The authors also note that the incidence is higher in obese patients. Montz et al. [84] conducted a large survey with 3,217 responses from surgeons detailing 4,385,000 procedures. Only 933 herniae are reported and of these, 167 occurred despite closure of the fascia defect.

There is some debate about the smallest port site that requires closure. Sanz-Lopez et al. [31] suggest that all defects larger than 5mm should be closed, although they also reported a patient presenting with a hernia at a 5mm port site, and claim that other authors have noticed the same, although no references are provided. Comajuncosas et al. [32] reported that over 80% of trocar site hernia occurred in defects greater than 10mm, however it is noted that a significant number of herniae also occur at sites less than 5mm. Closing of such defects in infants is of particular importance as their small intestine is proportionally

smaller than that of an adult, resulting in a greater risk of herniation [33]. Waldhaussen [33] also claims that 5mm ports are difficult to close due to difficulty accessing the fascia through the small hole. This claim is affirmed by Sanz-Lopez et al. who also cite obesity as impeding access. Obesity is also reported as a risk factor for developing incisional herniae post-operatively [6, 32, 85], most likely due to the difficulty of closing the defect in these individuals and the likelihood of increased IAP [38, 49].

Author	Port Size	$N_{procedures}$	Incidence of Hernia
Kadar et al. [5]	10mm	429	0.23%
Kadar et al. [5]	12mm	161	3.1%
Bowrey et al. [6]	10mm	320	3%
Boldo et al. [46]	10mm	27	22%
Helgstrand et al. [78]	Not Reported	7626	1.3%
Birdi et al. [79]	Not Reported	555	0.36%
Immè et al. [37]	10mm	150	2%
Coda et al. [82]	12mm	1287	1%
Duca et al. [83]	10mm	9542	0.18%
Nassar et al. [34]	5mm & 10mm	870	1.8%
Azurin et al. [80]	10mm	1300	0.77%
Sanz-Lopez et al. [31]	10mm	123	1.6%
Mayol et al. [81]	10mm	403	1.5%
Montz et al. [84]	Not Reported	4385000	0.00021%

Table 3.2 – Various reports of the incidence of trocar site herniae following laparoscopic surgery.

While there is much debate about the size of trocar defects that need to be closed, it is clear that closure of large defects is essential. For simplicity, a standard practice of closing all defects would be ideal, although this would not be possible using a direct visualisation method. A complete overview of the physiology of the incisional hernia can be found in Section 2.4.

3.5. Meshes

Prosthetic meshes (e.g. Figure 3.5), usually manufactured from nylon, polytetrafluoroethylene (PTFE) or polypropylene, among other materials, are commonly used in the repair of hernia defects [86-94]. The main purpose for their use is to permit tension-free repair of a defect in the abdominal wall. Using sutures to re-approximate the edges of a defect induces tensile loading in the stitches, which can increase the probability of failure [95]. A mesh simply covers the defect, prohibiting viscera from herniating and thus permitting natural healing of the defect. While mesh repair of traditional hernia defects is common, use of meshes to cover trocar holes and prevent incisional herniae has not yet been evaluated by large studies [12, 32]. As such, the majority of mesh analysis is from a traditional hernia repair point of view but it is still applicable to mesh use for trocar defects and serves as a suitable starting point for development of a trocar site mesh solution.

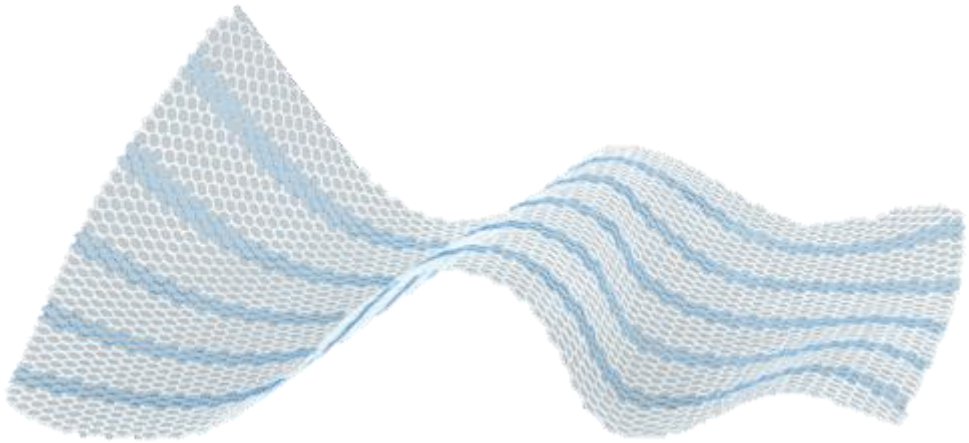

Figure 3.5 – Sample piece of polypropylene mesh manufactured by PFM Medical (Köln, Germany).

3.5.1. Mesh Techniques

Traditionally, hernia repair involved open abdominal surgery comprising re-approximation of the edges of the hernia defect and suturing the defect closed. The first reported hernia repair using a prosthetic mesh was by Usher et al. [96] in 1958. A number of studies have been conducted recently that compare the efficacy of traditional suture repairs to more modern mesh repairs, and all have found mesh repair to be superior. Pavlidis et al. [97] found that while operating time for meshes was longer, complication rate and recurrence rate was significantly lower and the time to return to normal life was shorter

than for suture repair. Similar findings are reported by Sauerland et al. [98] in a retrospective study of 446 patients, and by Burger et al. [95] in a clinical trial. Interestingly, Israelsson et al. [99] found mesh repair to be cheaper when time as an inpatient and on sick leave are taken into account. This study also reports a significantly higher recurrence rate after suture repair of the defect.

3.5.2. Mesh Fixation

Typically, meshes are fixed to the patient's abdominal wall by sutures, tacks or glue [100-102]. There is significant debate as to the best or most effective method of fixation. Being a long-standing, traditional operative method, sutures are the most obvious choice, however with advances in manufacturing, materials and laparoscopic medical devices, tacks have become a popular alternative. Similarly, fibrin glue◊ has been used extensively by some authors who strongly advocate its benefits [103]. There is also some discussion on the benefits or disadvantages of using absorbable fixators instead of permanent ones [104].

Descottes et al. [103] conducted a large prospective study examining the effectiveness of fibrin sealant and found it to be a particularly good alternative to tacks or sutures. Patient pain levels, recurrence of the hernia and the rate of other complications were all low. The results of their findings agree with the results of other authors who conducted randomised controlled trials on mesh fixation methods, including Lovisetto et al. [105] and Olmi et al. [106]. The non-traumatic nature of this fixation method seems to reduce the incidence of post-operative pain for patients. However, in a small study, Boldo et al. [107] found that while fibrin sealant has a lower rate of certain complications, it has a higher recurrence rate and costs more than traditional methods, although these findings were not statistically significant. Schwab et al. [108] reported that fibrin sealant results in less pain and is equally as effective as tack fixation, while Khaleal et al. [109] concluded that fibrin sealant should be the fixation of choice because of the associated reduced pain.

Most authors seem to agree that the use of tacks results in more long term post-operative pain than sutures, although short term post-operative pain is worse for sutures. Beldi et al. [102] conducted a small, yet clearly reported, randomised controlled trial comparing sutures and tacks, and concluded that short-term pain was worse for patients in the suture group. Nguyen et al. [110] found that pain for patients who underwent suture fixation was

higher initially, but long-term pain was greater for patients who underwent tack fixation. Interestingly, Bansal et al. [111] found that pain as a result of tack fixation is permanently worse than pain from sutures. Eriksen et al. [112] found patient reports of bad post-operative pain after tack fixation, but did not compare it to any other method and suggested that non-invasive closure, such as fibrin sealant, might reduce pain. Since pain is found to decrease with time, and ultimately becomes negligible for most patients, Nguyen et al. recommend that pain should only be a minor factor in deciding the post-operative closure method. Lepere et al. [113] investigated resorbable clips as a possible solution for minimizing long-term pain and found a low rate of complications, little pain and no recurrence of the hernia. However, there was no control in the trial and no comparison was made to any other closure method. Similarly, Byrd et al. [104] compared titanium tacks to resorbable tacks in pigs and found no difference in the efficacy of fixation between the two methods and also reported less adhesions in the resorbable tack group.

Some authors reported that meshes do not need to be fixed at all. Sajid et al. [114] and Tam et al. [115] reported that no mesh fixation is just as good as tack fixation. Both authors conducted a literature review of randomised clinical trials comparing tack fixation to mesh fixation. Tam et al. identified six studies while Sajid et al. identified eight (the same six as Tam et al., plus two more) and each came to the independent conclusion that tack fixation of a mesh statistically results in a similar amount of complications and recurrences. Similarly, Bell et al. [116] conclude that a 3-dimensional contoured mesh that follows the geometry of the abdomen does not need to be fixed to the abdominal wall.

3.5.3. Mesh Overlap

The amount by which a mesh overlaps the defect it is closing is an important factor when placing a mesh. Too little overlap can result in failure of the closure, while too much mesh is wasteful and may increase complications [15].

There have been no randomised controlled trials conducted on the optimum mesh size or mesh overlap for various defect sizes. Such a trial would be ethically difficult as some patients could be at a significantly greater risk of a hernia recurrence if the mesh used is too small, requiring them to undergo a revision surgery. There have been few laboratory or mathematical studies of mesh overlap [19, 20, 117].

Binnebosel et al. [19] conducted a study using a custom built rig where a number of mesh types and overlaps were investigated. There is no report of any validation of the rig, but the authors found that a mesh overlap of 3cm was sufficient to prevent mesh dislocation in most cases. Only a small number of defect sizes were examined in this study, and it is likely that for very small defects a 3cm overlap would be a significant over-estimation. Similarly, for a very large defect, it is probable that a 3cm overlap would be too small.

Mathematical calculations by Hollinsky et al. [20] indicate that the mesh overlap is dependent on defect size, as might be expected, with mesh size required to increase linearly with hole diameter. The authors recommend a mesh that is three times the diameter of the defect it is to repair, but consider friction as the only force resisting mesh dislocation and do not incorporate terms for tack or suture pull-out.

Aside from these few investigations, most literature on overlap recommends using a constant 50mm overlap on all defects, regardless of size [13, 15-18, 118, 119], while some recommend a larger overlap to be certain of no recurrences [14, 120] and others recommend a slightly smaller overlap [121-123].

Authors including Conze et al. [13], Sharma et al. [18], Schumpelick et al. [17], Phillips et al. [15] and Ponsky et al. [16] all reported on the efficacy of a 50mm overlap, mainly citing experience of low recurrence rates. Only Phillips et al. mention that there is no minimum overlap ratio reported in the literature. This use of 50mm is based purely on standard practice and has not been subject to investigation, though no other authors acknowledge this.

Schumpelick et al. [17] conducted a review of literature on overlap and hernia recurrence and presented evidence for using at least a 50mm overlap to reduce recurrence, but still reported incidences of recurrence up to 10%. Edwards et al. [14] instead used mesh overlap of up to 10cm in 27 patients and reported no recurrence. However, while a large overlap achieved the goal of eliminating recurrences, it is likely that there was significant waste of mesh with associated higher costs. Similarly, Amato et al. [120] used very large overlaps of up to 12cm and again reported no recurrence. The authors did not discuss mesh overlap as a factor, but rather aimed to maximise overlap in all cases.

Bay-Nielsen et al. [124], Carbonell et al. [125] and Stumpf et al. [126] all reported on the difficulties that can be encountered trying to achieve an optimum mesh overlap. Bone, tendons and other underlying structures can limit the overlap that can be achieved in some cases. The authors emphasise how it is important to place a mesh in such a way that avoids these complications where possible and to be aware of the increased risk associated with meshes that cannot avoid these structures.

In all of the literature, except the mathematical study by Hollinsky et al. [20] and the study by Phillips et al. [15], no authors refer to the importance of hole diameter in determining mesh size. This could be particularly dangerous in the repair of very large herniae where a 50mm overlap may not be sufficient, but also allows for an "over repair" of very small defects which could possibly be adequately closed by smaller meshes.

3.5.4. Mesh Complications

While the use of meshes is widespread, they are not without complications. The most common complication is mesh adhesion to the abdominal viscera. Other complications can include mesh migration or shrinkage, complications relating to the fixation method and mesh erosion into an organ.

3.5.4.1. Mesh Adhesion

Jenkins et al. [127] conducted a study of patients presenting for laparoscopy subsequent to a mesh hernia repair and examined the adhesion tenacity for different mesh types. It was discovered that adhesion-related complications are associated with the properties of the mesh, with an uncoated macroporous mesh having the most tenacious and prevalent adhesion formation and the DualMesh®[6] having the least prevalent and least tenacious adhesions. The DualMesh®, made of PTFE, is designed to have a textured surface to allow tissue ingrowth on its parietal[◊] side and a smooth surface to discourage adhesions on its visceral side. In a study on rabbits, Kiudelis et al. [128] also proved the efficacy of PTFE

[6]DualMesh® is a PTFE surgical mesh made by W. L. Gore and Associates (Newark, USA).

meshes concluding that Proceed®[7], a PTFE mesh also with a textured layer to allow ingrowth and a smooth bio-absorbable layer to prevent adhesions, was the best mesh to minimise adhesion formation. Similarly, both Amid et al. [129] and Borrazzo et al. [130] discovered that polypropylene meshes with a bio-absorbable coating result in fewer adhesions. It would appear, therefore, that it is the bio-absorbable coating or smooth layer, designed to minimise adhesions, that improves the efficacy of these meshes relative to others, although this does not seem to have been explicitly examined by any author.

The true incidence of adhesions can only be discovered by surgical examination, thus only patients that undergo revision or subsequent surgery can be positively identified to have adhesions. Chelala et al. [131] found that 53% of their re-operated patients had developed adhesions. Jenkins et al. found a higher rate of adhesions (64 – 100%), although the sample size for each mesh investigated was up to 90% smaller than that of the Chelala et al. study. Despite this high incidence of adhesions, they only become a problem if they begin to cause the patient pain or if further surgery is required. Nonetheless, a mesh that shows reduced incidence of adhesions would be favourable over other meshes to reduce the probability of adhesion-related problems.

3.5.4.2. Other Complications

There have been many case reports of complications around mesh repairs including mesh migration [86-90, 94], mesh erosion [91-93], mesh infection [132] and mesh rejection [133].

In a case study and subsequent review of the literature, Agrawal et al. [134] found that the choice of mesh type and shape, as well as the fixation method, influences mesh migration. In addition to causing pain and discomfort for the patient, mesh migration leaves the defect uncovered which may increase the probability of recurrence of the hernia. Lo et al. [135] made similar findings that correct fixation of the mesh and accurate mesh placement is essential to minimise migration.

Confounding the problem of migration is mesh dislocation, which was studied by Śmietański et al. [136]. The authors examined how the human abdominal wall moves with

[7]Proceed® is a PTFE surgical mesh made by Ethicon, Inc. (Somerville, USA).

body movement and discovered that during certain movements, the abdominal wall can stretch by up to 100%, requiring a mesh to double in size. However, this finding is somewhat questionable given the high reported stiffness of the abdominal wall by authors who conducted mechanical tests (Section 3.3.1). Nonetheless, this stretching of the mesh is likely to put significant loading on the tacks or sutures that are fixing the mesh in place and highlights the need for the mesh to have a similar stiffness to the tissues of the abdominal wall.

Infections are not as common as other complications. Hofbauer et al. [137] found an incidence of three in 500 (0.6%) and Taylor et al. [138] reported an incidence of just one in 1100 (0.09%). Thus it is evident that the incidence of mesh infection is low and most were treated with antibiotics or similar. Only two authors reported complete immunological rejection of the mesh by the patient [133, 137].

3.6. Conclusion

It is clear that while there is a good understanding of intra-abdominal pressure (IAP), there is a poor understanding of the effect that it has on the tissues of the abdominal wall. The structural properties of these tissues have been poorly defined in the literature and there is little agreement amongst authors. There is a demonstrable gap in knowledge between the understanding of the magnitude of IAP and the effect it has on surgical defects in the abdominal wall. It is clear that this gap needs to be bridged with a goal of understanding the fundamental behaviour of the abdominal wall, rather than its behaviour in relation to medical conditions or injuries.

It is also clear that there is a significant interest in the incidence of trocar site hernia (TSH) after laparoscopic surgery. Examples of studies from 13 authors were given that establish an average incidence of 2.75%. This clearly identifies the need for a more robust solution to wound closure after laparoscopic surgery as wound closure has been cited by many as the key risk factor in developing TSH.

Many authors investigating hernia repair, which is very closely related to the field of laparoscopy and involves injuries very similar to the defects created by laparoscopic trocars, have identified tension-free closure solutions as the state-of-the-art method for

repairing hernia defects. While meshes are not without their complications, and issues do still exist around fixation and adhesion, it is clear that mesh solutions are far superior to traditional suture based closure of hernia defects. However, there is still little literature on the idea mesh overlap for various defect sizes, with standard practice based on empirical evidence rather than scientific study of the engineering relationship.

4. Project Approach

It has been suggested previously that a mesh-based closure method for trocar◊ wounds created in laparoscopic surgery is effective in closing the wound and preventing development of a trocar site hernia◊ [12].

The overall aim of this study is to develop a rig to evaluate wound closure techniques for trocar wounds. A number of subprojects have been defined within this project, each of which will comprise a chapter of this thesis.

This project aims to develop tools to tests the hypothesis in a pre-clinical, laboratory setting. Thus no clinical trials of devices were conducted on animals or humans. Some animal tissue was used for mechanical testing to develop surrogate materials for use in the laboratory. Additionally, a small observational study of surgical patients was conducted in a hospital setting. Ethical approval was sought, as necessary, for these tasks.

A fundamental understanding of the intra-abdominal pressure environment is required to understand its role in the development of trocar site hernia and to reveal the implicated layers of the abdominal wall in advance of developing a surrogate. A simple mathematical analysis and associated anatomical and physiological discussion are presented in Chapter 5.

To facilitate laboratory testing in a clean, repeatable and controlled manner, a mechanical surrogate of the abdomen was designed to replicate the human abdominal environment. It was required to hold small intestine or a surrogate intestine material as well as an abdominal wall or surrogate. Application of a representation of intra-abdominal pressure should cause the small intestine to extrude through a defect in the abdominal wall. The design and operation of this rig is described in Chapter 6.

To simulate a hernia, the rig must contain a representation of the small intestine that can extrude thorough a defect in the abdominal wall. Porcine small intestine is easily attainable and have been reported to accurately replicate human tissue [139, 140]. However, as with all meat products, they deteriorate rapidly. A surrogate material was therefore developed

to replicate the extrusion properties of small intestine for the purpose of trial-and-error testing of prototype devices and techniques in the rig. Selection of this surrogate material is discussed in Chapter 7.

Similar to the small intestine, the use of a real abdominal wall also may not feasible for large-scale trial-and-error testing of closure solutions and a surrogate material is required. The rectus sheath was identified as the tissue of interest and detailed mechanical tests were conducted to evaluate its structural properties, which were not readily available in the literature. These mechanical tests are described in Chapter 8 and may lead to the development of a surrogate material in the future.

To evaluate the performance of the rig, a clinical study of the intra-abdominal pressure required to cause a hernia in a freshly created, open trocar site was conducted in St. Vincent's University Hospital, Dublin. This study is described in Chapter 9. The results permitted modification of the experimental rig to ensure that it accurately replicated the hernia development environment following laparoscopic surgery.

Finally, application of the surrogate abdomen to study mesh overlap requirements for defect closure and evaluate of the rig's performance as a pre-clinical testing environment was conducted and is described in Chapter 10.

5. Intra-Abdominal Pressure

5.1. Introduction

Intra-abdominal pressure (IAP) is a natural pressure within the abdominal cavity that exists because the abdominal cavity is a sealed compartment bordered by muscles. At rest, the abdomen has a positive pressure of 1-1.5kPa [39-41]. In ill patients, this can rise to 2-2.5kPa [42]. During strenuous exercise, IAP can rise to 20kPa, but this will not be sustained for long periods and will, most likely, not occur in patients recovering from surgery. The maximum pressures realised in these patients will most likely be due to coughing or vomiting which both result in an IAP of 11kPa [41, 52].

The role of intra-abdominal pressure in the loading of individual abdominal wall structures has not been published in the literature and it is not immediately clear which of the many layers of the abdominal wall are stressed at high IAP. Furthermore, while the magnitude of the stress in the abdominal wall as a whole has been estimated [57], it is expected that only some of the layers of the abdominal wall be loaded in most high IAP situations, and this has not been previously examined.

The aim of this chapter is, therefore, to examine the physiology of IAP generation and estimate the stress in tissues that would be under load in high and low IAP scenarios with the goal of identifying the key tissues implicated in hernia formation as a result of high IAP.

5.2. Generation of Intra-Abdominal Pressure

IAP is generated through the action of the diaphragm and the abdominal muscles. Typically, in an abdominal straining manoeuvre, the glottis◊ is closed and the muscles of the abdominal wall are tensed and rigid. The diaphragm contracts, causing it to descend and reduce the volume of the abdominal cavity. A certain amount of blood and other fluids is expelled from the abdominal cavity, however, due to blood pressure, not all of the blood can be expelled. Some of the gaseous content of the cavity can be compressed, but there is only, on average, about 115ml of gas in the abdominal cavity [141].

5.3. Approximation of the Volume of the Abdominal Cavity

Assuming that the abdominal cavity can be approximated as the shape of an elliptical hemi-cylinder, the volume can be calculated by estimating the relevant radii and length of the shape. Duez et al. [142] used computerised tomography (CT) to obtain images of the abdominal cavity and used computer software to measure distances within the cavity (Table 5.1, Figure 5.1). However, an unusual formula was used to calculate the volume as 5L (half the product of the three measured lengths). Instead, applying Equation 5.1 (volume of an elliptical hemi-cylinder) yields a volume of 7.9L.

$$\frac{1}{2} \times L \times \pi \times r_1 \times r_2 \qquad \text{Eqn. 5.1}$$

Talasz et al. [143] investigated the movement of the diaphragm and other abdominal muscles during breathing and coughing by examining MRI images of patients, and found that the diaphragm descends by approximately 30mm during coughing with an associated reduction in waist diameter of approximately 10mm. This agrees with a similar study by Reber et al. [144] who also investigated diaphragm movement during normal breathing. Since a larger IAP is generated during coughing than during normal breathing, the values from Talasz et al. are used for this analysis (Table 5.1). Applying Equation 5.1 using the Talasz dimensions gives a new, diminished volume of 6.4L.

	Rest [142]	Pre-Cough [143]
Length [mm]	341	304
R_1 [mm]	141	141
R_2 [mm]	104	94.5
Volume [L] (Equation 5.1)	7.9	6.4

Table 5.1 – Dimensions of the abdominal cavity, from [142] and [143].

Considering that there is only, on average, 115ml of gas in the abdomen [141], this indicates that an amount of blood must be expelled from the abdomen to reduce the volume from 7.9L to 6.4L (a reduction of 1.5L). Abdominal straining manoeuvres have been cited to reduce venous blood return to the heart and thus evoke a vagal reflex◊ resulting in a slowing of the pulse [43] which evidences the interaction between the generation of IAP and the vascular system.

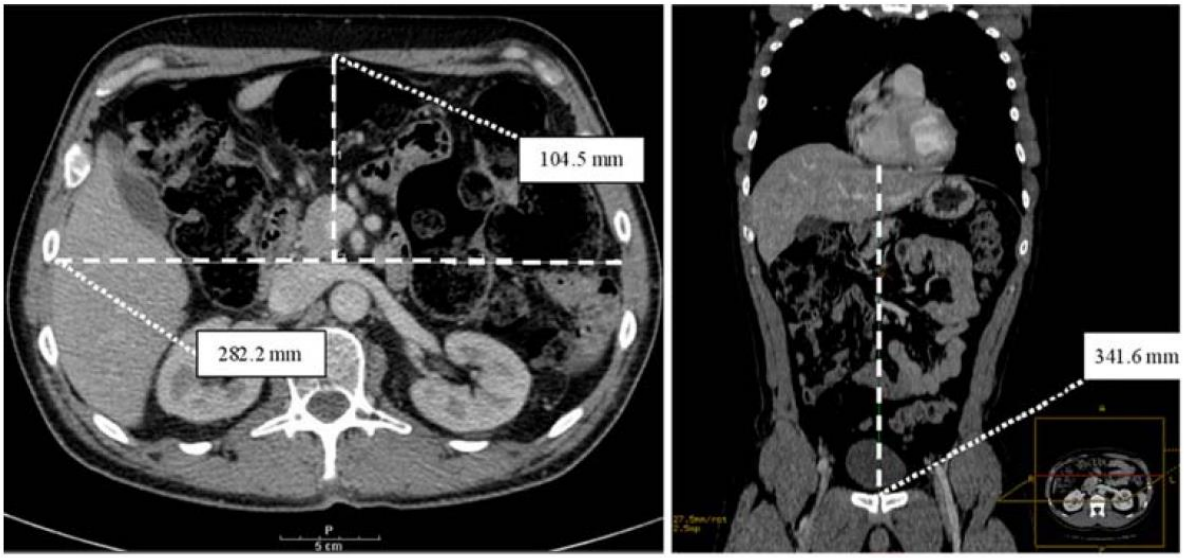

Figure 5.1 – Dimensions of the abdominal cavity, from [142].

If the abdomen was a completely sealed vessel containing an ideal gas, a reduction in volume of 1.5L (7.9L to 6.4L), or 19%, would, based on Boyle's Law (Equation 5.2), equate to a 19% increase in pressure. Given a resting IAP of 1kPa (Section 3.2) this would only generate an IAP of 1190Pa during a cough; significantly lower than the 11kPa reported by Cobb et al. [41]. However, with only 115ml of gas in the abdomen, a portion of blood must be expelled from the abdomen via the venous and arterial network to allow for the volume change. Central venous pressure is approximately 2kPa [145] but blood can only flow proximally due to the presence of valves. Diastolic arterial blood pressure is approximately 10.5kPa [146], thus to expel blood via the arterial network, the IAP must exceed 10.5kPa.

$$PV = k \qquad \text{Eqn. 5.2}$$

Overall, due to the complexity of the abdomen, and indeed the human body as a whole, it is quite difficult to accurately define the exact physiology behind the generation of high IAP. It is likely that a combination of factors is employed, including the compression of the small gas volume and the expulsion of an amount of blood through both the venous and arterial networks. This analysis, however, also highlights the possibility for variation of IAP between individuals. There are a number of variable factors involved, including the degree of muscle activation, the volume of gas in the abdomen, the venous and arterial blood pressures of the patient, as well as the BMI[◊] of the patient [38]. It is also likely that a supine

obese◊ patient will have a higher IAP than a supine person of normal BMI due to the weight force of central fat pressing on the abdominal cavity.

5.3.1. Thin Walled Pressure Vessel Formulation

Modelling the abdomen as a cylindrical pressure vessel, a thin walled pressure vessel assumption can be applied to understand the stress in the abdominal wall. An internal pressure within the abdominal cavity causes a stress in the abdominal wall. The abdominal cavity is bordered superiorly◊ by the diaphragm, which attaches to the ribs and spine and inferiorly◊ by the pelvis. Any loading in the craniocaudal◊ direction will (at least partially) be reacted by the spine, pelvis and legs.

In the passive case, when the patient is at rest, there is a static pressure within the abdomen of ≈1kPa [39, 42, 49]. The outward force caused by this pressure is resisted passively through tension in the fascia◊ and probably other layers of the abdomen. Laplace's equation for stress in the wall of a pressure vessel can be used to describe the stress in the abdominal wall (Equation 5.3). Using a radius of 200mm, a pressure of 1kPa and a thickness of 20mm [147] in this equation yields a hoop stress of approximately 10kPa at rest.

$$\sigma = \frac{Pr}{t} \qquad \text{Eqn. 5.3}$$

When the muscles of the abdomen are activated, they must first develop enough force to counteract this 10kPa tension force due to the static pressure within the abdomen. Upon relieving this tension, the contracting muscles will begin to reduce the volume of the abdominal cavity. Doing so will reduce the dorsoventral◊ radius of the 'cylindrical pressure chamber' which will result in increased IAP, as above. Subsequently, as the diaphragm contracts, the volume continues to reduce and the pressure continues to rise.

5.4. Discussion

5.4.1. Effects of Pressure on the Anatomy

Intra-abdominal pressure is generated by the combined action of the abdominal muscles, the diaphragm and the glottis. Leith et al. [44] provide a detailed description of the physiology of coughs by dividing a cough into four main stages; inspiration, compression,

expiration and cessation. It is mentioned that coughs vary quite considerably both between patients and within patients, depending on the reason for the cough. For the purposes of this study, the compression phase is of most interest as it is during this phase that IAP rises substantially.

After inspiration, the glottis closes and seals the inhaled air into the lungs. Simultaneously, the abdominal and thoracic muscles are activated forcefully. This causes both intra-abdominal and intra-thoracic pressures to rise. The compression phase lasts approximately 0.2s. The glottis is then voluntarily released and the diaphragm relaxes. The pressure difference between the atmosphere and the abdominothoracic cavity is equalised with rapid flow of air from the lungs.

As the forces in the abdominal wall during periods of raised IAP are not discussed in the literature, Sections 5.4.1.1 and 5.4.1.2 outline the loading of the various tissues. Due to the number of interacting layers and the various causes for raised IAP, it is likely that the stress environment is complex and varied. Therefore, in this discussion, two situations will be examined: a case of raised IAP with activation of the abdominal muscles and a case of raised IAP without activation of the abdominal muscles.

5.4.1.1. Activation of the Abdominal Muscles

Activation of the abdominal muscles can permit a particularly high IAP – up to 33.5kPa [41]. This pressure is created by using the abdominal muscles to brace the abdominal wall, resulting in an inner diameter of the abdominal cavity that is slightly smaller than the resting inner diameter of the cavity (Table 5.1). Subsequent contraction of the diaphragm considerably reduces the volume of the abdominal cavity, resulting in increased intra-abdominal pressure. Since contraction of the abdominal muscles reduces the circumference of the abdomen, it is expected that the *transversalis fascia* and peritoneum◊ will not be under tension. When the muscles contract, however, tensile forces will be generated at the insertions with tendons or aponeuroses, as these are in series with the muscles (Figure 5.2). Contraction of the internal and external oblique muscles and the *transversus abdominis* would therefore result in tension in the anterior◊ and posterior◊ rectus sheath, as well as in the *linea alba*. Defects in these layers, caused by abdominal surgery, would be opened by this tension. An IAP during coughing of 11kPa in an abdominal cavity of radius 200mm

and rectus sheath thickness of 2mm would result in a hoop stress in the rectus sheath of 1.1MPa (Equation 5.1). Associated IAP could cause structures within the abdominal cavity to push out through the defects, which had been opened by this tension in the rectus sheath causing a hernia◊.

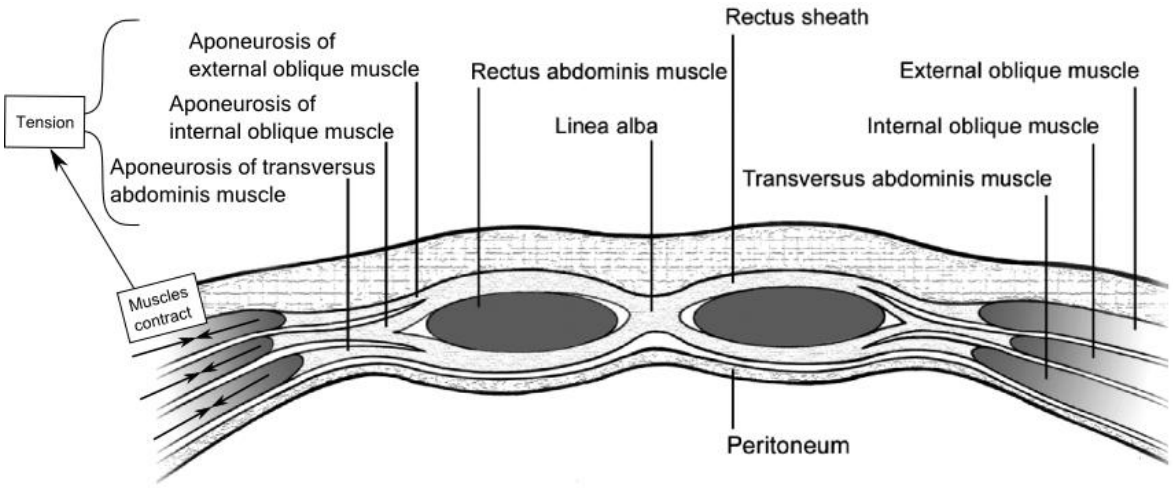

Figure 5.2 – Layers of the abdominal wall, adapted from [148].

Laterally◊, where there is no rectus sheath, it might also be possible for structures to extrude through the abdominal wall, but in this case it would most likely be due to defects or injuries caused to the muscle during surgery that limits its ability to effectively contract, thus leaving an opening for the formation of a hernia.

5.4.1.2. No Activation of the Abdominal Muscles

During normal quiet breathing the abdominal muscles are not activated [40]. Contraction of the diaphragm reduces the craniocaudal diameter of the abdominal cavity and, to maintain the volume and pressure of the cavity, the dorsoventral diameter increases. In a situation where the volume cannot be kept constant, e.g. the maximum dorsoventral diameter is reached, the pressure within the cavity will build. In this case, all of the layers of the abdominal wall, including the peritoneum, rectus sheath and *transversalis fascia* are likely to be under tensile loading because of the small IAP. This tension should not be particularly high, however, as reported variation in IAP during normal breathing is only 1kPa. As above, assuming a radius of 200mm and an abdominal wall thickness of 20mm, stress in the abdominal wall would only be of the order of 10kPa.

5.4.2. Limitations of the Assumptions

This analysis is based purely on verbal reports from surgeons and an engineering-oriented analysis of the structure of the abdominal wall. Experimental analysis of the loading scenario would be difficult, if not impossible, with current technology, as it would be necessary to install strain gauges on each individual layer of the abdominal wall and record the strain at various IAPs and muscle loading configurations. Nonetheless, at some point this information will be needed in order to clearly understand the exact interactions of the abdominal wall structures.

The skin and fat are not considered at all in this analysis. While this is considered as a suitable assumption due to the compliant and elastic nature of the skin and the very low toughness and strength of the fat, it is likely that both layers do have some impact on the loading scenario. In supine obese patients, the large layer of fat tissue will press downwards on the abdominal cavity and increase the pressure within the abdomen.

Biological variations in the thickness of the abdominal wall layers, or even in the tone of the abdominal muscles, could significantly affect the loading of the abdominal wall layers. These variations could be natural, or could be due to surgery or other co-morbidities as is frequently the case in obese patients.

5.5. Conclusions

The exact loading scenario of the abdominal wall layers during coughing, breathing and other movement is difficult to determine and it is likely that a number of loading conditions hold true for various scenarios. It is therefore hard to predict which layers of the abdomen will be in tension or will be unloaded in patients recovering from abdominal surgery who are likely to develop incisional hernia, however the above analysis suggests that the rectus sheath is likely to be under a stress of the order of 1MPa as a result of an IAP of 11kPa due to a cough.

Reports from patients suggest that the most common time of hernia formation is during strenuous use of the abdominal muscles such as during fits of coughing, straining for bowel movements or during heavy lifting, and this corroborates with the above analysis of the activation of abdominal muscles case.

To facilitate the design of a closure mechanism it is necessary to understand the anatomy of the abdominal wall clearly. However, due to the complexity of the wound healing scenario, it is not possible to develop a single clear description of how a hernia forms. It would seem that the most important layer to close after a laparoscopic surgery is the rectus sheath. It is crucial that this closure is effective and capable of withstanding significant tensile loading.

6. Surrogate Abdomen Rig Design

6.1. Introduction

During concept development, it is essential for a device to be rigorously tested to ensure that it conforms to expectation. This testing can take a number of forms, including finite element computer modelling, laboratory testing or pilot testing of the device in its intended application. Typically, medical devices will undergo detailed lab testing, subsequent animal trials and finally, human trials. Animal and human trials are expensive, complex and must adhere to detailed and strict ethical guidelines. To minimise the use of these trials it is often prudent to test the device in a laboratory setting – either using animal tissue from a butcher or using surrogate materials. Such tests permit repetitive trial-and-error testing in an easily controlled environment, allowing an iterative design process to take place.

Some authors have developed mechanical rigs, with attachments for animal tissue, that aim to replicate the *in vivo* environment for the tissue or physiology under investigation. For example, Schwab et al. [108] developed a rig to mimic intra-abdominal pressure for testing of mesh techniques in hernia◊ repair, and Podwojewski et al. [149] examined animal abdominal walls in a rig designed to mimic the natural environment of the abdominal wall.

Investigation of wound closure techniques requires iterative testing of prototype devices. For simplicity, this is most efficiently done in a laboratory using either surrogate materials or real animal tissues in a rig that mimics the *in vivo* abdominal environment. There are no commercially available solutions that are specifically designed to test abdominal closure methods and, at the same time, mimic the intra-abdominal pressure environment that causes complications after operative procedures.

6.2. Concept

A mechanical surrogate of the abdomen was envisaged to replicate the post-operative environment of the abdomen. It would contain small intestine (or a suitable surrogate material) which would be capable of herniating through a defect in an abdominal wall (or a suitable surrogate). Intra-abdominal pressure would be represented by a pressure

generation system which would have the effect of forcing the small intestine out through a defect in the surrogate abdominal wall. The rig would be small, lightweight and easy to operate.

6.3. Design

A rig was designed and built in the mechanical engineering workshop in Trinity College, Dublin. A rectangular box-shaped rig (200mm × 150mm) was designed to represent the abdominal cavity (Figure 6.1). This box would contain a strong, oversized balloon connected to a compressed air supply. Activation of the compressed air supply at a known pressure would fill the balloon with air which would subsequently apply pressure to the material sitting on top of it. As the balloon was oversized, there was no energy expended in stretching the walls of the balloon.

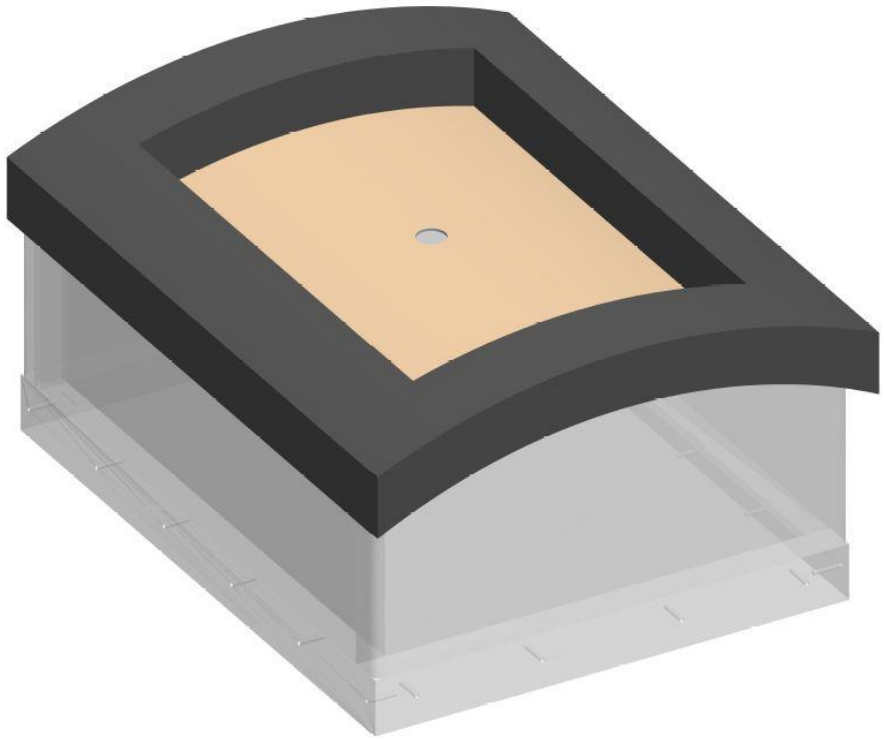

Figure 6.1 – Surrogate abdomen rig with a Perspex box to hold the balloon and small intestine and a curved lid to replicate the curvature of the abdominal wall.

To represent the circumferential curvature of the abdomen, the top of the rig was given a radius of curvature of 200mm [71]. Longitudinal curvature of the human abdomen was assumed to be infinite, thus no longitudinal curvature was applied. The lid of the rig was designed to have the same curvature as the base and to contain a large rectangular hole

(170mm × 120mm) in the middle, almost the same size as the rectangular box. This lid would hold the abdominal wall in place on top of the box containing the small intestine and the balloon. The lid was tightly affixed to the base using a cable and a system of pulleys to prevent slippage of the abdominal wall layer on application of pressure. The surfaces in contact with the abdominal wall were lined with a nutmeg grater (Figure 6.2) to improve gripping of the belly and prevent slippage under high pressure.

Figure 6.2 – Nutmeg grater.

A compressed air pipe network (Figure 6.3) was designed to allow accurate control of air pressure up to 20kPa in a way that would allow the pressure to be set on a regulator while the balloon was still isolated from the system. A dual regulator system was used to allow initial coarse pressure setting followed by more accurate fine adjustment on a precision regulator. A network of valves would permit the air entry into the balloon thus applying pressure to the contents of the rig. An exhaust valve could be activated to return the system to atmospheric conditions.

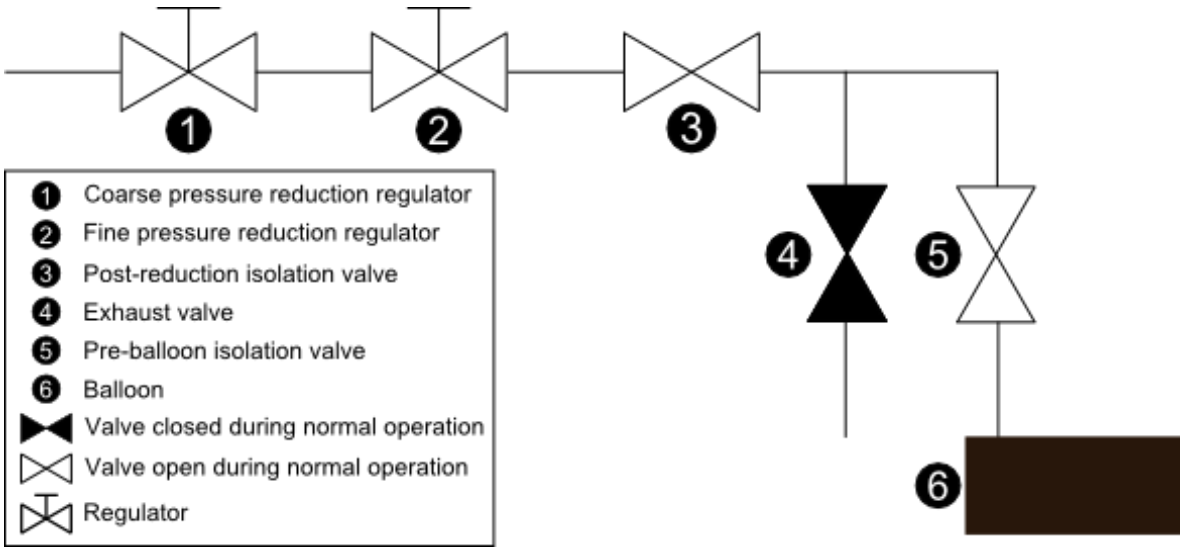

Figure 6.3 – Compressed air pipe network.

6.4. Operation

Set up and operation of the rig requires either real or surrogate materials for the abdominal wall and the small intestine. The following steps are followed for set up of the rig:

1. The balloon is fully deflated and inserted into the bottom of the rig with its air connection protruding through the tight fit hole in the base of the rig.
2. The rig is filled to capacity with intestine placed on top of the pressure balloon.
3. The abdominal wall is placed on top of the rig.
4. The lid is placed on top of the abdominal wall and secured to the base of the rig in a manner that will avoid slippage of the abdominal wall during testing.
5. The rig is placed in its stand and connected to the compressed air system.

The abdominal wall should contain a defect that will allow intestine material to extrude, replicating the formation of a hernia. The pressure is set and the valves are opened to apply this pressure, via the balloon, to the contents of the rig. Extrusion of the intestine, if applicable at that pressure, should be observed through the defect. Testing of closure methods can then be conducted by closing the defect and again applying the pressure to the system. No extrusion of small intestine at the maximum pressure would indicate the success of the closure method. Repeated tests can be conducted for statistical analysis, with some variability expected between samples, especially if using animal tissue.

6.5. Conclusion

The rig was constructed easily and operated as designed. A partial validation of its operation was conducted using data obtained from a study of real human intra-abdominal pressure (Chapter 9) and a preliminary study on mesh overlap was conducted as proof of the capabilities of the rig (Chapter 10).

7. Small Intestine

7.1. Introduction

Suitable surrogates to model biological tissues are needed for early-stage design and testing of wound closure devices. For physical modelling, materials ideally need to be clean, stable, replicable, cheap and reproduce the dominant mechanical characteristics of the native tissue. Physical models made from materials which satisfy these conditions provide a powerful platform for trial-and-error testing in the early stages of device assessment, prior to *in vivo* testing, which is increasingly resource intensive. Often it is neither possible nor necessary to replicate all properties of the native tissue, and engineering judgement is required to determine which aspects must be faithfully reproduced in the surrogate material. Differences between the surrogate material and the native tissue may sometimes be accounted for through a conversion factor.

To develop a surrogate abdomen environment to aid in the design of a tension-free wound closure method for post-operative defects in the abdominal wall, a surrogate to represent the small intestine must be found. However, limited data on the mechanical properties of the small intestine are available in the literature, and there appear to be none relevant to the behaviour of intestinal tissue during hernia◊ formation. As discussed in Chapter 3, some studies have been conducted on the tensile mechanical properties of human and animal small intestine [74, 75]. Bellini et al. [72] conducted biaxial tensile tests on porcine intestine and subsequently performed computational modelling to simulate the passage of endoscopy capsules through the small intestine. However, during incisional hernia formation, the small intestine is under a compressive load from the intra-abdominal pressure and intestine material is forced out through a small defect in the abdominal wall. This extrusion process is what needs to be replicated in the development of a surrogate abdomen for wound closure assessment. Accordingly, a surrogate material must have similar extrusion properties as the small intestine in the conditions experienced within the abdomen.

If a suitable surrogate intestine material can be identified, physical testing of wound closure methods can be achieved with greater biofidelity. Since the extrusion properties of small intestine are unreported to date, the extrusion properties of fresh cleaned and non-cleaned porcine small intestine were tested in an extrusion environment similar to the abdomen and a number of cheap and readily available surrogate materials were assessed for their capacity to mimic the observed extrusion behaviour of the biological tissue.

7.2. Methods

7.2.1. Custom Testing Rig Development

An extrusion rig, custom designed to conduct these tests (Figure 7.1 and Figure 7.2), was attached to a Zwick Roell Z005 machine (Zwick/Roell GmbH Ulm, Germany) in which a displacement-controlled compression could be applied. The rig incorporated:

1. An aluminium base with legs and a 55mm diameter hole to allow for similar extrusion pressures as experienced during abdominal muscle activity, as per [41].
2. A Perspex tube, inner diameter 55mm sitting flush on the aluminium base.
3. An aluminium plunger with a diameter of 54.5mm to allow for friction free movement.
4. A piece of 0.5mm thick silicone sheeting with a 13mm hole in the centre to simulate a 10mm trocar◊ hole with some enlargement due to operative manipulation.

The silicone sheeting was placed between the aluminium base and the Perspex tube. The Perspex tube was then pressed hard against the aluminium base and secured with cables so that the silicone could not slide. The Perspex tube was filled with material (Section 7.2.2) and the system was attached to the Zwick machine. Displacement-controlled crosshead movement was used to apply a force to the content of the tube and cause it to extrude through the 13mm hole in the silicone sheeting. Silicone sheeting was selected as it deforms slightly, thus creating a conical shaped channel for the extruded material, somewhat replicating the slightly compliant nature of the tensed abdominal wall.

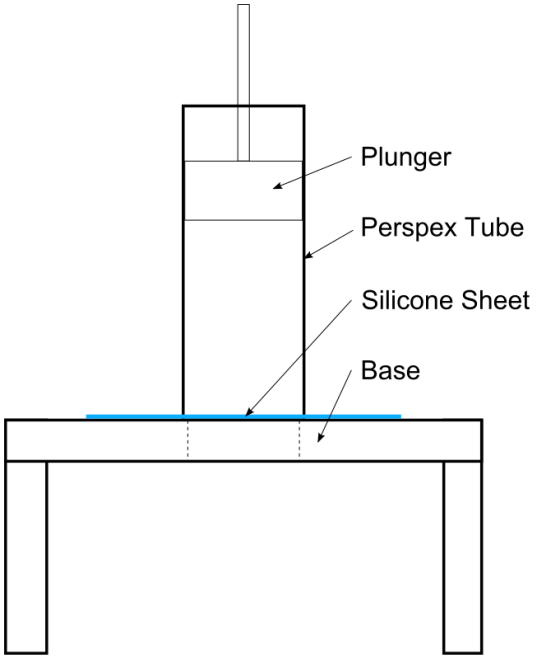

Figure 7.1 – Line drawing of the extrusion rig.

Figure 7.2 – Photograph of the extrusion rig.

7.2.2. Materials Tested

Tests were conducted on fresh non-cleaned small intestine, fresh cleaned small intestine, silicone gel, edible gelatine (jelly), dough (regular and oatmeal) and reconstituted powdered potatoes (RPP), see Table 7.1.

	Material	Number of Tests
1	Fresh non-cleaned small intestine.	3
2	Fresh cleaned small intestine	9
3	Silicone gel (EGel 3000, ACC Silicones, Bridgewater, England)	2
4	Edible gelatine (Chivers Brand, Premier Foods, Dublin)	2
5	Regular dough	9
6	Oatmeal dough	2
7	Reconstituted powdered potatoes (RPP) (Knorr Brand, Unilever, Dublin)	9

Table 7.1 – List of materials tested.

Non-cleaned small intestines were harvested from three month old female pigs and cleaned small intestines were sourced from a local abattoir. The non-cleaned fresh small intestines

were harvested in-house[8]. There was no washing and the mesenteries◊ were left intact. The cleaned small intestines were removed from slaughtered animals, washed inside and outside and the mesenteries were completely removed.

All other materials tested were composed of readily available food products. The regular dough mixture was composed of a combination of plain flour, tap water, table salt, sunflower oil and white wine vinegar (Table 7.2). The ingredients were mixed together in a saucepan on a low heat for 5-7 minutes until the dough was dry to touch. It was then kneaded for two minutes by hand.

Ingredient	Quantity
Plain Flour	40g
Tap Water	400ml
Table Salt	495g
Sunflower Oil	20ml
White wine vinegar	6ml

Table 7.2 – Regular dough ingredients.

Oatmeal dough was made from a mixture of rolled oats, plain flour and tap water. The flour and oats were mixed together and water was slowly added to the mixture and stirred in. Table 7.3 shows the ingredients and their quantities.

Ingredient	Quantity
Plain Flour	150g
Rolled Oats	110g
Tap Water	100ml

Table 7.3 – Oatmeal dough ingredients.

RPP was made using Knorr Powdered Mashed Potato (Unilever, Dublin) in a ratio of 5ml of tap water to 1g of powdered potato mixture.

[8] Ethical approval for the use of porcine small intestine from pigs slaughtered in the bio-resources department was granted by the Trinity College Ethics Committee.

Three samples of intestine, RPP and regular dough were tested at each extrusion rate (nine samples for each material in total). Only two samples of oatmeal dough, edible gelatine and silicone gel were tested, as the results were drastically different from small intestine. Three samples of non-cleaned small intestine were tested. These three samples were taken from a single three month old female pig. Samples were frozen until testing, defrosted at 4°C and tested at room temperature. The nine samples of cleaned small intestine were taken from one pig aged 26-28 weeks of unknown gender. Samples were frozen within four hours of harvesting, defrosted at 4°C prior to testing and tested at room temperature. Various regions of the small intestine were not distinguished for these tests.

7.2.3. Test Conditions

Crosshead movement rates of 7.5mm/min, 15mm/min and 30mm/min in the Zwick machine were used to investigate viscoelastic effects. These rates were chosen from a base rate of 7.5mm, which was considered significantly slower than any *in vivo* pressure generation, and was doubled for each test until the force required to extrude material exceeded the maximum force the machine could apply. Due to a strong odour, the fresh non-cleaned small intestine were only tested at 15mm/min for operator welfare reasons, which in itself is an argument for suitable surrogate intestine materials. Three tests were conducted on each of the other materials at the three rates listed above to test for repeatability. Room temperature during testing was constant at 20±1°C. Video recordings (Panasonic DMC-FT1, Panasonic, Osaka, Japan) were taken of each test to permit graphical analysis and force, crosshead displacement and time were recorded by the Zwick computer software.

7.2.4. Yield Strength Evaluation

In order to normalise the extrusion force and to account for the geometry of the system, the following equation was used to calculate the "yield strength" of the material. Although the equation assumes that the material is a continuous, incompressible solid, it does provide a measure of the pressure required to extrude the material regardless of the geometry of the system:

$$Y = \frac{P}{ln(R)} \qquad \text{Eqn. 7.1}$$

where Y is the yield strength of the material, P is the pressure applied, and R is the ratio of the initial diameter to the final diameter. This equation will be used to assess the yield strength of the materials tested.

7.3. Results

Preliminary evaluation showed that the silicone gel and the gelatine were wholly unsuitable as surrogate intestine materials (see Section 7.4 for more details). Therefore, no further results for silicone gel and gelatine will be presented. For the remainder of the data, a graphical comparison between the extrusion behaviour of the cleaned and non-cleaned small intestine is first presented. Following this, a graphical comparison between the extrusion behaviour of the cleaned small intestine compared to the dough and RPP is shown. Finally, the force versus extrusion behaviour of the cleaned small intestine, the dough and the RPP at different extrusion rates is given.

7.3.1. Graphical Comparison Between Cleaned and Non-Cleaned Small Intestine

Figure 7.3 shows a graphical comparison of the three tests at 15mm/min crosshead displacement with cleaned small intestine compared to the only test with non-cleaned small intestine (also at 15mm/min).

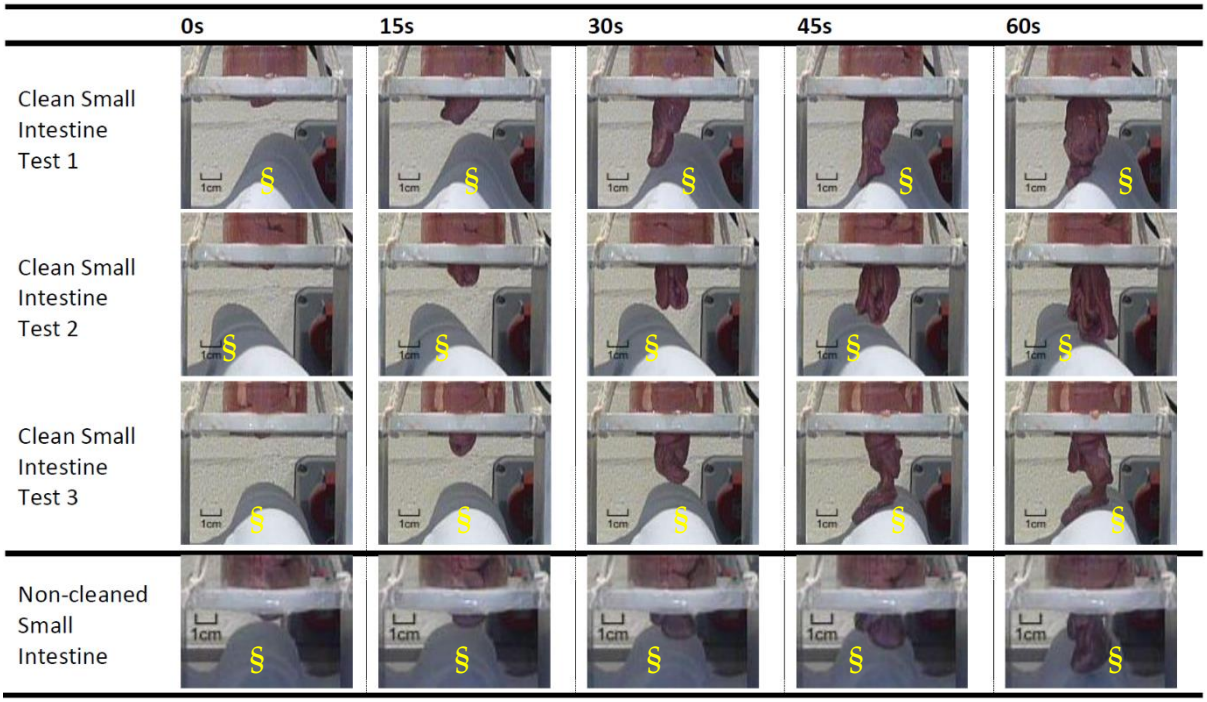

Figure 7.3 – Graphical comparison of cleaned and non-cleaned small intestine. The object marked with "§" is tissue paper to protect the machine from the biological samples.

7.3.2. Graphical Comparison Between Cleaned Small Intestine and Surrogate Materials

Figure 7.4 shows a graphical comparison of the extrusion properties of cleaned small intestine compared to dough and RPP at rates of 7.5mm/min, 15mm/min and 30mm/min. Images were taken at 60s for 7.5mm/min, 30s for 15mm/min and 15s for 30mm/min, thus the crosshead displacement in each image is constant at 7.5mm. For brevity, only graphical results from one test at each rate are shown. Oatmeal dough was similar to standard dough, but performed slightly worse, requiring a higher force; again, for brevity, the results are omitted.

Rate [mm/min]	Small Intestine	Dough	Reconstituted Powdered Potato
7.5	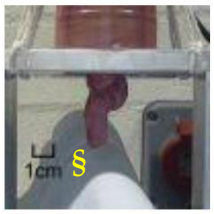	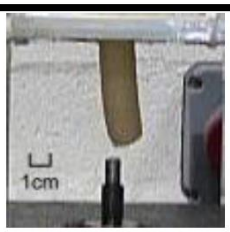	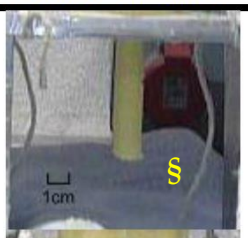
15	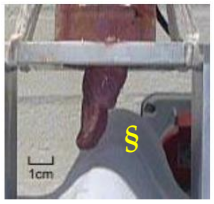		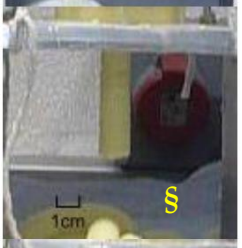
30	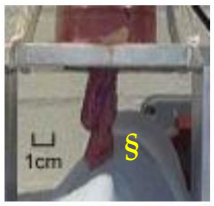	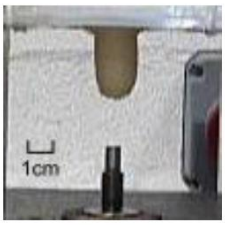	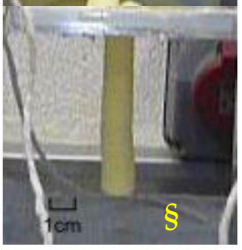

Figure 7.4 – Still captures from videos of extrusion tests at a crosshead displacement of 7.5mm. Object marked with "§" is tissue paper to protect the machine from the perisible samples.

7.3.3. Force-Extrusion Relationships

The average and standard deviation of the force exerted by the Zwick machine to achieve extrusion of the material is plotted against crosshead displacement for each extrusion rate in Figures 7.5, 7.6 and 7.7. Force-displacement curves are shown for cleaned small intestine, RPP and dough at each of the three rates. Table 7.4 shows the average extrusion force for each material at the different rates tested. This was obtained by averaging the force after

3mm of crosshead displacement to eliminate the ramp part of the force. Also detailed is the yield strength of the material, as derived from Equation 7.1.

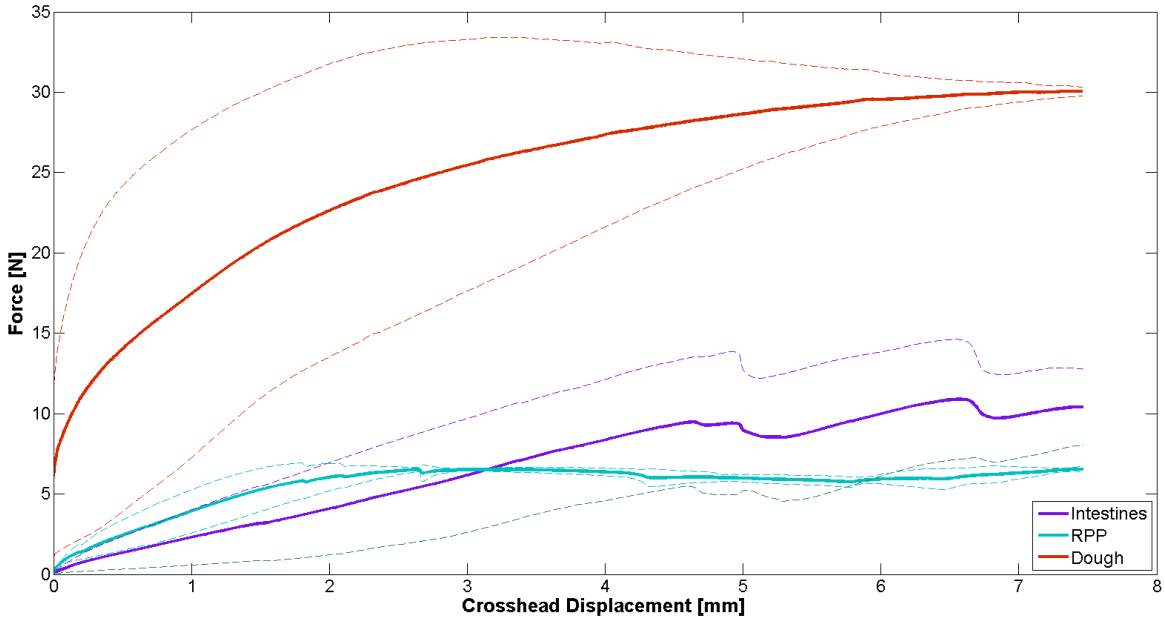

Figure 7.5 – Force-displacement curves for intestine, RPP and dough at 7.5mm/min showing average force-displacement curves +/- one standard deviation.

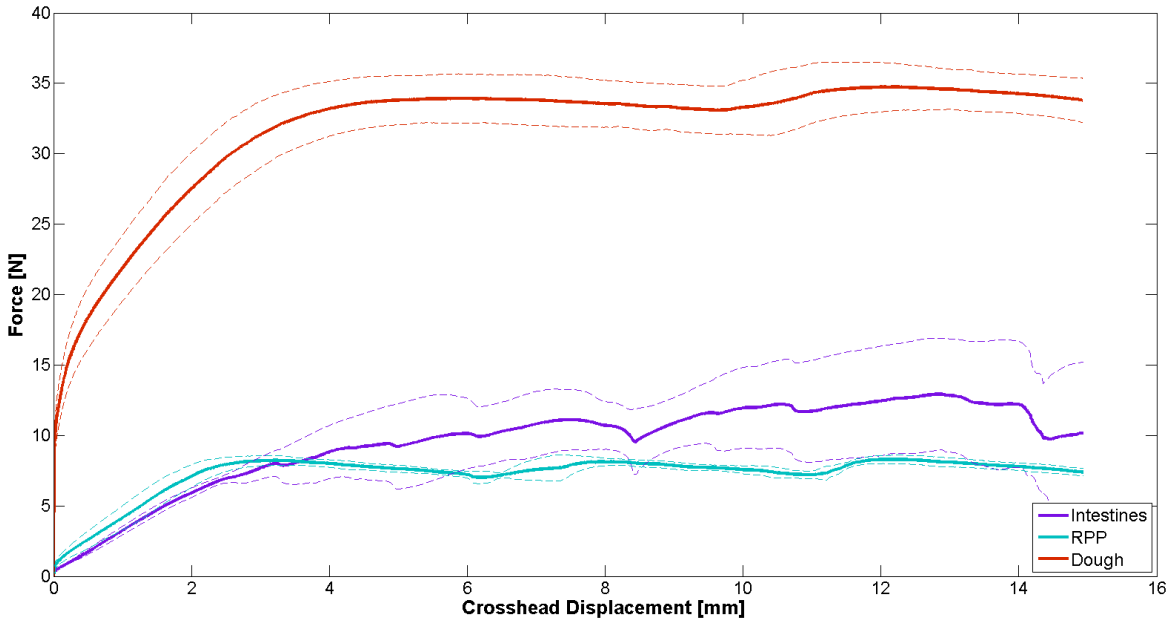

Figure 7.6 – Force-displacement curves for intestine, RPP and dough at 15mm/min showing average force-displacement curves +/- one standard deviation.

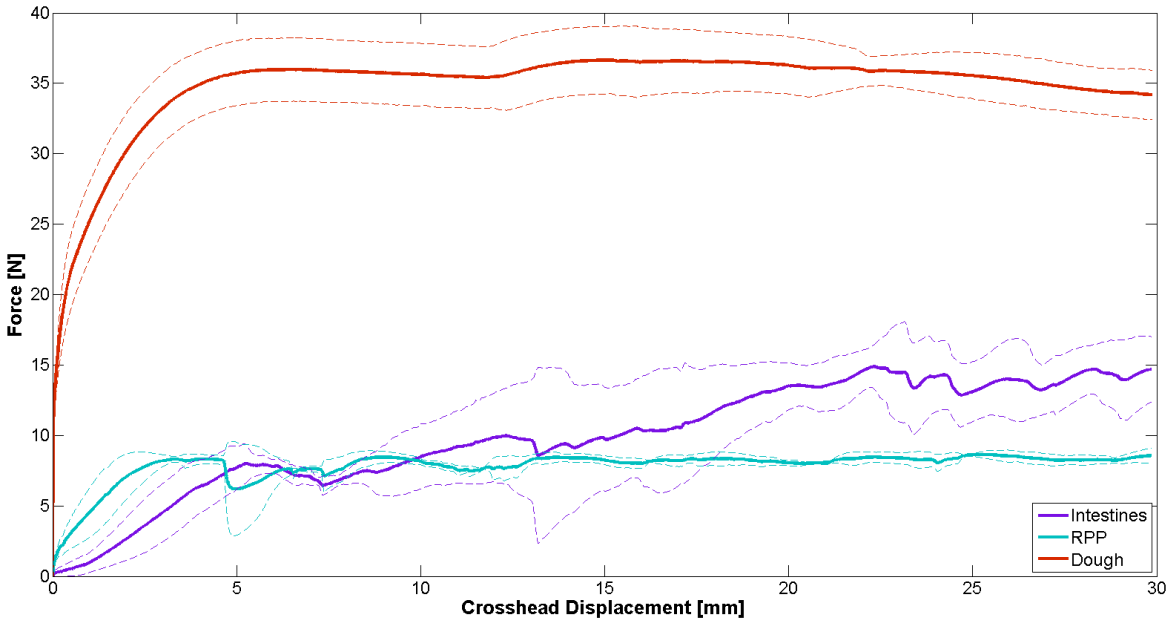

Figure 7.7 – Force-displacement curves for intestine, RPP and dough at 30mm/min showing average force-displacement curves +/- one standard deviation.

	Force [N]			Yield Strength [N/mm^2]		
	7.5mm/min	15mm/min	30mm/min	7.5mm/min	15mm/min	30mm/min
Dough	28.49 (3.43)	33.77 (1.75)	35.71 (2.02)	1310 (158)	1552 (80)	1642 (93)
RPP	6.16 (0.12)	7.77 (0.27)	8.1 (0.26)	283 (6)	357 (12)	372 (12)
Intestine	9.06 (3.54)	10.8 (2.61)	10.8 (2.01)	417 (163)	497 (120)	496 (92)

Table 7.4 – Average extrusion forces and material yield strengths for dough, RPP and small intestine at the three extrusion rates presented as mean (standard deviation).

A measure of the viscoelasticity of small intestine, RPP and dough is presented in Figure 7.8, Figure 7.9 and Figure 7.10, by showing the force-crosshead displacement curves for each of the three rates on one graph for each material.

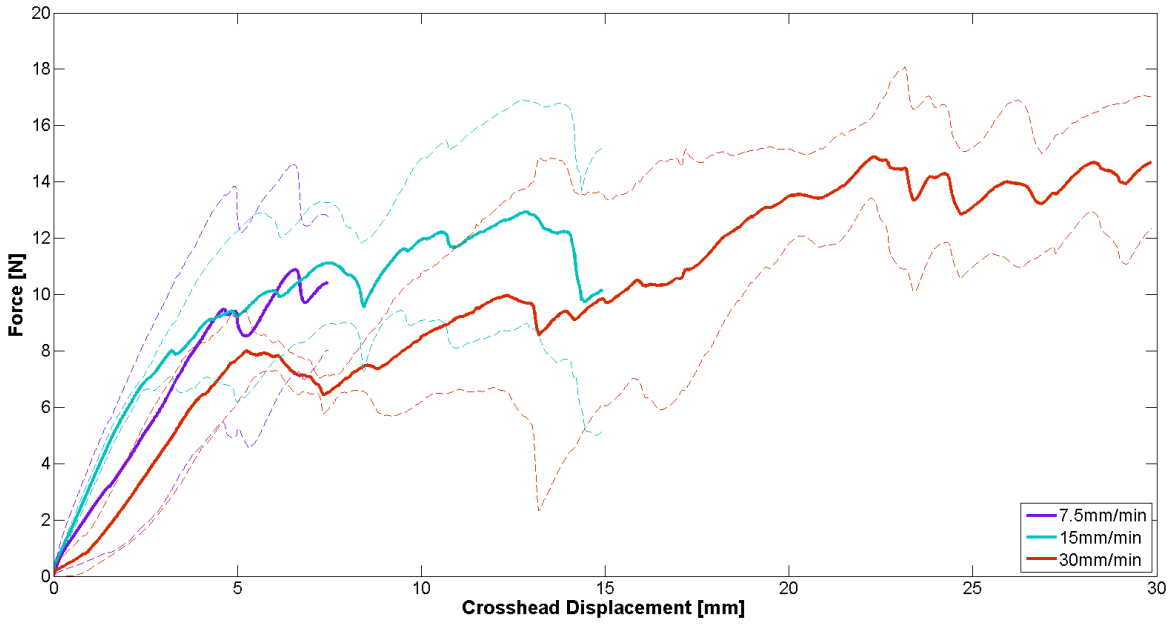

Figure 7.8 – Average force-displacement curves for small intestine at the three extrusion rates +/- one standard deviation.

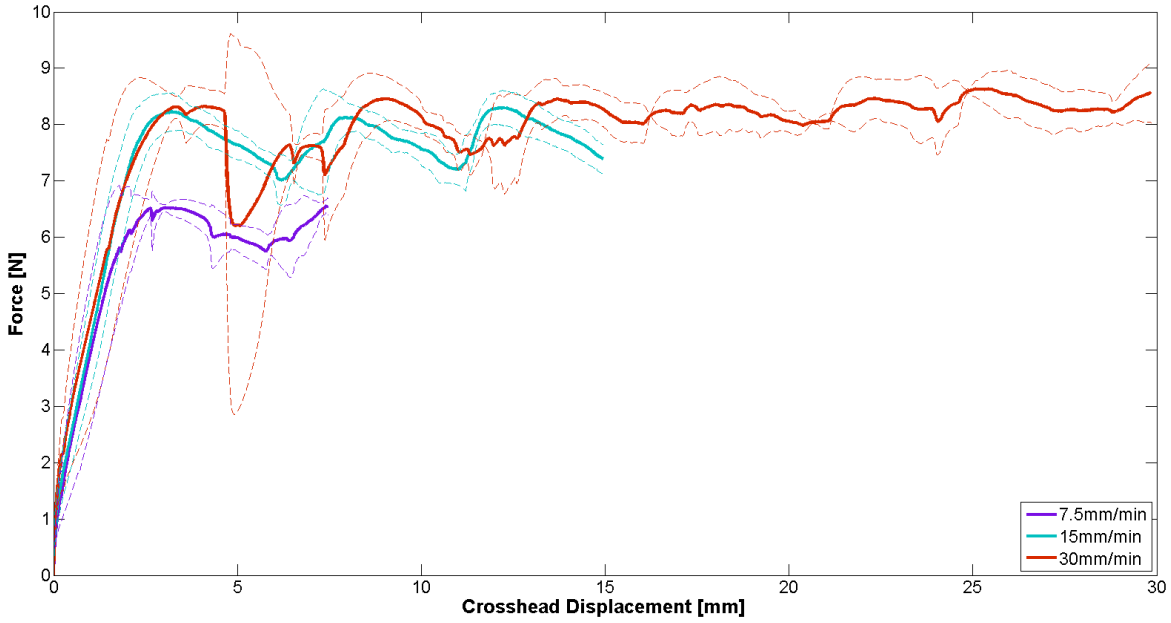

Figure 7.9 – Average force-displacement curves for RPP at the three extrusion rates +/- one standard deviation.

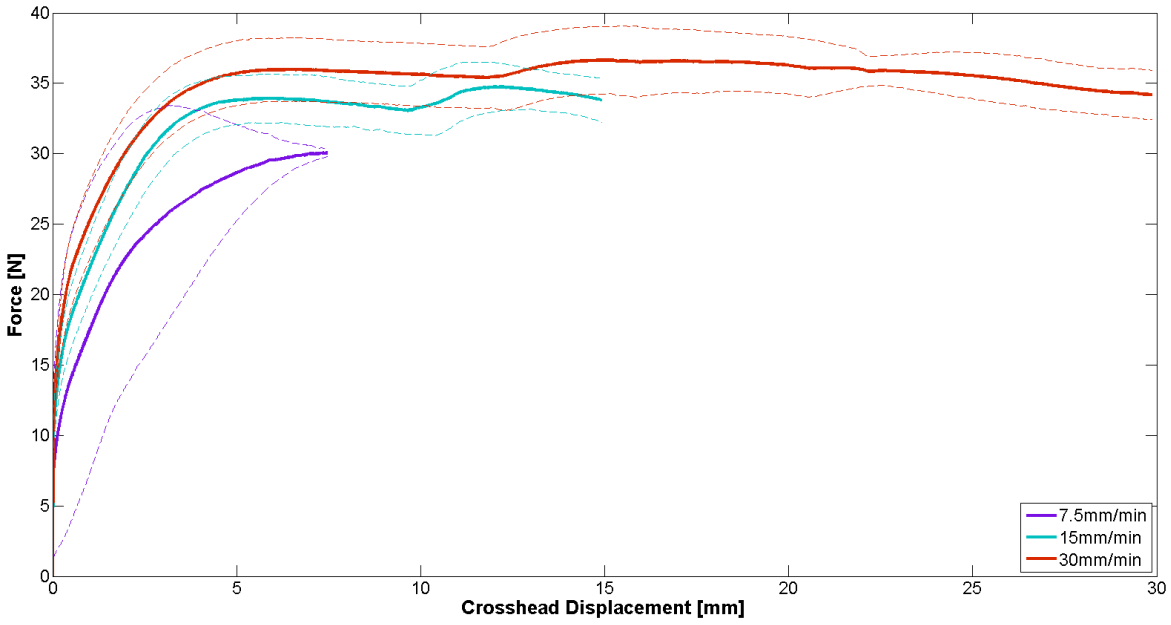

Figure 7.10 – Average force-displacement curves for dough at the three extrusion rates +/- one standard deviation.

7.4. Discussion

Comparison of the three tests using cleaned small intestine show some variability which is to be expected with biological tissue (Figure 7.3). However, Figure 7.3 also shows that the cleaning process had little effect on the extrusion behaviour of the small intestine. The amount extruded, particularly up to 30 seconds, is very similar and the shapes match well. The cleaned small intestine had the mesenteries removed, whereas the non-cleaned small intestine did not. At crosshead displacements exceeding 7.5mm, more cleaned intestine emerges than non-cleaned intestine and this is most likely due to the presence of mesentery on the non-cleaned small intestine. Given the highly unpleasant odour associated with the non-cleaned small intestine (to the extent that it was not possible to continue testing them), this is a very useful finding as it facilitates the use of cleaned small intestine if required. Nonetheless, since even cleaned intestine is an unstable material and subject to rapid decay, the requirement for a surrogate for mechanical testing remains obvious.

Preliminary tests on the surrogate materials indicated that the silicone gel and edible gelatine were wholly unsuited to be surrogate materials. The surface tension of the silicone gel resulted in a high friction contact with the Perspex tube of the extrusion rig and the

gelatine had a low shear strength and extruded at a low force, almost like a liquid. Similarly, oatmeal dough proved to be unsuitable due to its high shear strength.

Initial graphical comparisons between ordinary dough, reconstituted powdered potato (RPP) and cleaned small intestine showed similar extrusion properties for both dough and small intestine in this specific test environment. Figure 7.4 graphically shows a broad agreement between the amounts of dough and intestine extruded at 7.5mm of crosshead displacement for each rate, while the amount of RPP extruded is slightly more (mean difference of between 7% and 37%). However, this similarity is a reflection of the compressibility of the materials rather than their extrudability. In order to assess the extrusion properties, the force-crosshead displacement characteristics and the related yield strength are considered.

7.4.1. Yield Strength

Figures 7.5, 7.6 and 7.7 show that the dough requires approximately three to four times more force to extrude the same amount as the small intestine. In contrast, the RPP extrudes slightly more easily than intestine, with the force required for the RPP approximately 30% less than the force required for the small intestine. A surrogate intestine material should ideally be slightly more extrudable than the native tissue to give a margin of safety, suggesting that RPP would make a better surrogate material.

Table 7.4 details the average constant extrusion force for each material. This was obtained by averaging the force after 3mm of crosshead displacement to eliminate the ramp part of the test. However, simple evaluation of the force does not quantify the fundamental behaviour of the material as the force required will obviously be dependent on the geometry of the system. In the case of extrusion, it is useful to normalise the force over the area to which it is applied (pressure), but also to account for the size and shape of the orifice through which the material is being extruded. This normalisation is often formatted to give the yield strength of the material. For flow of a fluid, such as a Newtonian polymer melt flow, the yield strength is the product of the viscosity of the material and the shear strain rate. For the tests reported here, the viscosity of intestine is difficult to estimate as the material is not a liquid. Additionally, the tests conducted in this study were quasi-static, at a maximum rate of 30mm/min, resulting in a very low shear strain rate. An alternative

estimate of yield strength comes from the mechanics of extrusion of solids (Equation 7.1). While the components of this equation are readily available from the test reported here, the intestine is not a continuous solid. Nonetheless, Equation 7.1 provides a normalised form of the extrusion force for these experiments using the assumption that the material is an incompressible continuous solid, there is no external friction and that there is no die angle. This provides a more generic explanation of the findings of this paper, ignoring the effects of rig geometry and it is clear from Table 7.4 that, compared to the dough, the yield strength of RPP is much more similar to that of the small intestine. The yield strength of RPP is less than the yield strength of small intestine by about 30% on average. However, due to the intestine variability, a Student's t-test revealed no statistically significant difference between mean extrusion force, and hence yield strength, for RPP and small intestine at the 95% confidence interval for the rates tested, with *P*-values ranging between 0.14 and 0.3. In contrast, there was a statistical difference between the extrusion force, and hence yield strength, for dough and small intestine with *P* values ranging between 0.0001 and 0.002. These results reinforce the suitability of RPP as a surrogate intestine material for hernia modelling.

7.4.2. Variability

There was more variability in the amount of small intestine extruded compared to the amount of dough or RPP for the same test conditions. It was only possible to quantify the amount of RPP extruded up to a crosshead displacement of approximately 7.5mm, as after this point the extruded piece broke off. The variability with the small intestine is similar to that which is observed in most biological tissue, and is presumably related to local variations in structure and composition, though this was not tested. For a surrogate material, repeatability is generally a desirable characteristic, and this is evident from the low standard deviation for the RPP, see Table 7.4 and Figure 7.9.

7.5. Conclusions

Results show little difference between cleaned and non-cleaned specimens of porcine intestine. The tissue exhibits typical biological variability, but showed no clear viscoelasticity when extruded at rates between 7.5mm/min and 30mm/min. Evaluation of

potential surrogate materials to represent the extrusion properties of small intestine showed that silicone, gelatine and dough are unsuitable, but RPP exhibits very similar extrusion behaviour compared to fresh cleaned porcine small intestine at extrusion speeds between 7.5mm/min and 30mm/min. It is concluded that RPP is a clean, repeatable, cheap and suitable surrogate intestine material for physical ventral◊ hernia modelling.

8. Rectus Sheath

8.1. Introduction

The non-linear, viscoelastic nature of biological tissues makes their structural properties inherently difficult to classify, and thus it is difficult to select or develop surrogate materials to represent the tissues in physical models. Modelling for development of medical devices can be computer based [72, 150, 151] or done using physical tests [152, 153] or a combination of both. For all modelling techniques, some knowledge of the structural properties of the relevant biological tissues is required. Robustly developed models can provide a powerful platform for preliminary design and testing in advance of *in vitro* and *in vivo* testing.

This chapter presents a characterisation of the structural properties of the rectus sheath and follows the characterisation of the small intestine (Chapter 7) – the other tissue implicated in herniae◊. The rectus sheath (Section 2.2.2), a fibrous layer encompassing the *rectus abdominis* muscle, is often implicated in hernia formation and is the key tissue resisting high IAP (Chapter 5). There is limited data on the structural properties of this tissue with varying protocols and conflicting results [66, 68, 69]. Rath et al. [68] studied human rectus sheath in uniaxial tension but reported only maximum breaking stress and elongation and did not report on the deformation profile of the tissue which is necessary for generating accurate surrogate materials. Martins et al. [66] measured uniaxial stress-strain behaviour in human tissue in both fibre and cross-fibre directions but reported large scatter with stresses between 2.5MPa and 20MPa and failure stretches of up to 2.6, which seem doubtful. A number of statistical tests compared fibre and cross-fibre orientations, effects of BMI, gender etc. but the sample size in each case was quite small, limiting the statistical power of the tests. Ben Abdelounis et al. [69] recently examined the effect of various loading rates on the fibre direction response of human tissue in uniaxial tension. Unlike Rath et al. and Martins et al., the authors used an image-based method to measure the strain and address slippage at the tissue-grip interface, a phenomenon which may account for some of the findings of Martins et al. However, their sample size was small, with only three subjects included in the study in total.

It is clear that there is poor agreement between the limited amount of data in this field. The aim of this study was, therefore, to characterise the structural properties of the porcine rectus sheath with a view to understanding the behaviour of the tissue under loading from intra-abdominal pressure.

8.2. Methods

Twenty porcine abdominal walls were sourced from a local pig abattoir. All pigs were aged 26-28 weeks old and all females were nulligravid. Animals were slaughtered and dissected in the abattoir as per their standard procedures where the abdominal walls were harvested and frozen pending collection. They were subsequently kept frozen at -20°C until testing in the laboratory. Prior to testing, abdominal walls were defrosted at 5°C±1°C for 40 hours.

8.2.1. Uniaxial Tests

8.2.1.1. Sample Preparation

Abdominal walls were dissected to isolate the anterior◊ rectus sheath. The tissue was immediately placed in Phosphate Buffered Saline (PBS) solution to prevent it from drying out. Fat and muscle were meticulously removed from the samples.

Tissue was dissected into fibre direction and cross-fibre direction specimens (Figure 8.1). Due to the significant anatomical variations between animals and the crude method of dissection of the abdominal wall from the pig carcass, standardised specimen sizes were not practical. Instead, rectangular specimens between 12 and 20mm wide and between 16 and 66mm long were cut. Samples were labelled and stored in PBS until immediately prior to tensile testing. Sixteen fibre direction and sixteen cross-fibre direction samples were tested in total.

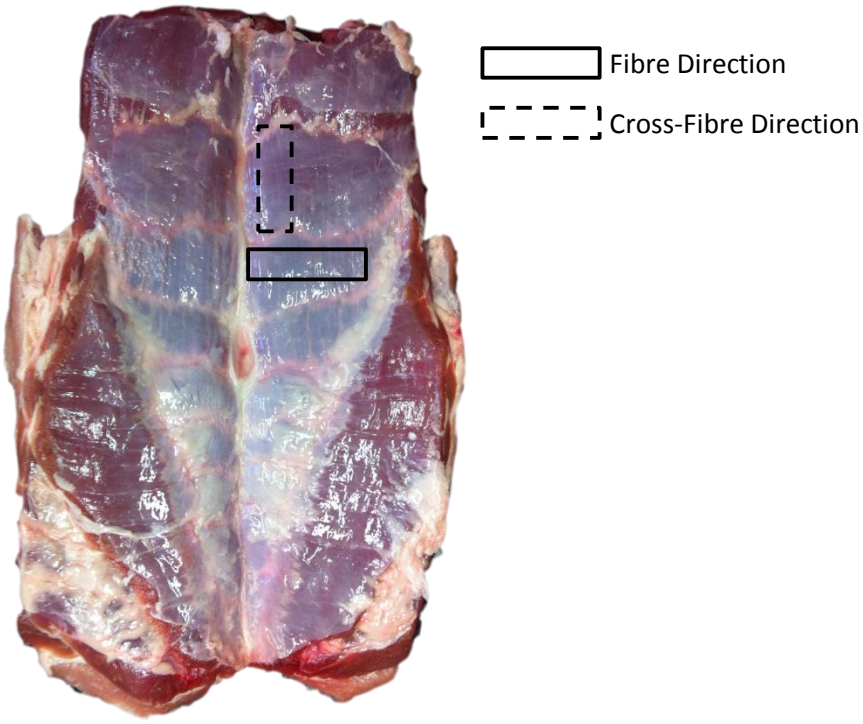

Figure 8.1 – Posterior◊ view of a porcine belly showing the fibre and cross-fibre directions.

8.2.1.2. Testing

A jig was employed to improve alignment of specimens in the grips (Figure 8.2a). Grips were covered in grade P60 sandpaper to improve gripping. To prevent tissue damage during gripping and ensure continuity across tests, grip bolts were tightened using a torque wrench to 0.2Nm which was found empirically to minimise both slippage (grips too loose) and tissue damage (grips too tight).

The width, thickness and mass of each sample was recorded prior to gripping. After gripping, the grip-to-grip distance (characteristic length) of the tissue was measured and recorded. A grid of six dots was applied to the centre of the sample for graphical analysis of the strain (Figure 8.2b). Samples were tested under displacement-controlled uniaxial tensile loading in a Zwick Roell Z005 machine (Zwick/Roell GmbH Ulm, Germany). A preload equal to the weight of the sample was applied and the post-preload grip-to-grip separation was recorded by the machine for strain analysis. Samples were stretched under controlled displacement at a rate of 10% of the characteristic length per minute to avoid any viscoelastic effects. Samples were stretched until failure (>20% drop in the force applied).

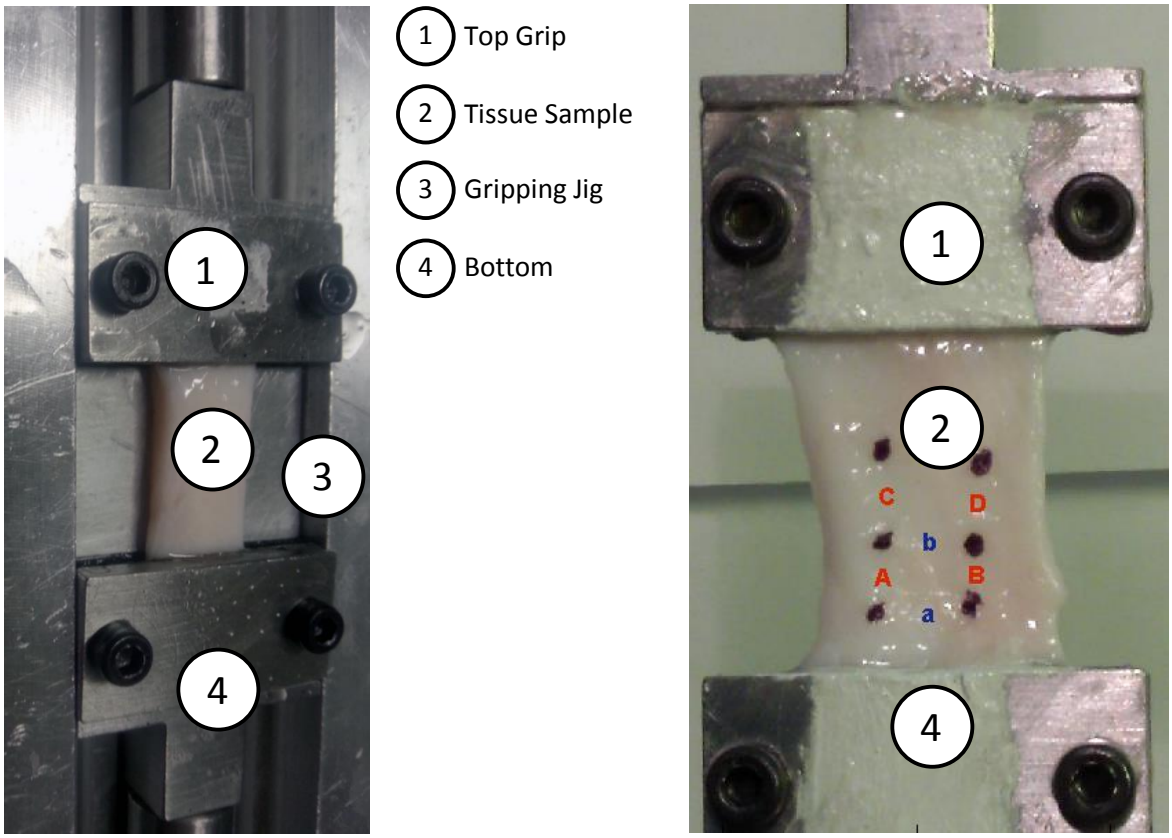

(a) (b)

Figure 8.2 – (a) Gripping jig and (b) gripped sample in the Zwick machine.

Throughout the test, a high definition Samsung HMX-QF20 camera (Samsung Electronics Co., Gyeonggi-Do, Korea) was used to record the motion of the dots by capturing an image of the sample at two frames per second.

8.2.1.3. Results Analysis

Custom Matlab code, used previously by Takaza et al. [67] was used to analyse the motion of the dots as recorded by the high definition camera. The code identified and tracked the vertical and horizontal motion of the dots. This permitted analysis of intra-specimen strain variation between pairs of dots, as well as global stretch through an average calculation of the motion of each of the dots. Engineering stress was calculated from the applied force and the original cross-sectional area. A time history of the stress applied to the tissue was imported from the Zwick data file and plotted against the graphically determined stretch to achieve a stress-stretch plot for each sample tested.

An average stress-stretch plot that would represent the average of each of the response curves, and maintain the same overall shape for fibre and cross-fibre direction samples was generated as follows:

1. Each curve was divided into the same predetermined number of discrete points.
2. Points were numbered from one to n, with shorter curves having a higher density of points.
3. The stress and stretch at each point was averaged over all of the curves in a particular direction.

An additional 0.1MPa preload to reduce the scatter in the results was applied to overcome challenges in identifying the unstrained sample length. This preload represents only 2-5% of the maximum stress applied to the samples.

8.2.2. Biaxial Tests

8.2.2.1. Sample Preparation

As with the uniaxial tests, the abdominal walls were dissected to isolate the anterior rectus sheath. The tissue was immediately placed in Phosphate Buffered Saline (PBS) solution to prevent it from drying out. Again, fat and muscle were meticulously removed from the samples.

A custom bladed punch was used to cut square samples 39.5mm × 39.5mm. Samples were labelled and stored in PBS until testing. A custom gripping jig was used to ensure equal placement of four fish hooks along each edge of the sample. Hooks were spaced at 11mm intervals along each edge (Figures 8.3 and 8.4) to ensure equal distribution of the force throughout the sample.

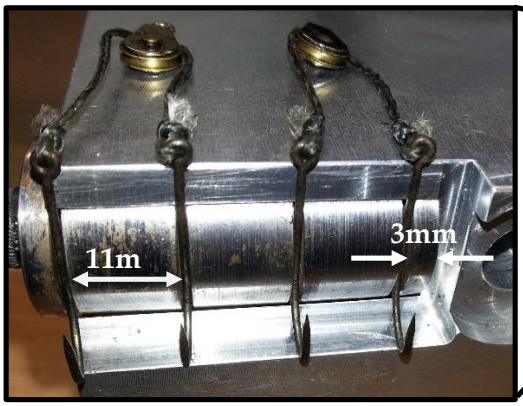

Figure 8.3 – One edge of the gripping jig with hooks.

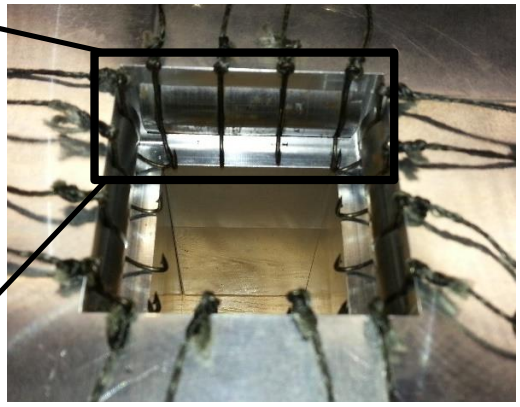

Figure 8.4 – Complete biaxial gripping jig.

8.2.2.2. Testing

A custom designed equi-force biaxial testing rig [154] (Figure 8.5) was used to apply equal tensile force to each of the four sides of the square specimen using a simple wire and pulley system connected to a Zwick Roell Z005 (Zwick/Roell GmbH Ulm, Germany) testing machine. With the sample connected to the rig, a pre-load was applied to straighten the sample out and lift if off the base of the rig (approx. 3N). By running an inked toothbrush over a sieve, a speckled pattern of black drawing ink was applied to the tissue for subsequent digital image correlation (Figure 8.6). Images were recorded on a high definition camera Samsung HMX-QF20 camera (Samsung Electronics Co., Gyeonggi-Do, Korea) at a frame rate of 2fps.

Samples were subject to displacement-controlled tension via the Zwick machine, but the biaxial testing rig allowed for anisotropic stretching of the material while maintaining an equal force on each hook. Thus, the force applied was determined by the stiffness of the fibre direction (stiffer) while the direction of largest strain in the tissue was the cross-fibre direction (more compliant).

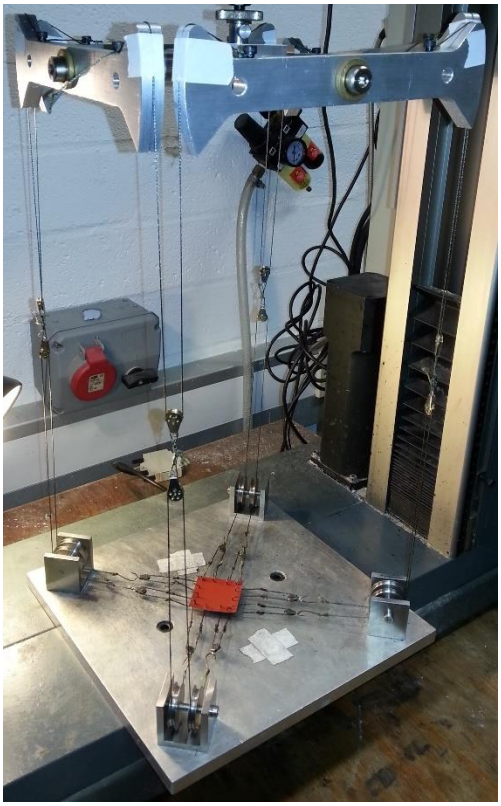

Figure 8.5 – Equi-force biaxial testing rig.

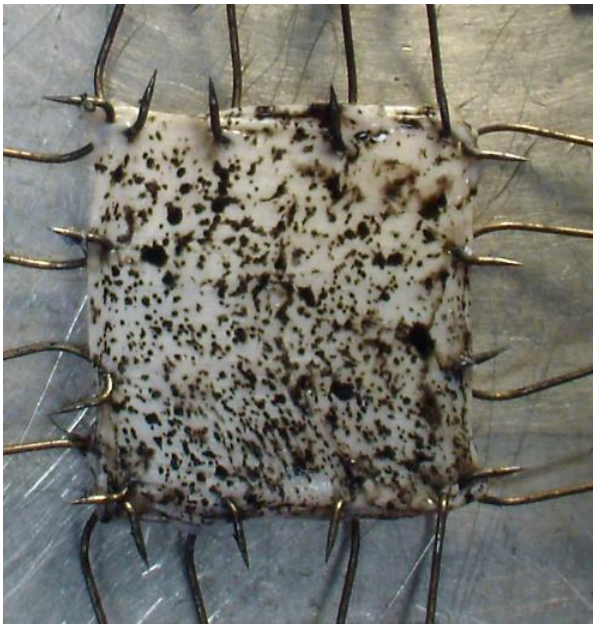

Figure 8.6 – Sample under equi-force biaxial tension.

8.2.2.3. Results Analysis

Digital Image Correlation (DIC) was conducted using freely available Matlab code [155] (see Section 8.4 for validation). This method of strain analysis was used as the fishing twine strained under loading and the fish hooks sometimes caused significant local deformation of the tissue while leaving corner regions unstressed. Force measurements were recorded by the Zwick machine. Average stress-stretch plots were created for the fibre and cross-fibre directions in the same way as for uniaxial samples (Section 8.2.1.3).

8.2.3. Statistical Methods

Time history control charts with 3σ limits were used to ensure there was no time bias affecting the results (operator experience, etc.). Normal probability plots were generated for the stretch and stress at failure to ensure the assumption of normality applied. ANOVAs were generated to ensure that the variation between each run of tests (pig belly) was not significantly different from the within group variation (i.e. that the variation between pig bellies was not significantly different from samples within each belly). A Student's t-test

was conducted to compare the stress-stretch response of fibre and cross-fibre direction specimens.

8.2.4. Computational Modelling

Computational modelling of the uniaxial and biaxial tests was conducted using FeBio [156] to assess the ability of a fibre-reinforced hyper-elastic model to reproduce the observed experimental results and to assess the effect of gripping the sample on its stress state at the end of the test.

A first-order Ogden model represented the tissue matrix and an exponential power law represented the fibres [157], with the following strain energies (Ψ):

Ogden:

$$\Psi = \sum_{i=1}^{N} \frac{c_i}{m_i^2}\left(\lambda_1^{\widetilde{m}_i} + \lambda_2^{\widetilde{m}_i} + \lambda_3^{\widetilde{m}_i} - 3\right) + U(J) \qquad \text{Eqn. 8.1}$$

where λ_x are the deviatoric stretches, c and m are material constants and $U(J)$ represents the volumetric component, where J is the determinant of the deformation gradient tensor. The volumetric component is computed based on the bulk modulus.

Exponential Power Law:

$$\Psi = \frac{\xi}{\alpha\beta}\left(e^{\alpha(\tilde{I}_n - 1)^{\beta}} - 1\right) \qquad \text{Eqn. 8.2}$$

where α, β are material constants and ξ is a measure of the fibre modulus and $\tilde{I}_n$ is the square of the fibre stretch.

A custom Matlab code, used previously by Takaza et al. [158] was employed to find the optimum material properties to represent each sample in both the fibre and cross-fibre directions. In the cross-fibre direction, the fibres are not under any loading, thus the experimental results from these tests were used to optimise the Ogden model parameters for each of the 16 samples. These parameters were then averaged and used for the fibre direction optimisation, which used an uncoupled combination of a first-order Ogden model, representing the matrix and an exponential fibre law representing the fibres. The

Matlab optimisation algorithm, in both cases, interacted with FeBio to minimize the sum of squared difference between the experimental force displacement data and the FeBio force displacement data.

Two uniaxial simulations were conducted for each of the fibre and cross-fibre directions to assess the influence of gripping on the mid-sample stress-stretch relationship. Ideal geometries, matching the average geometries of fibre and cross-fibre direction specimens respectively, were created and meshed using 3,200 hexahedral elements. Simple uniaxial tension (without gripping) was first applied at a rate of 10% of specimen length per minute, similar to the physical tests and the stress-stretch response of an element at the centre was exported. In a second simulation, gripping of the tissue was simulated prior to uniaxial tension. Gripping simulation was achieved by applying equal compression of 20% to both sides of the specimen in the region under the grips. The final configuration after gripping was taken as the initial condition for subsequent uniaxial tension. Again, tension was applied at a rate of 10% of the specimen length per minute and the stress-stretch response of the same element was exported for comparison purposes.

A biaxial simulation was then conducted using the average material parameters from the individual simulations of each of the uniaxial tests and the results were compared to the average experimental biaxial results.

8.3. Results

8.3.1. Uniaxial

Figures 8.7 to 8.10 show typical uniaxial fibre and cross-fibre direction results of stretch against time. “Vertical stretch” is the stretch response of the tissue in the direction of the applied load and “horizontal stretch” is the corresponding lateral contraction of the tissue in the direction orthogonal to the load. Plots show stretch as calculated from tracking dots.

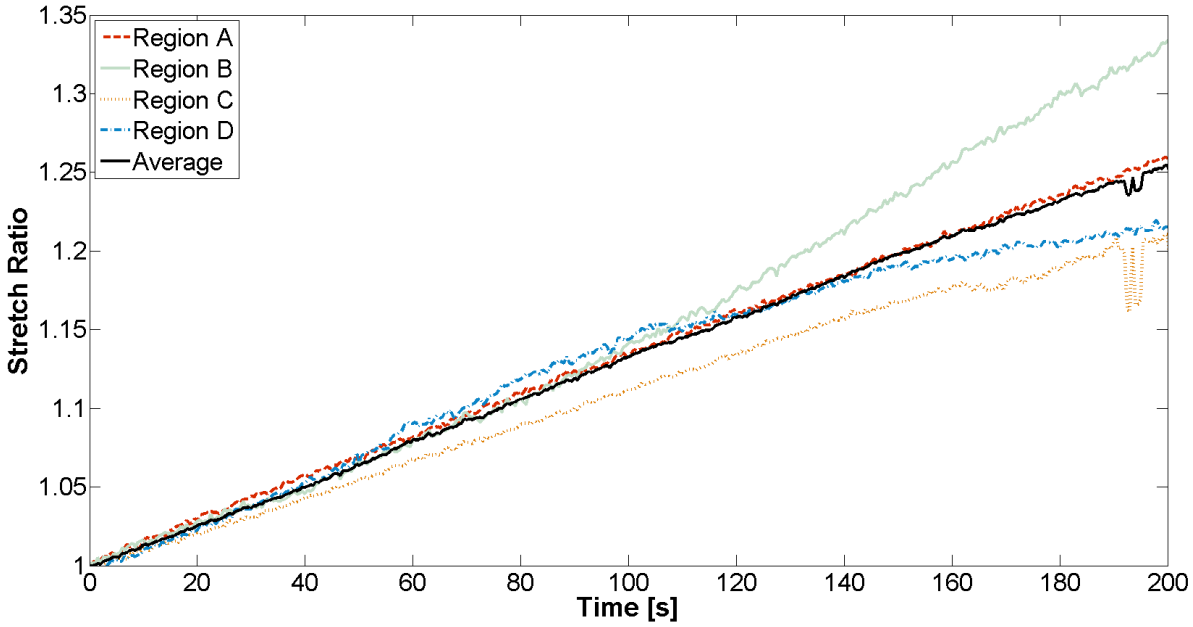

Figure 8.7 – Vertical stretch in the individual regions of a cross-fibre direction sample plotted against time.

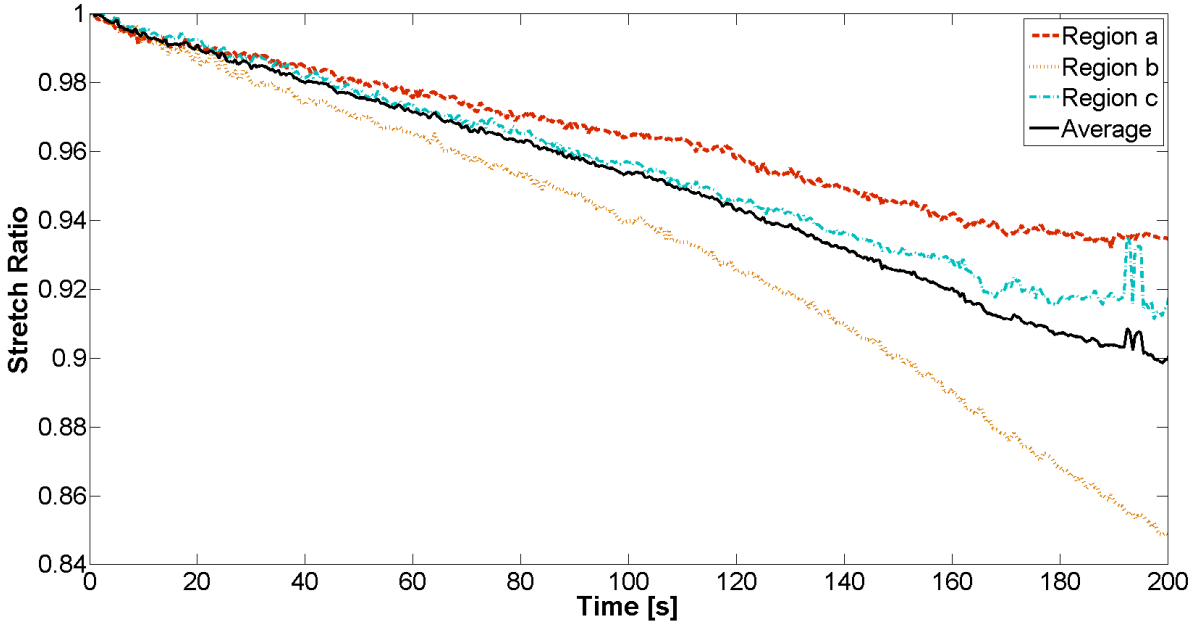

Figure 8.8 – Horizontal stretch in the individual regions of a cross-fibre direction sample plotted against time.

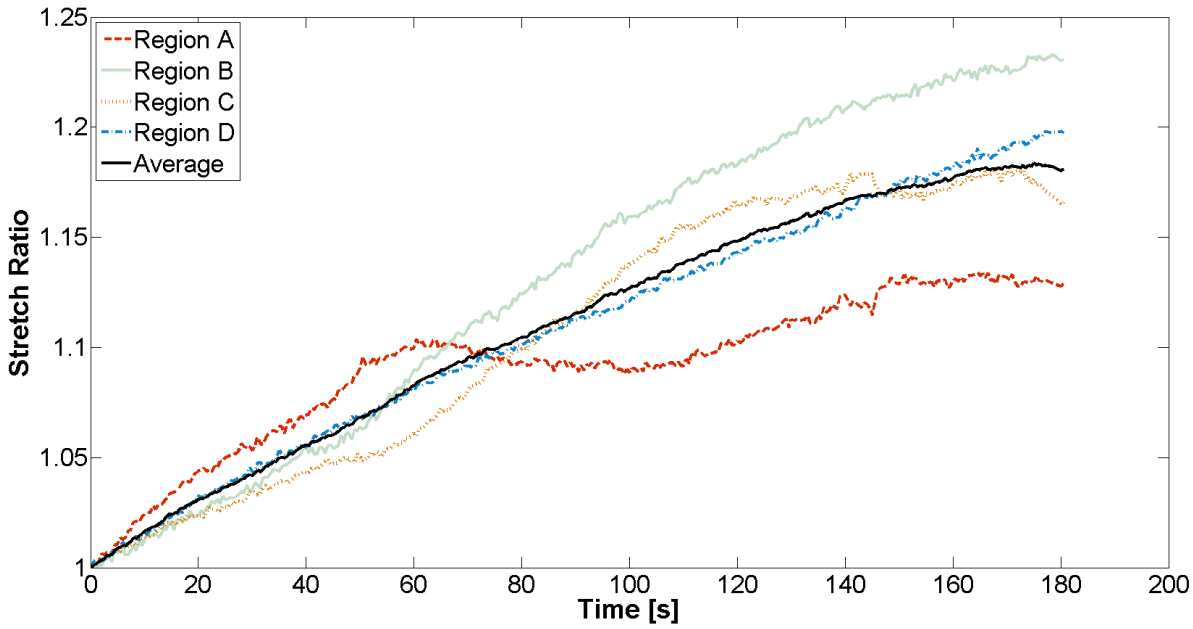

Figure 8.9 – Vertical stretch in the individual regions of a fibre direction sample plotted against time.

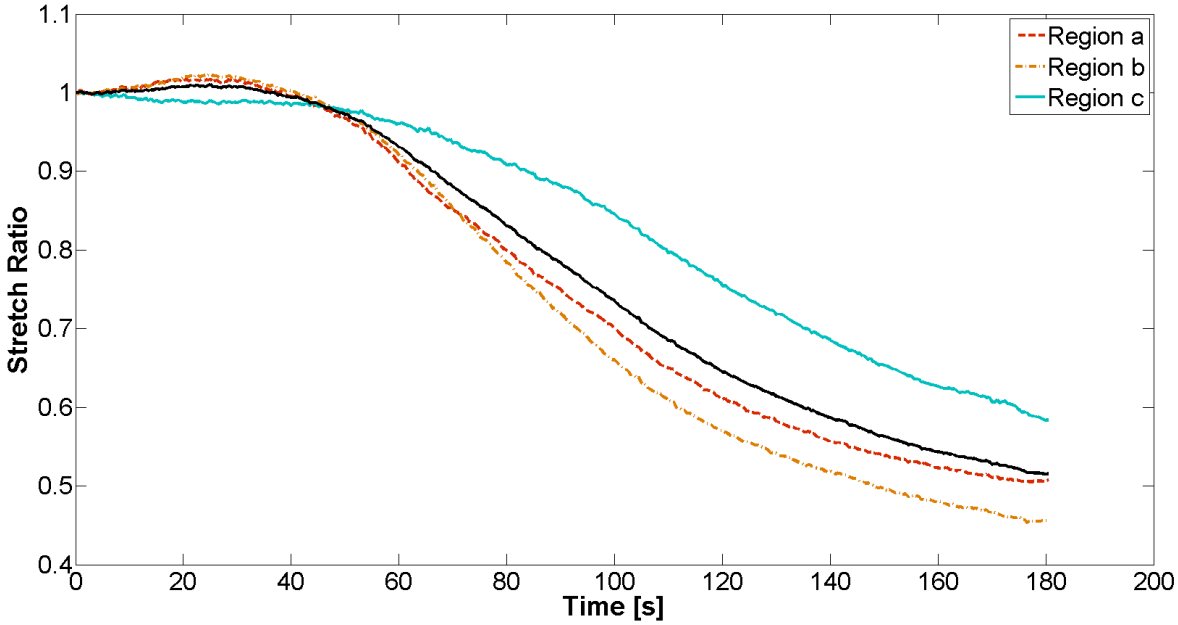

Figure 8.10 – Horizontal stretch in the individual regions of a fibre direction sample plotted against time.

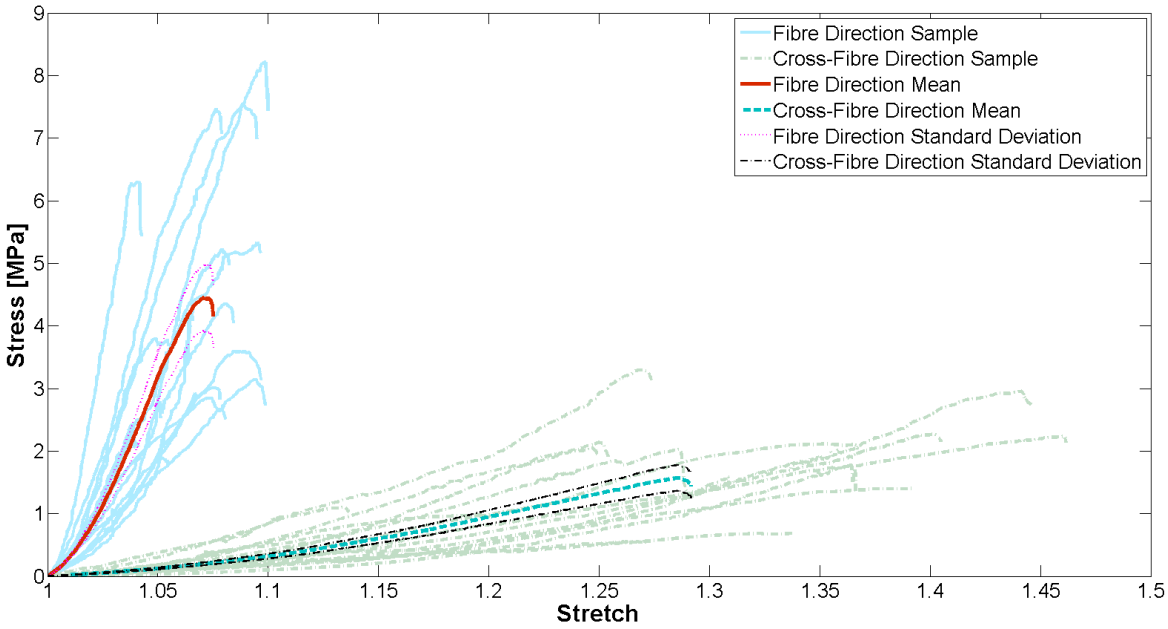

Figure 8.11 – Stress-stretch plots for fibre and cross-fibre direction samples.

8.3.2. Biaxial

Figures 8.12 and 8.13 show raw displacement for a fibre direction and a cross-fibre direction sample respectively. Raw displacement was obtained from Digital Image Correlation analysis of a video recording of the test. Figure 8.14 shows stress-stretch results from each of the 14 biaxial tensile tests and an average stress-stretch curve for both the fibre and cross-fibre directions, obtained using the method outlined in Section 8.2.1.3.

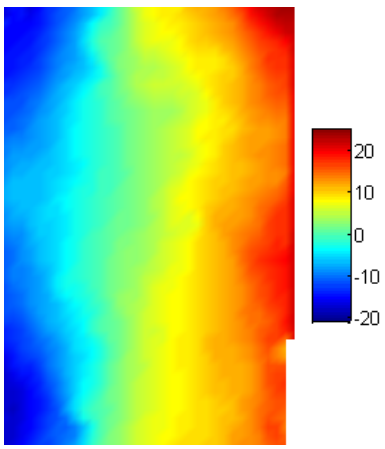

Figure 8.12 – Typical fibre direction sample raw displacement as recorded by DIC code.

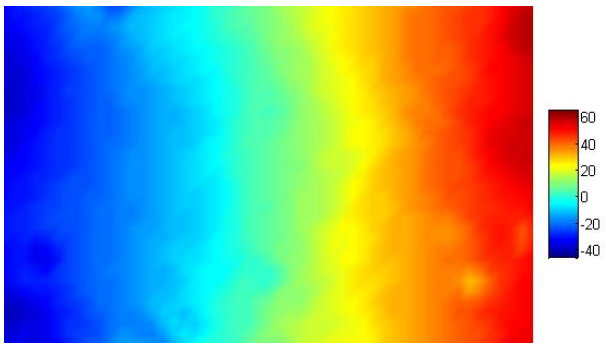

Figure 8.13 – Typical cross-fibre direction sample raw displacement as recorded by DIC code.

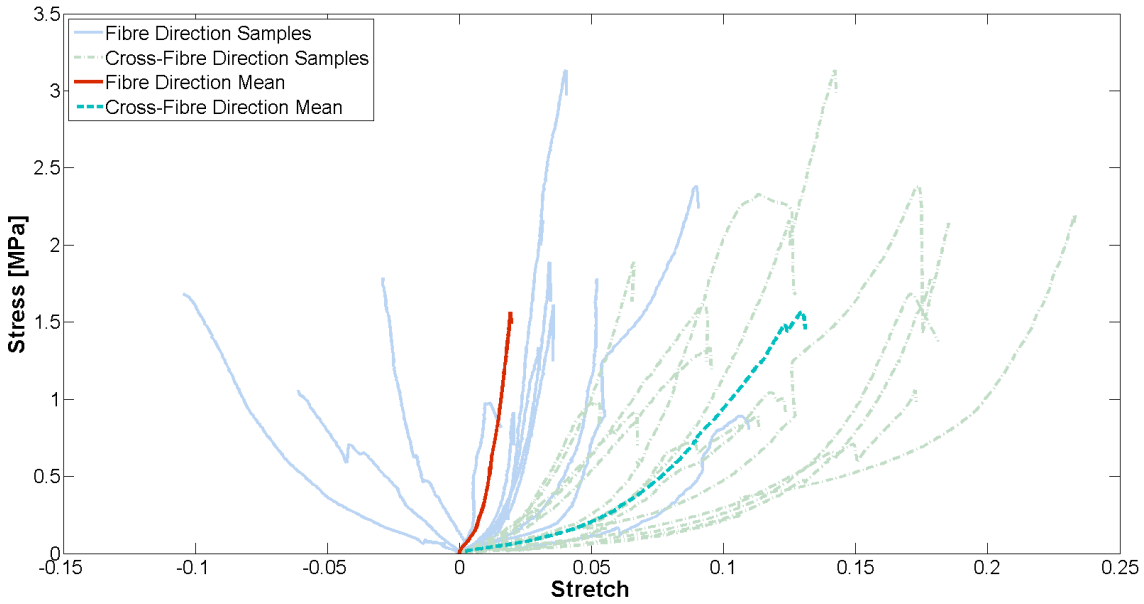

Figure 8.14 – Biaxial stress-stretch plots for all samples.

8.3.3. Computational Modelling

The average and the ranges of the predicted model parameters from fitting to the uniaxial data are presented in Table 8.1. The goodness of fit of the computational stress-stretch data to the experimental stress-stretch data is shown in Table 8.2 in terms of R^2 and the sum of squared difference. Plots of the fit for a fibre direction and a cross-fibre direction sample are shown in Figures 8.15 and 8.16 respectively.

	First Order Ogden Model		Exponential Power Law Model	
	C	M	Beta	Ksi
Mean	0.057	8.203	2	0.3424
Range	0.016-0.119	1-14.01	2-2	0.162-0.864

Table 8.1 – FeBio material model parameters.

	Cross-Fibre Direction Samples		Fibre Direction Samples	
	R^2	SSQD	R^2	SSQD
Mean	98.1%	0.391	96.3%	18.1

Table 8.2 – Average goodness of fit of computational data to experimental data for all samples.

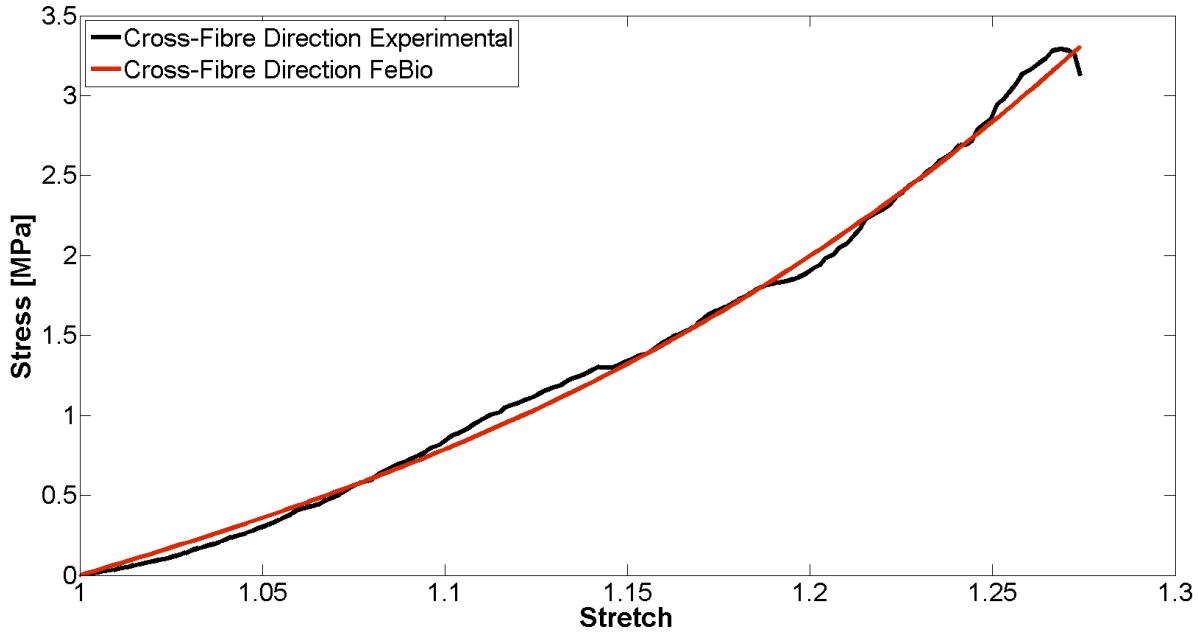

Figure 8.15 – Fit of FeBio stress-stretch results to experimental results in the cross-fibre direction.

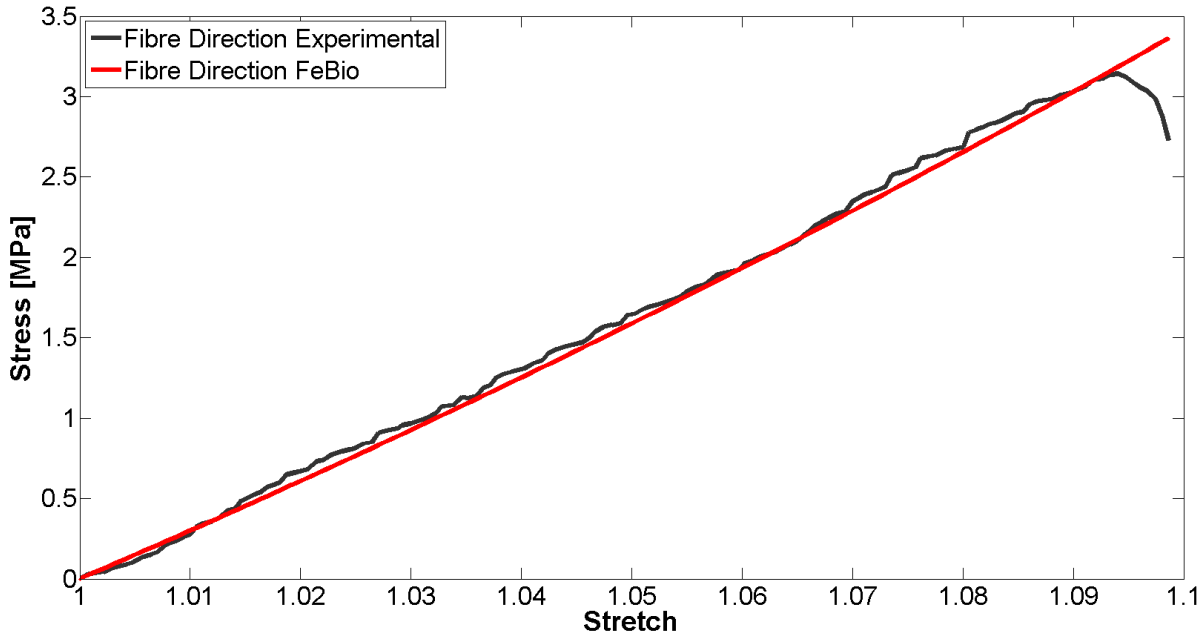

Figure 8.16 – Typical fit of FeBio stress-stretch results to experimental stress-stretch results in the fibre direction.

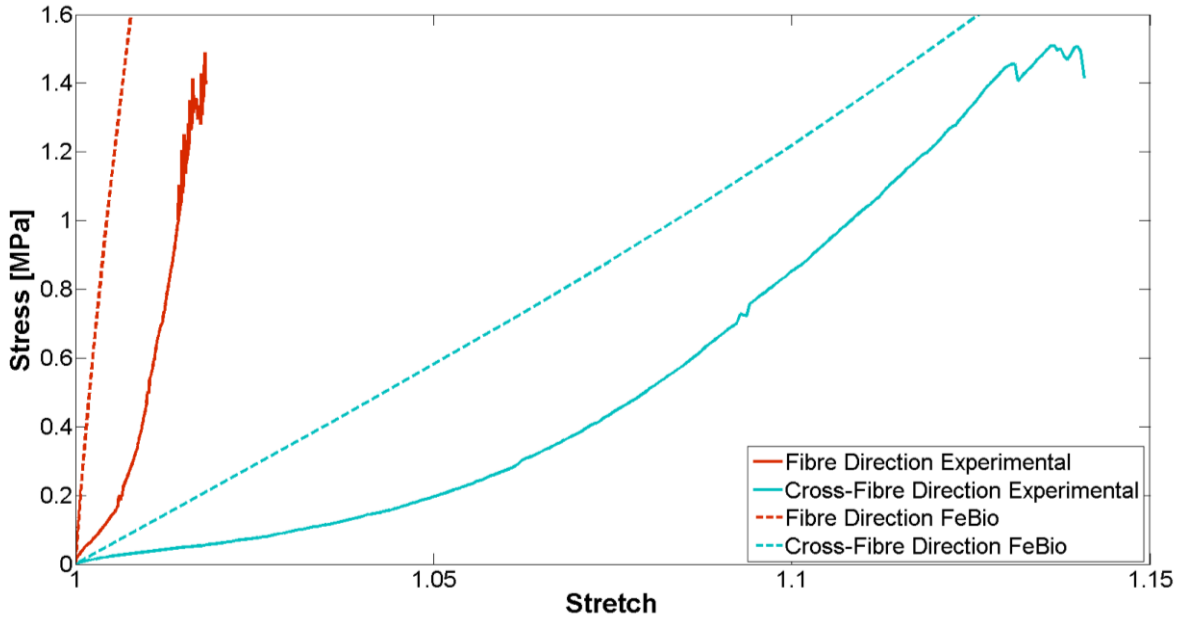

Figure 8.17 – Fit of biaxial FeBio stress-stretch results to experimental biaxial stress-stretch results.

8.4. Validation of Strain Measurement Techniques

Strain measurement techniques were validated by checking the results manually using printed images and a ruler to measure the initial and final distances between the dots. Figure 8.18 and Table 8.3 give an example of this validation for the uniaxial case.

Digital image correlation code was validated similarly. Easily identifiable speckles within the pattern that could be found in both the first and last image were selected and their movement was assessed by measuring the distance between two such points in the first and last images. The stretch ratio obtained was compared to the global stretch ratio reported by the DIC code. An example is given in Table 8.4.

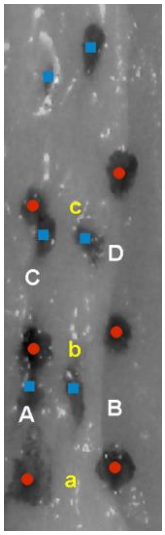

Figure 8.18 – Validation of the dot tracking method. The initial position of the dots is shown in red, the final position is shown in blue. The ratio of the distance between the final points to distance between the initial points gives the stretch.

Region	A	B	C	D	a	b	c
Software	1.16	1.11	1.11	1.2	0.5	0.5	0.49
Ruler	1.16	1.12	1.11	1.2	0.5	0.5	0.49
Error	0%	0.9%	0%	0%	0%	0%	0%

Table 8.3 – Results of the validation of the dot tracking method.

Region	Fibre Direction	Cross-Fibre Direction
Software	0.95	1.11
Ruler	1.02	1.13
Error	7%	2%

Table 8.4 – Results of the validation of the DIC method.

8.5. Discussion

Despite the importance of the rectus sheath in IAP loading, there is uncertainty regarding its structural properties. Uniaxial tensile tests were conducted on 32 samples of porcine rectus sheath (16 with fibre and 16 cross-fibre) and biaxial tests were conducted on 14 samples.

8.5.1. Uniaxial

Figures 8.7 to 8.10 show the horizontal and vertical stretch ratios for both the fibre and cross-fibre direction samples. The stretch in each of the regions A, B, C and D (vertical) or a, b, c (horizontal) is shown, as well as an average stretch across all regions (see Figure 8.2 for a description of regions). There is a noticeable variation in the stretch in each region of the samples and the average stretch was found to be less than the machine stretch in all cases indicating that, despite best efforts, there was some slippage at the grips. This can be explained by the inhomogeneous nature of biological tissue and highlights the need to analyse the strain on a regional basis and average rather than using machine crosshead displacement, as was done elsewhere [66, 68].

The stress-stretch response for each sample in both directions is shown in Figure 8.11. There is some variability, which can mostly be attributed to biological variation between the samples. ANOVA showed that the variation between samples was more significant than the variation between pig bellies used, providing confidence to the assumption that no difference in response exists between pigs (P=0.18).

It is clear that there is a considerable difference between the fibre and cross-fibre direction samples. This was found to be statistically significant at the 99.9% level (P<0.001). Breaking stretch values for the cross-fibre direction samples were much larger (1.3) than for the fibre direction samples (1.07) and the respective ultimate stress values were much lower (1.6MPa vs 4.5MPa).

8.5.1.1. Comparison with other authors

Comparison plots showing data from Rath et al., Martins et al. and average data from this study are shown in Figure 8.19 [66, 68]. Rath et al. only reported breaking stress and strain, thus straight line plots for their data are shown. Results from Martins et al. are doubtful due to the significant variation, the very high stress and the large elongation reported. It does not seem likely that the tissue would elongate by up to 2.6 times while under uniaxial tension. Given the complications experienced in the current study with sample gripping, necessitating the use of a torque wrench to ensure good gripping without damaging the tissue and the use of image-based strain analysis to avoid problems with sample slippage,

it seems likely that slippage occurred in the Martins et al. tests. It is clear from this plot that there is significant disagreement between this study and previous studies. Both Rath et al. and Martins et al. relied on the grip-to-grip separation to determine strain, which is known to be problematic [67] and was confirmed by this study to overestimate the strain (thus underestimate the stiffness) of the tissue.

Figure 8.20 compares current results with recent data from Ben Abdelounis et al. evaluating the uniaxial stress-strain response of human rectus sheath in the cross-fibre direction only. Ben Abdelounis et al. also used image analysis techniques to measure the strain, very similar to the methods employed in this study. This, coupled with the similarity in the responses observed, provides confidence in the current results, particularly in the cross-fibre direction. Furthermore, the comparison suggests that the uniaxial behaviour of human (Ben Abdelounis et al.) and porcine (current study) rectus sheath is similar [69].

Due to the unusual behaviour of the tissue, it was not possible to quantify the Poisson's Ratio in these experiments. During gripping, the tissue in contact with the grips spread in the horizontal direction under the compression of the grips causing the tissue to expand in the horizontal direction under uniaxial tension (Figure 8.22).

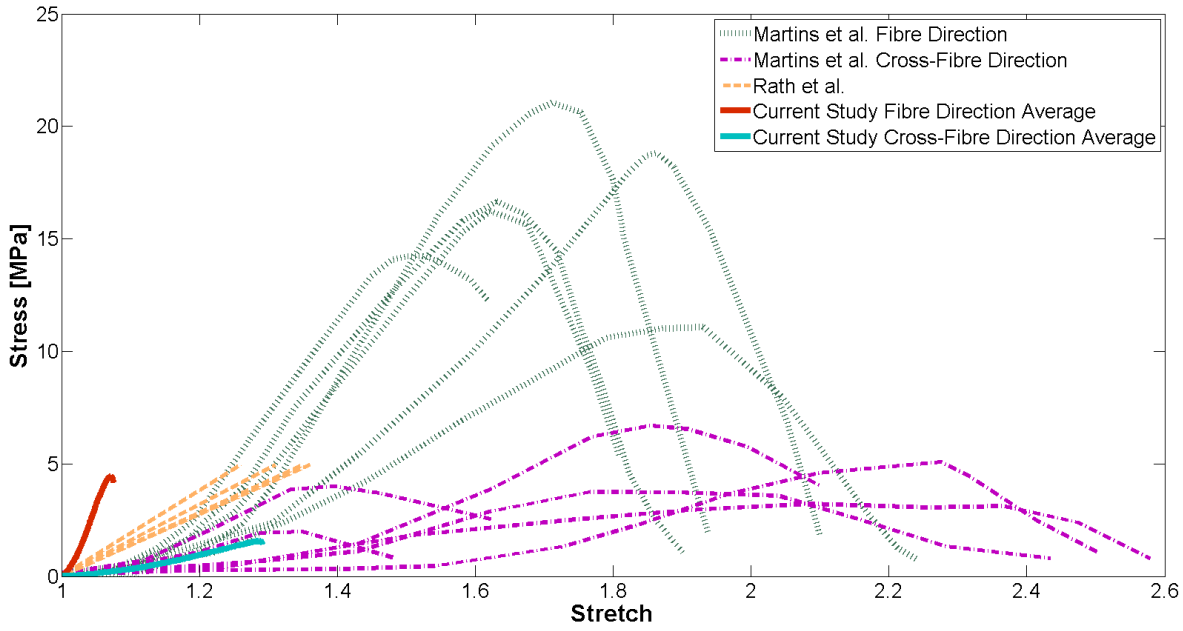

Figure 8.19 – Comparison between the current study and the results of Martins et al. [66] and Rath et al. [68].

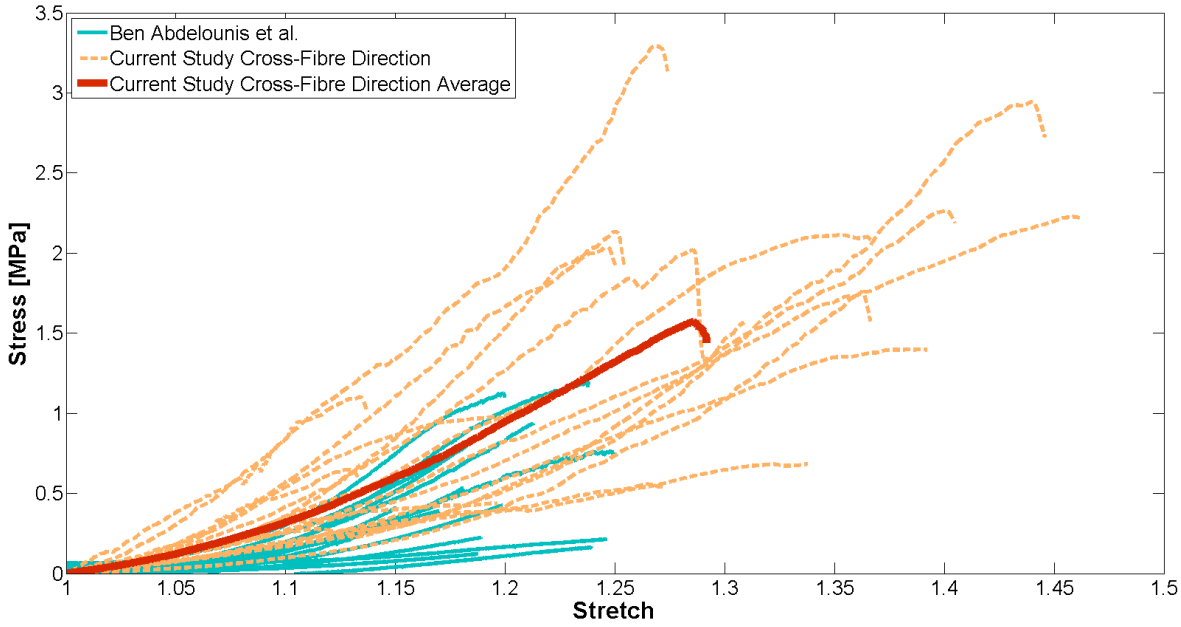

Figure 8.20 – Comparison between the current study and the results of Ben Abdelounis et al. [69].

8.5.2. Biaxial

Figures 8.12 and 8.13 show a raw displacement map of a typical sample, in the fibre and cross-fibre directions respectively, immediately prior to failure under biaxial loading. The sample is seen to stretch quite uniformly across its width in both directions. This gives confidence to the reported average strain measurements from the DIC code and shows that the global stretch it reports is representative of the stretch within the sample. There is no region of the sample that stretches unusually.

Figure 8.14 shows the fibre direction and cross-fibre direction stretch for each biaxial sample. The samples were square and the force was equal in each direction, leading to equal stress in both the fibre and cross-fibre directions. The fibre direction was significantly stiffer than the cross-fibre direction, stretching 16% less for the same stress. Average curves for both directions were obtained in the same way as for the uniaxial case, described above in Section 8.2.1.3.

In some cases contraction occurred in the fibre direction while the tissue elongated in the cross-fibre direction under biaxial tensile loading (see left-hand side of Figure 8.14). This is believed to be due to a large difference between fibre direction and cross-fibre direction

stiffness and is corroborated by an analysis based on linear elastic transverse isotropy, where the stress-strain relationship is:

$$\begin{bmatrix} \varepsilon_L \\ \varepsilon_T \\ \varepsilon_{T'} \\ \varepsilon_{LT} \\ \varepsilon_{LT'} \\ \varepsilon_{TT'} \end{bmatrix} = \begin{bmatrix} \frac{1}{E_L} & -\frac{\vartheta_{TL}}{E_L} & -\frac{\vartheta_{TL}}{E_T} & 0 & 0 & 0 \\ -\frac{\vartheta_{LT}}{E_L} & \frac{1}{E_T} & -\frac{\vartheta_{TT'}}{E_T} & 0 & 0 & 0 \\ -\frac{\vartheta_{LT}}{E_L} & -\frac{\vartheta_{TT'}}{E_T} & \frac{1}{E_T} & 0 & 0 & 0 \\ 0 & 0 & 0 & \frac{1}{G_{TT'}} & 0 & 0 \\ 0 & 0 & 0 & 0 & \frac{1}{G_{LT}} & 0 \\ 0 & 0 & 0 & 0 & 0 & \frac{1}{G_{LT}} \end{bmatrix} \begin{bmatrix} \sigma_L \\ \sigma_T \\ \sigma_{T'} \\ \sigma_{LT} \\ \sigma_{LT'} \\ \sigma_{TT'} \end{bmatrix} \quad \text{Eqn. 8.3}$$

Equation 8.3 was used to predict strains under equi-force biaxial tensile loading for a range of fibre and cross-fibre direction stiffnesses (E_T and E_L respectively), derived from fitting to the experimental data (Figure 8.11), in which high fibre direction stiffness was paired with low cross-fibre direction stiffness and vice-versa (Table 8.5) to represent extreme experimental cases. A range of estimated Poisson's Ratios were used (Table 8.5), since these could not be derived directly from the experimental data. There are limitations to this analytical approach, in particular that the rectus sheath is non-linear and closer to a fibre reinforced composite than a transversely isotropic material. However, this approach yields contractile stretches in the stiffer direction in almost all cases except low ϑ_{LT} coupled with low E_T and high E_L (Figure 8.21). These results can be interpreted by considering energy minimisation concepts: under biaxial loading, when significant anisotropy is present, stretch in the stiffer direction may be contractile to reach a state of overall minimum potential energy.

As expected, Figure 8.14 shows that the stiffness of the tissue in biaxial tension is higher than in uniaxial loading, but the anisotropy is less pronounced. In the uniaxial case, the fibre direction is approximately 11× stiffer, on average, than the cross-fibre direction while in the biaxial case, the fibre direction is 7× stiffer on average. This may be because constraining in the cross-fibre direction has a greater influence on effective stiffness than constraining in the fibre direction.

Property	Range	Number of Values
E_T	2MPa – 15MPa	5
E_L	200MPa – 35MPa	5
ϑ_{LT}	0.4 – 0.5	21
ϑ_{TL}	0.2 – 0.4	21
$\vartheta_{TT'}$	0.8 – 0.6	21

Table 8.5 – Values used for various material properties for Hooke's Law analysis.

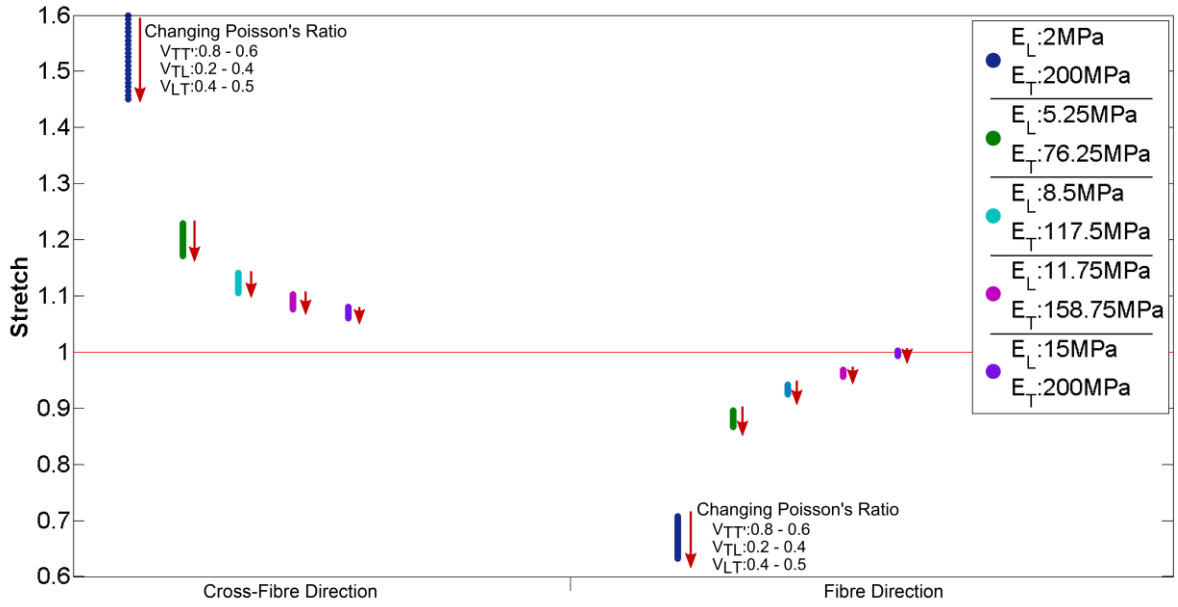

Figure 8.21 – Predicted strains from Hooke's Law analysis in fibre and cross-fibre directions for a range of Poisson's Ratios and Young's Moduli.

Figures 8.11 and 8.14 show that a stress of 1.6MPa seems to be a limiting factor in the cross-fibre direction for both uniaxial and biaxial tests. This may reflect the matrix strength and reveals the importance of the collagen fibre reinforcement in withstanding any stresses greater than 1.6MPa created by IAP.

8.5.3. Statistical Tests

Statistical tests showed no anomalies in the testing procedure. Control charts showed no time bias affecting the results and normal probability plots showed normality in the results. ANOVAs revealed that the variation between pig bellies was not statistically significantly different from samples within each belly, as above.

8.5.4. Computational Modelling

The Ogden model was a very good fit to the cross-fibre direction uniaxial experimental data, with high R^2 (98%) coupled with a low SSQD (0.391). The model for the fibre direction, which includes an uncoupled matrix represented by the Ogden model and an exponential power law representing the fibres also had a high R^2 (96%) and a SSQD of 18.1 (Figures 8.15 and 8.16 and Table 8.2).

The fit for the biaxial simulation (Figure 8.17) was not as good as for the uniaxial optimisation, but it still captures the essential difference in stiffness between the two directions. The material properties for this simulation were obtained from uniaxial optimisation and biaxial tension was applied. This did not account for any additional interactions between the two load directions and suggests that a more complex model might be required.

As noted previously, during gripping the tissue under the grips spread, creating a somewhat dog-bone shaped sample from a sample that was originally rectangular (Figures 8.22(a) and 8.22(b)). Upon application of uniaxial tension the tissue initially bulged in the lateral direction to re-create a rectangular specimen (Figure 8.22(c)) before beginning to narrow as would be expected (Figure 8.22(d)). As a result of this unusual movement of the tissue, accurate measurement of the horizontal stretch was not possible in most cases, thus the Poisson's Ratio could not be quantified. It is hypothesised that in the fibre direction case, the fibres become curved as a result of gripping. When tensile loading is initiated, these fibres straighten out, causing the sample to bulge outwards. Once the fibres are straight, the tissue can then behave as normal and contract in the unloaded direction. The FeBio simulation with the average model parameters was used to assess if gripping influenced the presented stress-stretch results.

It was found that the effect of gripping the tissue did not adversely affect the stress at the centre of the specimen. In the cross-fibre direction case, there was no difference in the stress-stretch curves for a gripped and a non-gripped sample (Figure 8.23). In the fibre direction, the stress in the gripped case was 5% less than in the non-gripped case (Figure 8.24).

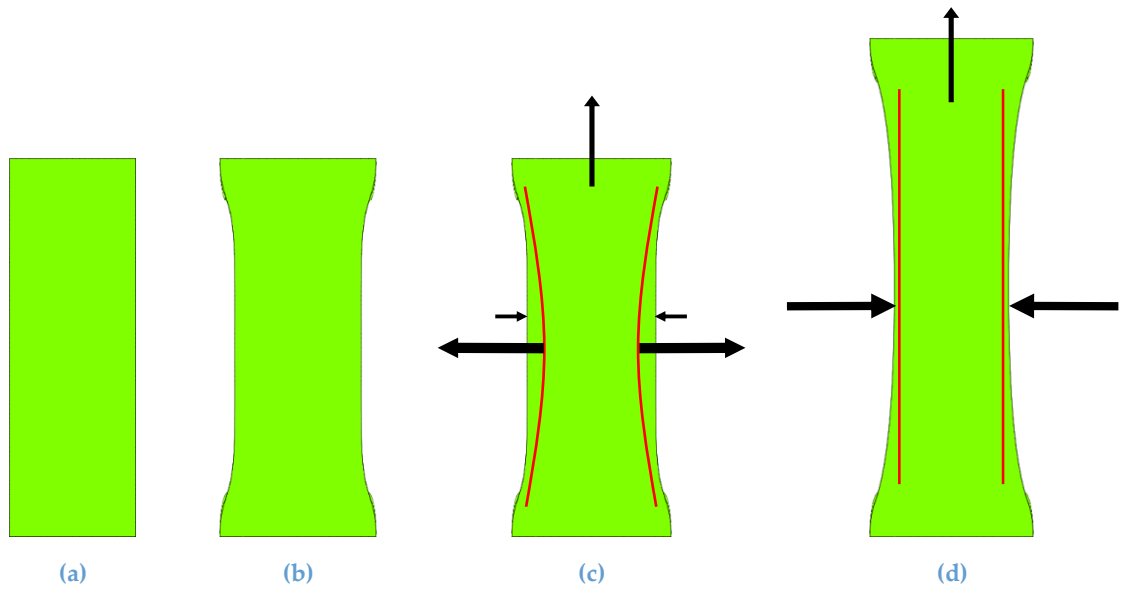

Figure 8.22 – Hypothesis for the bulging of the tissue in the fibre direction tests. In (a) to (b), the tissue is clamped in the grips, causing it to spread horizontally under the grips. (c) As the tissue is stretched, the force of the fibres trying to straighten outweighs the force of the matrix trying to contract. (d) When the fibres are straight, the tissue can contract as normal.

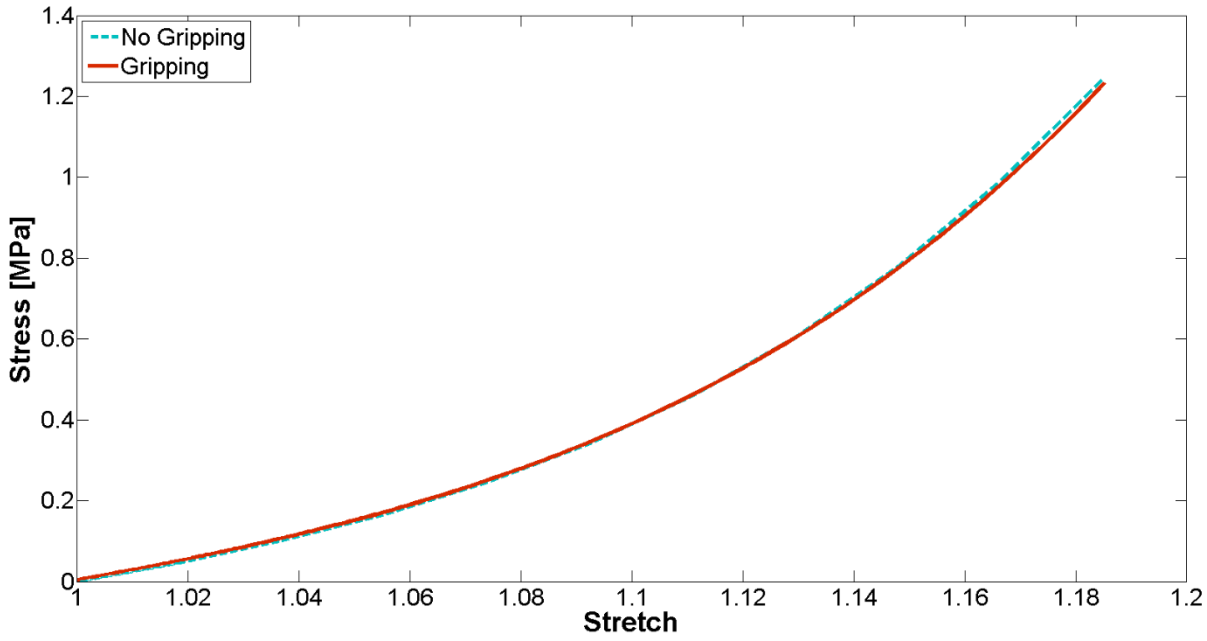

Figure 8.23 – FeBio stress-stretch plots for a gripped and a non-gripped cross-fibre direction sample.

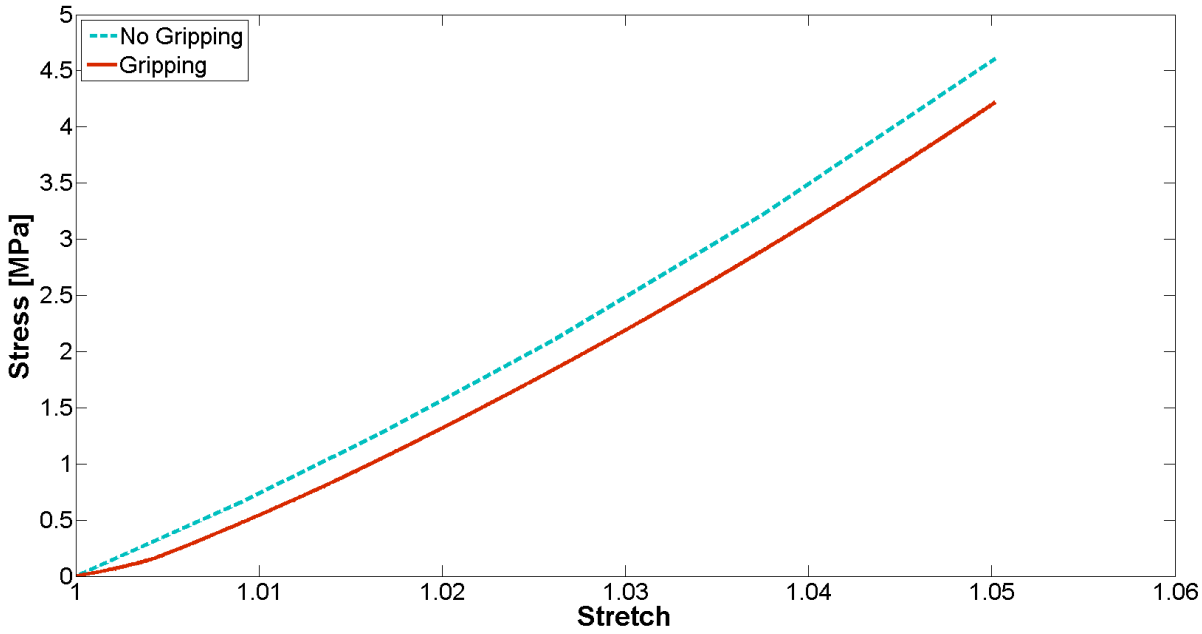

Figure 8.24 – FeBio stress-stretch plots for a gripped and a non-gripped fibre direction sample.

8.6. Conclusions

This study contributed to an understanding of incisional hernia formation through experimental and computer modelling of uniaxial and biaxial stress-stretch responses of porcine rectus sheath.

Characterisation of the uniaxial and biaxial tensile stress-stretch response of porcine rectus sheath using an image analysis method to evaluate stretch and maintaining constant, controlled parameters around age, weight, gender and gravidity of subjects allowed accurate analysis of the behaviour of rectus sheath. Complete stress-stretch curve profiles permit further computer modelling of the tissue.

The generation of preliminary material model parameters for this tissue will allow further work in the modelling of rectus sheath and further development of a computational model of the abdomen.

The results indicated that the response of porcine rectus sheath to uniaxial tension is similar to the response of human rectus sheath.

9. Surrogate Abdomen Evaluation

9.1. Introduction

An understanding of the intra-abdominal pressure (IAP) environment related to hernia◊ formation is important for the evaluation of the performance of the physical model of the abdomen. There are some detailed studies of IAP in the literature, including those by Cobb et al. [41], Campbell et al. [40], Marras et al. [50] and Iqbal et al. [52], but none investigate the effect of IAP on hernia formation or other similar complications. From an engineering perspective, a greater pressure within the abdominal cavity will result in a greater stress in the abdominal wall, leading to a greater likelihood of wound dehiscence◊. Subsequently, with a defect in the abdominal wall and increased pressure in the abdominal cavity a fluid organ, such as the small intestine, could easily be extruded. This can be confirmed empirically in a human subject when an anaesthetic begins to wear off before completion of surgery and an abdominal straining manoeuvre is initiated.

The aim of this chapter is to compare the IAP realised in surgery to those developed in the surrogate abdomen rig and examine the hernia formation behaviour of the rig.

9.2. Observational Study in Surgery

A small observational study was conducted on patients who were scheduled to undergo laparoscopic surgery in St. Vincent's University Hospital, Dublin to evaluate the IAP generated at various stages of the procedure. The study was designed and developed with evaluation of the surrogate abdomen in mind. Prof. Des Winter and Dr. Helen Mohan applied for ethical approval from the St. Vincent's Healthcare Group Ethics and Medical Research Committee and collected the data during a number of surgical procedures that they were conducting. Raw data was returned and is analysed herein.

9.2.1. Methods

The study was approved by the St. Vincent's Healthcare Group Ethics and Medical Research Committee. A prospective observational study of abdominal pressures in patients

undergoing abdominal surgery was conducted between January and July 2013. A total of seven patients participated, following written informed consent.

This study measured bladder pressure via the urinary catheter connected to an abdominal pressure manometer (UnoMeter™, UnoMedical, Birkerød, Denmark), as described by Gaidukov et al. [159]. The manometer was attached to the urinary catheter at the start of the case prior to draping[9]. The 0cm point (midclavicular line◊, in line with the anterior◊ superior◊ iliac spine) was marked using a skin marker, to avoid intraoperative discrepancies. All recordings were conducted with the table flat, with the patient either supine or in lithotomy◊. An abdominal straining manoeuvre (ASM - often incorrectly referred to as a Valsalva manoeuvre [43], Section 2.5.1) was performed by the anaesthetist[10] prior to closure of the wound to a maximum airway pressure of 4kPa.

Intra-abdominal pressure was measured at five intervals:

1. Preoperative baseline: following induction of anaesthesia at the start of the case immediately prior to draping.
2. Intraoperative baseline: at the end of the case before the ASM.
3. Abdominal straining manoeuvre: at the end of the case during the ASM.
4. Wound closure: patient anaesthetised with all wounds closed.
5. Awakening: maximum pressure during awakening from anaesthesia.

[9] A surgical drape is a sterile, fabric-like material used to isolate the surgical site from the rest of the patient's body and other possible sources of contamination (e.g. the bed). Draping is a technical process where surgical drapes are carefully placed to isolate the surgical site.

[10] An abdominal straining manoeuvre is normally performed autonomously by a conscious patient when attempting to exhale against a closed glottis◊ thus increasing intra-thoracic and intra-abdominal pressures (Section 2.5.1). This can be mimicked intraoperatively by the anaesthetist to check for intra-abdominal bleeding. To do so, the ventilator is switched off, the pressure relief valves are closed and the anaesthetist squeezes the manual ventilation bag until intra-thoracic pressure rises to a desired level, where it is held for a predetermined length of time. Relief valves are then opened and the ventilator is switched back on for mechanical ventilation to return to normal.

Exclusion criteria included patients with a short bowel due to previous resections, extensive abdominal scarring, those considered underweight on the basis of their BMI (BMI < 19), those under the age of 18, those with chronic lung disease and those whom the anaesthetist deemed unsuitable for ASM.

9.2.1.1. Statistical Methods

Simple average and standard deviation values were calculated for all data. Significance was investigated using Student's t-test at 95% confidence.

9.2.2. Results

Seven patients were recruited for inclusion in this study. Demographic data for each patient along with their history prior to the operation is presented in Table 9.1.

Gender	
Male	2 Patients
Female	5 Patients
Age	
Mean	51 years
Range	29-70 years
BMI	
Mean	26 kg/m2
Range	25-30 kg/m2
Port Sites	
Three	3 Patients
Four	3 Patients
Laparotomy	1 Patient
Steroids	
Yes	1 Patient
No	6 Patients
Previous Incisional Hernia	
Yes	1 Patient
No	5 Patients
Not Recorded	1 Patient

Disease	
Inflammatory Bowel Disease	4 Patients
Colorectal Cancer	3 Patients
Weight	
Mean	77kg
Range	63-98kg
Waist Circumference	
Mean	120cm
Range	93-130cm
Surgery Type	
Laparoscopic	5 Patients
Laparoscopic Converted	1 Patient
Laparotomy	1 Patient
Previous Abdominal Surgery	
Yes	4 Patients
No	3 Patients

Table 9.1 – Summary of patient demographics for all seven patients.

Abdominal pressure recordings at the five intervals are summarised in Table 9.2 and Figure 9.1. There was considerable variation in absolute values between patients, but the overall trend was similar, with highest pressures recorded at the end of the operation when the wound was closed and during awakening[11].

	Preoperative BL	Intraoperative BL	ASM	Wound Closed	Awakening
Mean	1003	767	1047	1516	1744
Median	747	700	933	1467	1867
σ	396	490	664	1059	773
Range	640 to 1467	0 to 1600	133 to 2266	133 to 3333	533 to 2600

Table 9.2 – Summary of IAP recordings in Pascals [Pa].

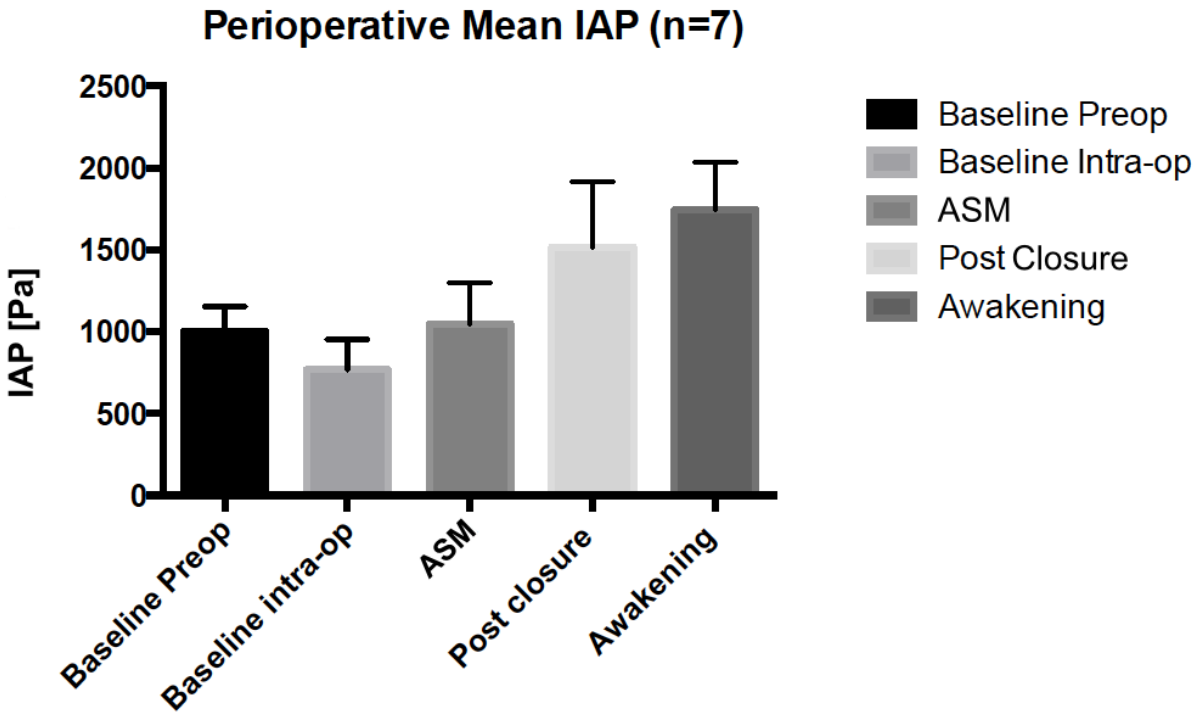

Figure 9.1 – Perioperative mean IAP and standard deviation.

[11] During awakening, the patient remains intubated◊ as the anaesthetic wears off. As the patient regains muscle control, the diaphragm begins to work again and the patient is ready to breathe autonomously. The patient begins to gag to try to expel the airway tube, causing an increase in IAP. At this point the patient is extubated by the anaesthetist.

9.2.3. Discussion

This observational study investigates how IAP changes throughout the course of a surgical procedure. The problem of post-operative hernia development at wound sites has existed for many years and still has a high incidence despite the increase in laparoscopic techniques [5-7, 32, 46]. From a bioengineering perspective, understanding the pressure within the abdomen, which is one of the root causes of the problem, can lead to novel and effective solutions.

The mean resting pressure, before the beginning of the procedure was 1kPa. This corroborates well with results from other authors [38-40, 49].

Straining for bowel movements, doing abdominal crunches (sitting up), vomiting and even climbing stairs can result in a significant increase in IAP (up to 11kPa [41, 52]). This is much higher than the pressures observed in the cohort during surgery. No herniae developed in the patients during the study, but it can be assumed that much higher pressures generated in these activities could cause an incisional hernia to develop in a poorly closed wound [7-9].

A limitation of this study is the small sample size, which limits the statistical power of the findings. However, it does give an insight into the pressures required to generate a hernia, by examining pressures during the ASM. Further studies could include a larger cohort with comparison between patients with a greater range of BMIs, and a follow-up to relate IAP at hernia formation to relevant post-operative complications.

Furthermore, due to necessary safety limitations, it was not possible to continue to increase the pressure, using the ASM, until hernia formation. Thus, the reported ASM pressures are all pressures at which hernia formation *did not* occur. This permits partial validation of the physical model using these pressures and pressures at which a hernia is observed in the rig.

9.3. Rig Validation

To maintain confidence in the results obtained from the rig, it is essential for it to be validated against experimental data. The rig is designed to replicate the abdominal

environment in a simplistic and repeatable way to permit recurrent testing of potential devices.

Observations were made during a small number of laparoscopic procedures conducted in St. Vincent's University Hospital, Dublin (as described above) where patients' IAPs were measured a number of times before, during and after a procedure. Using these results, along with the results of Cobb et al. [41] on normal IAP in humans, it is possible to test the efficacy of the rig to respond in a similar manner to the body.

9.3.1. Methods

9.3.1.1. Porcine Tissue

Initial validation was conducted using porcine small intestine and a porcine abdominal wall. The rig was assembled as described in Chapter 6 and a pressure of up to 10kPa was first applied to ensure the rig set-up and abdominal wall could withstand this pressure.

Subsequently, with the pressure released, a defect was created in the abdominal wall, through the umbilicus◊. An incision approximately 1cm in diameter was created in the skin and fat layers using a scalpel. The point of a blade was then used to puncture the *linea alba*. A trocar◊ port (Blunt Tip Trocar, Covidien, Dublin, Ireland) was introduced through the incision and pushed through the *linea alba* with the leading end of the trocar enlarging the initial small defect and ensuring a tight fit (Figure 9.2).

To ensure that a defect approximately the size of the trocar had been created, the pressure was again increased and it was confirmed that there were no leaks in the region of the trocar. With the pressure released, the trocar was removed and the defect was left open in the abdominal wall.

Pressure was then slowly increased until the intestine was observed to extrude through the open defect in a manner similar to a hernia. This pressure was recorded and the experiment was run twice more to test repeatability.

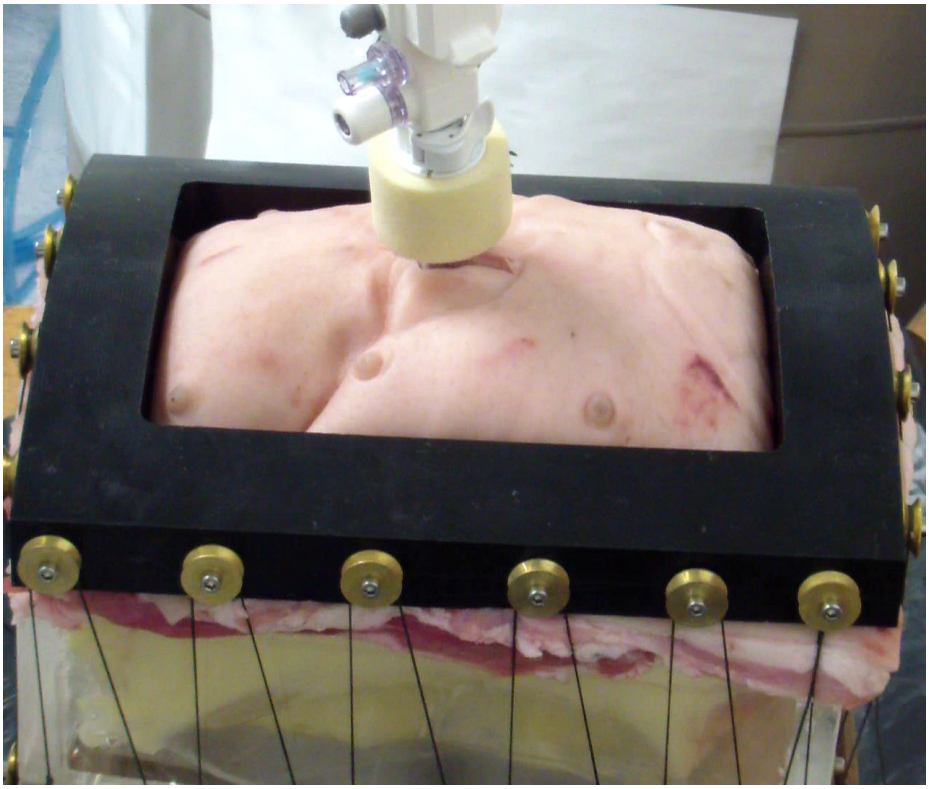

Figure 9.2 – Blunt Tip Trocar inserted into the abdominal wall in the surrogate abdomen rig.

The diameter of the defect was subsequently increased by 10mm and the experiment was run three times for this new defect size, recording the pressure at hernia initiation each time. Defect sizes from 10mm to 50mm were investigated.

9.3.1.2. Surrogate Small Intestine

Chapter 7 identified reconstituted powdered potatoes (RPP) as a suitable surrogate for small intestine extrusion. In order to further validate the rig, the tests described above were repeated using RPP. Again, five tests (10mm to 50mm defects) were conducted and each extrusion was conducted three times to test repeatability.

9.3.2. Results

Table 9.3 and Figure 9.3 show the actual pressure at hernia generation for various defect sizes and intestine materials (cleaned small intestine or RPP). Most IAPs are measured using a urinary catheter or naso-gastric tube, thus recording the intravesical[◊] (as above) or intragastric pressure. Anatomically, the small intestine does not lie on top of either of these organs. In the laboratory tests conducted in this study, however, the small intestine or RPP (hereafter referred to as intestines) were lying directly on top of the balloon creating the

pressure. Thus, the pressure created by the weight of the intestines acting on the area of the balloon has been subtracted from the pressure set on the regulator in order to compare the extrusion pressures in the laboratory tests to those recorded in the operating theatre.

Material	Hole Size	Mean Hernia Pressure
Intestines	10mm	5.88kPa (370)
Intestines	20mm	5.76kPa (391)
Intestines	30mm	5.52kPa (942)
Intestines	40mm	4.62kPa (421)
Intestines	50mm	4.20kPa (872)
RPP	10mm	5.8kPa (637)
RPP	20mm	5.6kPa (941)
RPP	30mm	4.8kPa (909)
RPP	40mm	4.4kPa (933)
RPP	50mm	3.5kPa (432)

Table 9.3 – Recorded pressures at hernia formation for both RPP and intestines at various hole sizes.

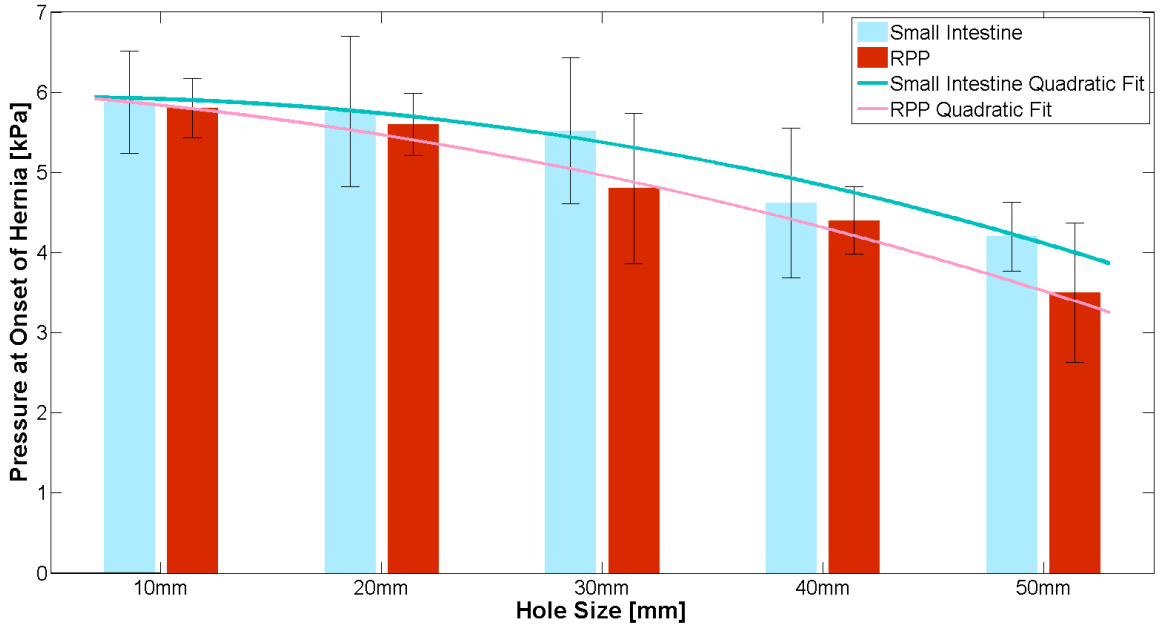

Figure 9.3 – Recorded hernia pressures for RPP and small intestine at a range of hole sizes with error bars (± one standard deviation) and quadratic fits for both materials.

Figure 9.4 shows a logistical regression between results from the perioperative tests (no hernia) and the laboratory tests (hernia formation) through a 10mm defect using RPP as surrogate intestines. Since there are no overlapping results between the sets of experiments, this regression effectively creates a step function. For comparison, a ramp function is also shown.

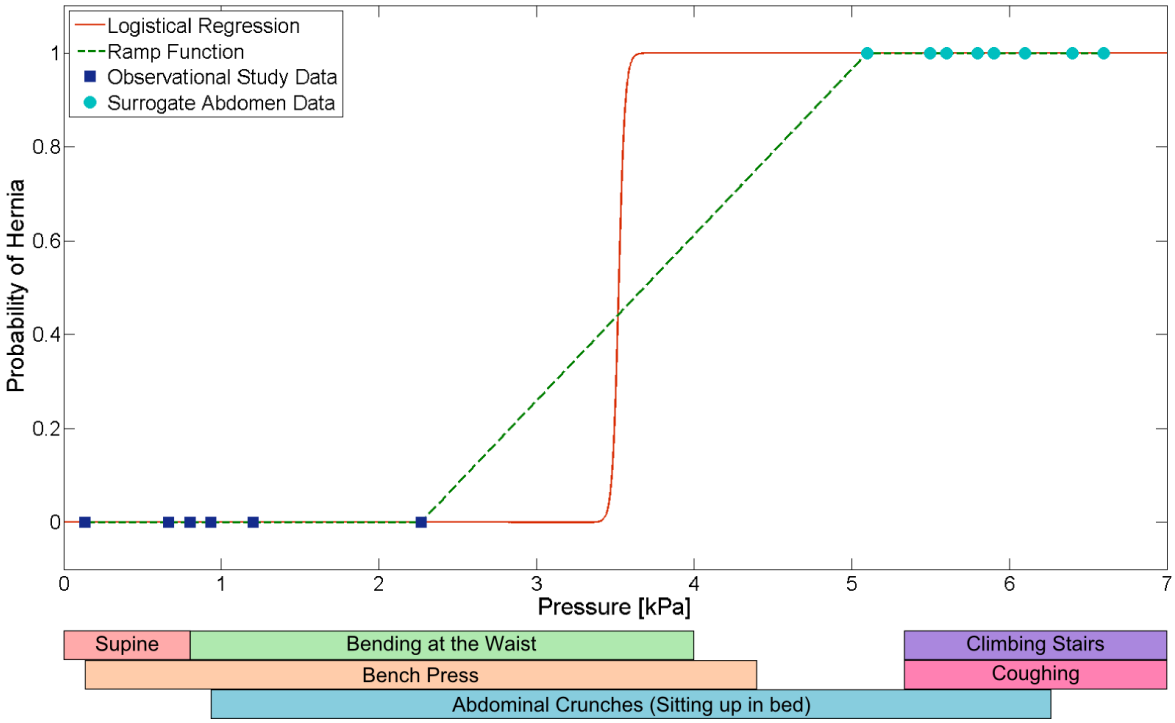

Figure 9.4 – Probability of hernia formation through an open 10mm defect predicted using a logistical regression and a ramp function. The horizontal axis also shows typical activities that generate such pressures, from [41]. In the experiments, these pressures were applied as static pressures which over-estimates their influence in hernia generation and provides for a factor of safety in this prediction.

9.3.3. Discussion

Table 9.3 and Figure 9.3 show that the pressure required to create a hernia decreases with increasing defect size, as expected. It is also clear that the porcine intestines are slightly harder to extrude than the RPP, as was similarly found in Chapter 7, though the difference in hernia formation pressure was not statistically significant. In Chapter 7, RPP was found to extrude at a force 30% less than intestines, however in the surrogate abdomen, the RPP extruded at a pressure only 10% less than intestines. The same information is shown in bar chart form in Figure 9.3 with error bars showing one standard deviation. A quadratic relationship is evident between the hernia development pressure and hole diameter, with the pressure reducing proportionally to the square of the hole size. Given the quadratic relationship between force, diameter and pressure (Equations 9.1 and 9.2), this is as expected and is evidence for the need to ensure adequate closure of large abdominal wall defects in particular.

$$Pressure = Force \times Area \quad \text{Eqn. 9.1}$$

$$Area = \frac{\pi D^2}{4} \quad \text{Eqn. 9.2}$$

The pressures available from the perioperative tests were all for cases where hernia did not occur. Hernia did not occur at those pressures in the rig, however it is not known at what pressure hernia should be expected. Given that RPP was found to be a good surrogate for intestines (Chapter 7) and that hernia was observed in the rig at a low IAP, it is concluded that the rig is broadly valid. A logistical regression is presented in Figure 9.4 which can be used to estimate the probability of hernia formation at a given pressure. However, as there are no overlapping cases, this logistical regression becomes a step function approximately half way between the highest no-hernia pressure and the lowest hernia pressure[12]. For comparison purposes, a ramp function between these two data points is also included. The development of a hernia *in vivo* may be dependent on a loop of small bowel being aligned with an appropriately sized defect along with the generation of sufficient IAP. Although, Figure 9.3 shows that this may not be as important as originally envisaged, since RPP extrudes only slightly easier than cleaned porcine intestines. However, the mesenteries◊ were not present in these laboratory tests which may have a small confounding effect (though this was not evident in the extrusion tests in Chapter 7). It is not possible to say with certainty at what pressure a hernia will form through a 10mm defect, but the data shows that it is between 2.1kPa and 5kPa. Considering the IAPs recorded by Cobb et al. [41], the risk activities for developing a hernia in an unclosed 10mm defect include bending at the waist and sitting up in bed, both of which could frequently be done by patients post-operatively. It is also clear that activities such as climbing stairs and coughing are high risk.

This data pertains to hernia formation at unclosed 10mm defects and thus incorporates a significant factor of safety over a patient who has undergone facial closure. The safest

[12] Logistical regression relates the probability of an event to an exponential function of the independent variable. The number and spread of the "event" and "non-event" cases will dictate the constants of the function, thus a probability of 0.5 will not necessarily be predicted for a value of the independent variable that is half way between the highest "non-event" value and the lowest "event" value.

considerations for the patient would be to assume that a risk of hernia begins at an IAP of 2kPa, and that risk escalates with increasing IAP thereafter with hernia very likely at pressures above 5kPa. As a result, closure of all trocar defects would be recommended given that almost all patients will either bend at the waist or sit up in bed, creating IAPs in the "at risk" range.

9.4. Conclusions

The perioperative tests provided an understanding of the IAP experienced throughout a laparoscopic procedure and interestingly showed that the highest pressure was when the patient was waking up. These perioperative observations also provided some data to partially validate the experimental rig.

The experimental rig performed as expected, with hernia formation at physiologically realistic pressures. Furthermore, hernia formation using RPP instead of real intestines happened at a lower pressure, facilitating some factor of safety, although there was no statistically significant difference.

A quadratic relationship between hole size and hernia development pressure was found. This is as expected given the relationship between force, pressure and area, and the quadratic relationship between diameter and area.

Complete validation of the surrogate abdomen's ability to predict the onset pressure for a hernia was not possible as there is no *in vivo* data on the pressure required to cause a hernia. Instead, *in vivo* data was obtained for pressures that do not cause a hernia and experimental data for pressures that do. This provides an "at risk" range of pressures, and thus activities, for hernia formation.

10. Mesh Overlap

10.1. Introduction

Implantable prosthetic meshes are commonly used as a tension-free repair method for abdominal wall and inguinal◊ hernia◊ defects [160]. Repairs can be performed by laparoscopic or open techniques. In both cases, the hernia is first reduced before a mesh is placed over the defect and sutured, tacked or glued in place. In some cases, sutures are used to close the defects, though current practice favours the use of mesh-based, tension-free repair [95].

Despite the recent surge in popularity of mesh-based repair of hernia defects, there is little scientific study on the optimum mesh overlap ratio that should be used [19]. A general "rule of thumb" reported by many authors is to use a 5cm overlap and this has been shown in a number of studies to be effective at preventing hernia recurrence [13-16, 18]. However, it would seem clear from an engineering point of view that there should be a relationship between the amount of overlap required and the size of the defect being repaired – with larger defects requiring larger overlaps. A mesh that is too large results in unnecessarily increased costs, the possibility of complications such as adhesions [15], and is wasteful. There has been little study of this relationship in the literature, with Hollinsky et al. [20] the only authors to examine the problem mathematically using insights from civil engineering; however it has not been verified experimentally. Furthermore, these calculations only incorporated the friction between the mesh and the abdominal wall and did not include parameters for the pull-out force of tacks or sutures that are often used to hold the mesh in place [100-102].

The physical model of the abdomen, described in Chapter 6 and evaluated in Chapter 9, is a suitable environment in which to assess these calculations and further examine the relationship between defect size and mesh size prior to animal or human trials.

Therefore, the aim of this chapter is to evaluate the mesh overlap requirement for various defect sizes. This will be done analytically by developing a mathematical relationship

between mesh size and defect size from first principles, and experimentally by studying the problem in the surrogate abdomen rig.

The purpose of the mathematical model is to develop an analytical, engineering understanding of the relationship between mesh size and defect size, including the effect of tacks and sutures used to anchor the mesh. Whereas the purpose of the experiments is to generate evidence to evaluate the mathematical model and to create a simple clinical recommendation for the required mesh size to close a defect.

10.2. Analytical Approach

Similar to the analysis of Hollinsky et al. [20], a mechanical understanding of the force balance between a mesh and the defect it is attempting to close can be used to develop a mathematical model relating an optimum mesh size to various hole sizes.

A mesh covering a defect in an abdominal wall is analogous to a membranous thin-walled pressure vessel. The stress in such a membrane is related to the pressure, the radii and the thickness of the membrane:

$$\frac{\sigma_1}{r_1}+\frac{\sigma_2}{r_2}=\frac{P}{t} \qquad \text{Eqn. 10.1}$$

with r_1 and r_2 being the radii of curvature of the membrane. Assuming the membrane is deformed in a spherical fashion through a circular hole (Figure 10.1), where $r_1 = r_2$, this equation simplifies to:

$$\sigma = \frac{Pr_{hole}}{2t} \qquad \text{Eqn. 10.2}$$

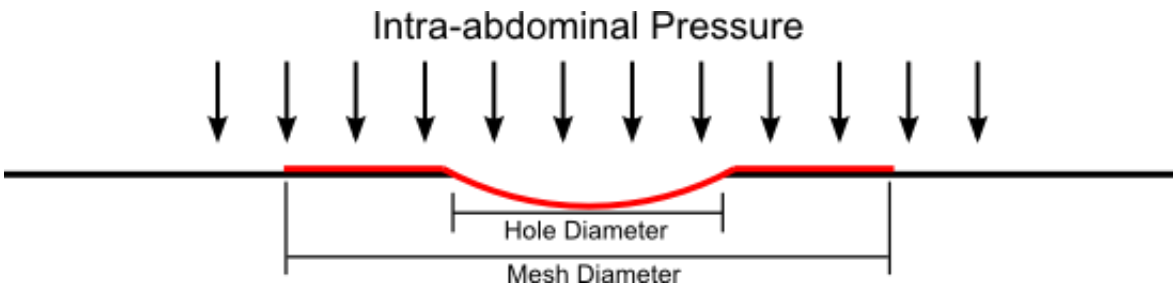

Figure 10.1 – Mesh placement to cover a circular hole deforming spherically due to an applied pressure.

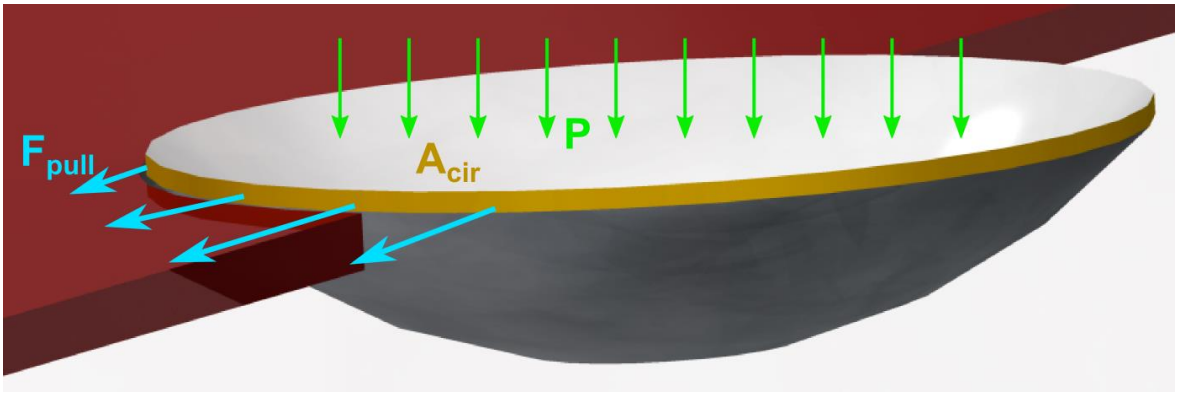

Figure 10.2 – A 3-dimensional representation of a mesh covering a defect with a cross-section showing pressure (P), tack pull-out force (F_{pull}) and circumferential area (A_{cir}).

This hoop stress in the membrane translates into a "pulling force" around the edge of the defect (Figure 10.2). The pulling force is equal to the stress in the mesh acting over the circumferential area of the mesh:

$$F_{pull} = \sigma A_{cir} \qquad \text{Eqn. 10.3}$$

$$A_{cir} = 2\pi t r_{hole} \qquad \text{Eqn. 10.4}$$

Combining Equations 10.2, 10.3 and 10.4 yields the pulling force in terms of the pressure and the radius:

$$F_{pull} = P\pi r_{hole}^2 \qquad \text{Eqn. 10.5}$$

Considering a force balance at the interface between the mesh and the abdominal wall, the in-plane membrane force from the mesh being pushed into the defect by the pressure (F_{pull}) will be balanced by the friction force ($F_{friction}$) of the mesh against the abdominal wall along with a number of tacks (n), which each fail at the tack pull-out force (F_{tack}):

$$F_{pull} = F_{friction} + nF_{tack} \qquad \text{Eqn. 10.6}$$

The friction force is a product of the pressure force acting on the annulus of mesh and the coefficient of friction:

$$F_{friction} = \mu P A_{annulus} \qquad \text{Eqn. 10.7}$$

The area of the annulus of the mesh is given by:

$$A_{annulus} = \pi\left(r_{mesh}^2 - r_{hole}^2\right) \quad \text{Eqn. 10.8}$$

Combining Equations 10.5, 10.6, 10.7 and 10.8 and rearranging for mesh diameter gives

$$m = \sqrt{\frac{h^2 + \mu h^2}{\mu} - \frac{4nF_{tack}}{P\pi\mu}}, \quad \text{Eqn. 10.9}$$

where m is the mesh diameter required to block the hole, h is the hole diameter, μ is the coefficient of friction, P is the intra-abdominal pressure, n is the number of tacks that must fail and F_{tack} is the pull-out force for a single tack.

This simplified analytical approach yields the mesh diameter (m) needed to effectively block a hole (of diameter h) given a specified maximum IAP (P), a tack pull-out force (F_{tack}) and a coefficient of friction between the mesh and the abdominal wall (μ). The number of tacks (n) required to fail for mesh failure to be considered must also be estimated.

10.2.1. Parameter Estimation

Values for IAP and coefficient of friction are available in the literature. According to Cobb et al. [41], a maximum IAP of just less than 20kPa is generated by coughing when standing. Hollinsky et al. conducted two separate experimental studies [20, 161] on the coefficient of friction between the mesh and the abdominal wall, with an average resulting coefficient of friction of 0.35.

Tack pull-out force has been studied by some authors [100, 162, 163], with a large range of reported values. van't Riet et al. [163] compared the pull-out force of tacks and sutures in porcine abdominal walls and the variation in tack pull-out force with the number of tacks used. It was found that adding tacks did not linearly increase the failure force as might be expected and that, in all cases, sutures had a significantly higher pull-out force.

Hollinsky et al. conducted two studies [100, 162] examining tack pull-out forces in rats and human cadavers. In the study in rats [162], the authors compared a variety of tacks and the change in their pull-out characteristics as adhesions developed. As expected, the presence of adhesions was found to increase the tack pull-out force. Results are presented as a pull-out stress and it is not clear what area this stress is acting over, thus it is not immediately possible to relate it to a force. Furthermore, the presence of adhesions in all cases makes

these results unsuitable for use in Equation 10.9. In the study in human cadavers [100], the authors investigated the efficacy of tacks and staples. It was found in all cases that tacks were superior to staples. Similar to van't Reit et al. [163], it was found that increasing the number of tacks did not linearly increase the total failure force. The pull-out forces from van't Reit et al. [163] and Hollinsky et al. [100] are summarised in Table 10.1.

No of Tacks	van't Reit et al. [163]		Hollinsky et al. [100]	
	Force per tack		Force per tack	
	Mean	Minimum	Mean	Minimum
1	28N	24N	-	-
2	21N	13.5N	17N	11.5N
3	21N	20N	-	-
4	18N	16N	18N	13N
5	16N	12N	-	-
8	-	-	16N	10.5N

Table 10.1 – Pull-out forces per tack showing mean and minimum, from [100, 163].

In the majority of cases a mesh will be fixed with at least four tacks. For safety purposes, it is best to assume that the tacks will fail at the minimum reported value rather than the average. Considering all of this evidence and safety considerations, a single tack pull-out force of 10N was selected for Equation 10.9. All estimated parameters for this equation are summarised in Table 10.2.

Taking diameters in millimetres and the pressure in megapascals, it is clear from preliminary evaluation of Equation 10.9 that for small hole diameters, the tack pull-out force dominates and could result in imaginary mesh sizes due to negative numbers within the square root. For the parameters used in this model (Table 10.2), this occurs for hole diameters up to 10.5mm. Furthermore, the equation calculates required mesh diameters smaller than the diameter of the hole for hole diameters up to 11.4mm.

Parameter	Value
μ	0.35
P	0.02MPa
F_{tack}	10N

Table 10.2 – Summary of constants for Equation 10.9.

A very small overlap, as calculated for hole diameters up to approximately 20mm is also not a plausible situation as the pull-out force of the tacks will be significantly reduced if they are very close to the edge of the hole. Regardless of the result of the calculation, it would be important to ensure a mesh overlap of 10 to 15mm to guarantee sufficient underlying tissue for solid tack placement.

Failure of the closure will occur when enough tacks fail to expose a sufficient portion of the hole for a hernia to occur. For example, in a circular mesh secured with four tacks at 90°, failure of one tack would cause the whole system to fail, whereas in a circular mesh with eight tacks at 45° it is likely that two or three tacks would have to fail for the closure system to fail. The number of tacks that must fail is also dependent on the circumference of the mesh and the size of the mesh overlap. It is difficult to predict how many tacks will have to fail in a given case to cause failure of the closure. Assuming tacks are placed every 10mm around the circumference of the hole, the number of tacks that would be required to fail for a particular mesh to fail was estimated (Table 10.3). The estimate was based on a minimum of 15-30% of the area of mesh becoming mobile if that number of sequential tacks failed. A particularly small mesh, with only four tacks, would only require one tack to fail for a large portion of the hole to become exposed. However, a larger mesh, secured with many tacks may require a larger number of neighbouring tacks to fail to expose the hole (Figure 10.3).

Hole Diameter	Estimated no. of tacks for failure
0-20mm	1
20-40mm	2
40-50mm	3

Table 10.3 – Number of tacks required to be pulled out to cause failure of the defect closure.

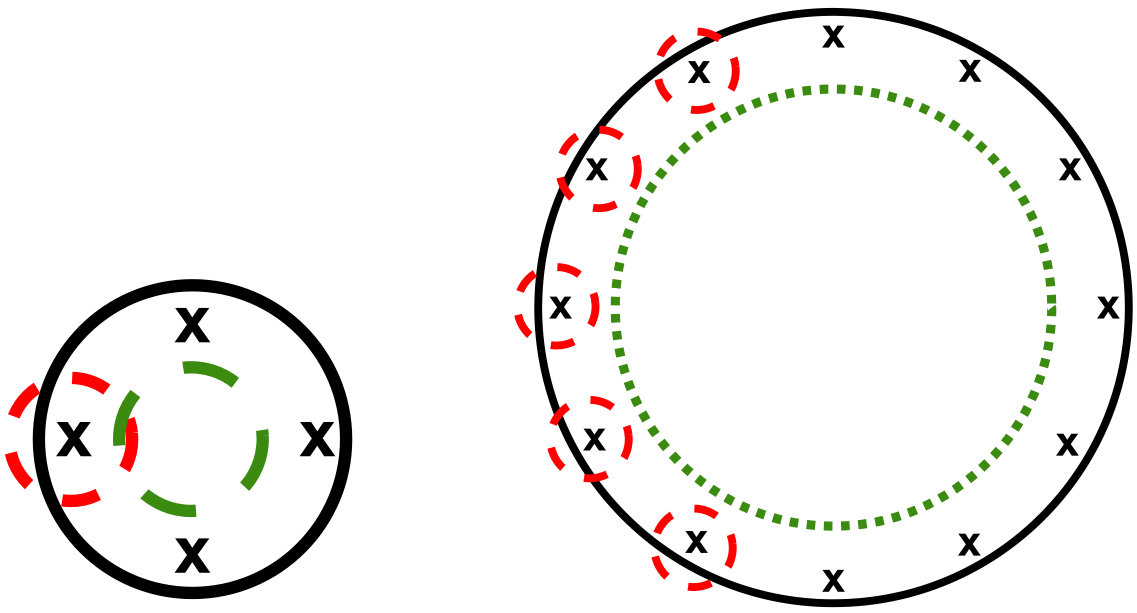

(a) (b)

Figure 10.3 – Number of tacks that must fail for the defect closure to fail. In (a), only one tack must fail as the mesh is small and only secured by four tacks. However, in (b), up to five tacks may need to fail before the defect closure will fail and expose the hole (shown in green).

10.3. Clinical Recommendation

Equation 10.9 is not practical for application during surgery when a decision needs to be made on the size of the mesh. Instead, a very simple calculation is required, ideally related to the defect size, for the surgical team to rapidly calculate the required mesh size. For simplicity, this calculation should not contain more than two parameters, which should be whole numbers.

Fitting a first-order polynomial to the experimental data provides a simple calculation for mesh size, with one multiplicative factor and one additive factor. This can be interpreted as:

$$mesh\ diameter = factor \times hole\ diameter + extra\ mesh \qquad \text{Eqn. 10.10}$$

This empirical mathematical model can be used quickly and easily in the operating theatre. The *"extra mesh"* factor can be increased as required to allow for a factor of safety over the experimental data.

10.4. Experimental Methods

Tests using the surrogate abdomen rig were conducted to experimentally assess the required mesh diameter to prevent hernia onset and provide for a clearer comparison between current practice [13-16, 18], the Hollinsky model [20] and the mathematical model described above.

Four porcine abdominal walls were sourced from a local pig abattoir. All pigs were aged 26-28 weeks old and all females were nulligravid. Animals were slaughtered and dissected in the abattoir as per their procedures where the abdominal walls were harvested and frozen pending collection. They were subsequently kept frozen at -20°C until testing in the laboratory. Prior to testing, abdominal walls were defrosted at 5°C±1°C for 40 hours.

Pieces of mesh (PhysioMesh™, Ethicon Inc., Somerville, USA) of diameter 20mm to 100mm in 10mm steps were prepared by cutting large pieces of mesh with a stencil.

Using plastic stencils and a scalpel, a 10mm diameter hole was created in the centre of the abdominal specimen (Figure 10.4). This defect was then closed using a 20mm mesh tacked in place using a laparoscopic tacker (Tacker™, Covidien, Dublin, Ireland) with tacks spaced every 10mm around the circumference (Figure 10.4).

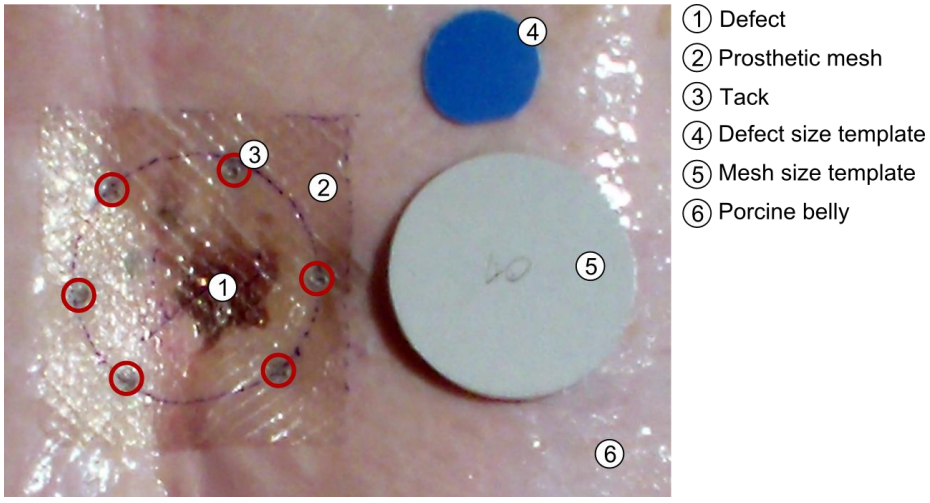

Figure 10.4 – Abdominal wall containing a defect closed with a tacked mesh.

The rig was set up for operation as described in Chapter 6. RPP was used to represent the small intestine as the RPP has been found to extrude at a slightly lower pressure than real small intestine which incorporates an extra factor of safety. It is also cheap, repeatable, clean

and easy-to-use (Chapters 7 and 9). A pressure was applied, beginning at 2kPa and increasing in 1kPa steps, until the RPP began to extrude through the defect, signifying mesh failure. This pressure was recorded, the mesh was removed and a mesh with a diameter 10mm larger was tacked in place.

When a particular mesh size was used that did not show signs of failure at 20kPa, the hole diameter was increased by 10mm and the process was started again.

This method was repeated for hole diameters of 10mm, 20mm, 30mm, 40mm and 50mm on each belly, resulting in a range of mesh sizes and failure pressures for a variety of hole diameters in a number of porcine abdominal walls.

To ensure that there was no effect of continually testing the same abdominal wall with increasing holes sizes, some spot checks were conducted using additional abdominal walls. In these spot checks a large hole diameter and corresponding mesh diameter were chosen and tested in isolation to ensure the result obtained was within the range observed in the sequential tests.

10.5. Results

Figure 10.5 shows a plot of failure pressure versus mesh diameter in millimetres for each hole size from 10 to 50mm. A mesh diameter of zero indicates no mesh was used and provides a baseline result for each set of tests. In each case the best-fit quadratic curve between the mesh size and the failure pressure is also given. Figure 10.6 shows the same hernia onset pressure recorded at various hole diameters for each mesh diameter.

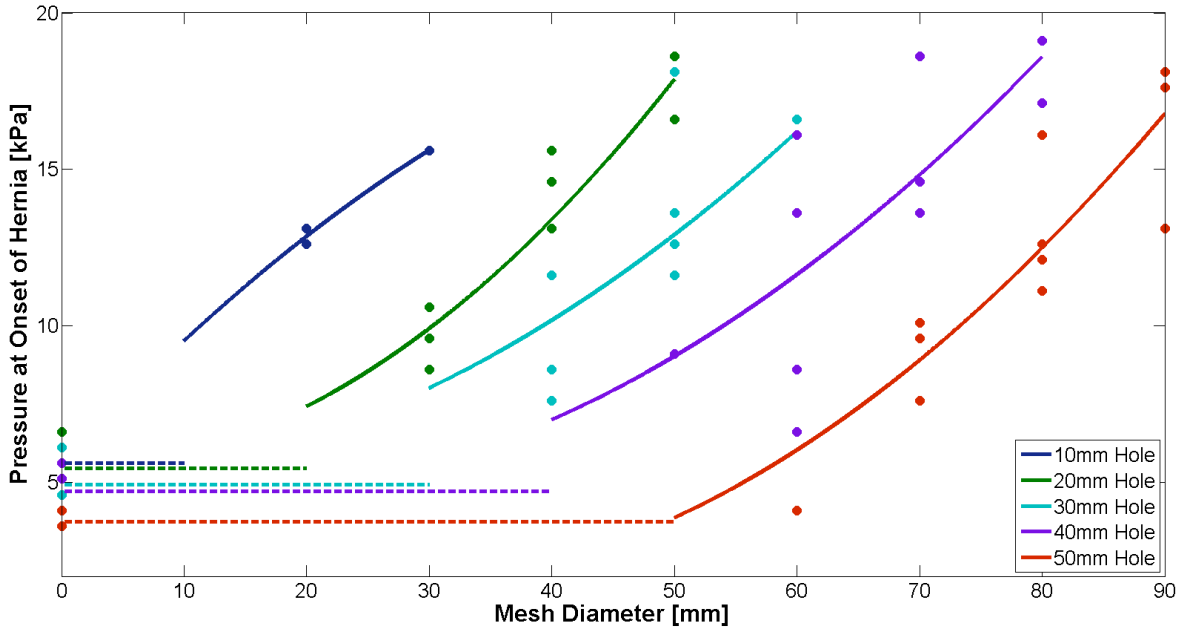

Figure 10.5 – Relationship between mesh diameter and hernia onset pressure for each hole size from 10 to 50mm.

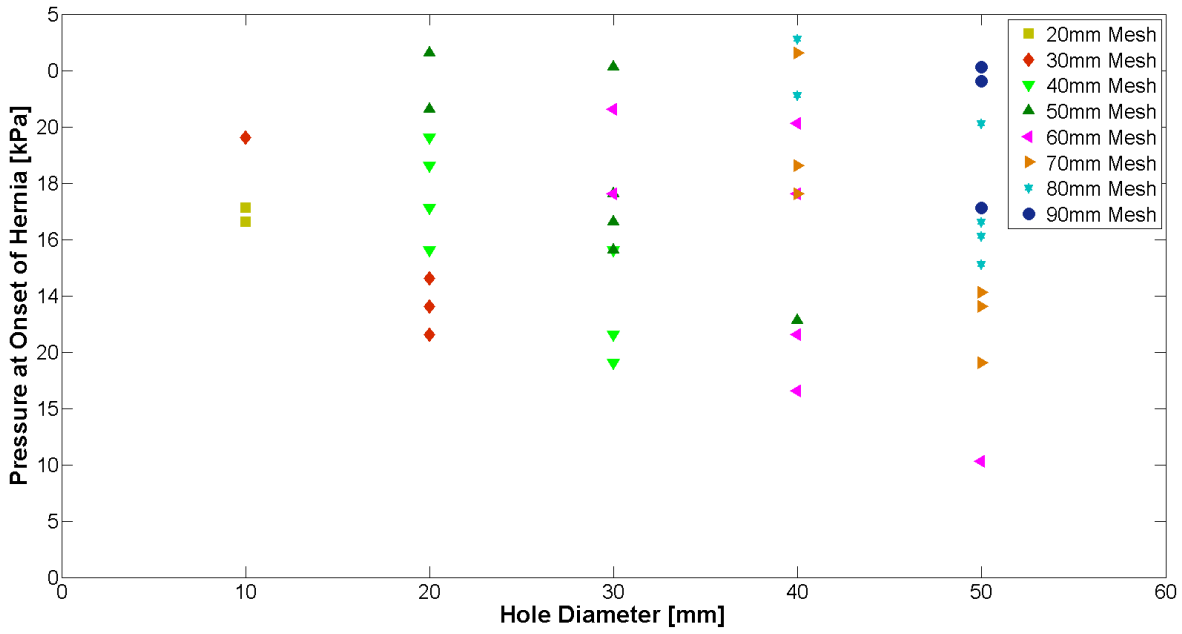

Figure 10.6 – Relationship between hole diameter and hernia onset pressure for each mesh size.

Figure 10.7 shows a 3-dimensional plot of hole diameter, mesh diameter and failure pressure. A quadratic surface has been fit to this data showing an increase in failure pressure with increasing mesh size for a given hole diameter. The surface fit the data with a correlation coefficient of 0.96 and separates regions corresponding to hernia formation (above the surface) and no hernia formation (below the surface).

The surface in is described by the equation:

$$P = 7.8 - 0.15H + 0.25M + 0.001H^2 - 0.008HM + 0.003M^2 \qquad \text{Eqn. 10.11}$$

where P is pressure in Pascals, and H and M are the hole and mesh diameters respectively in mm.

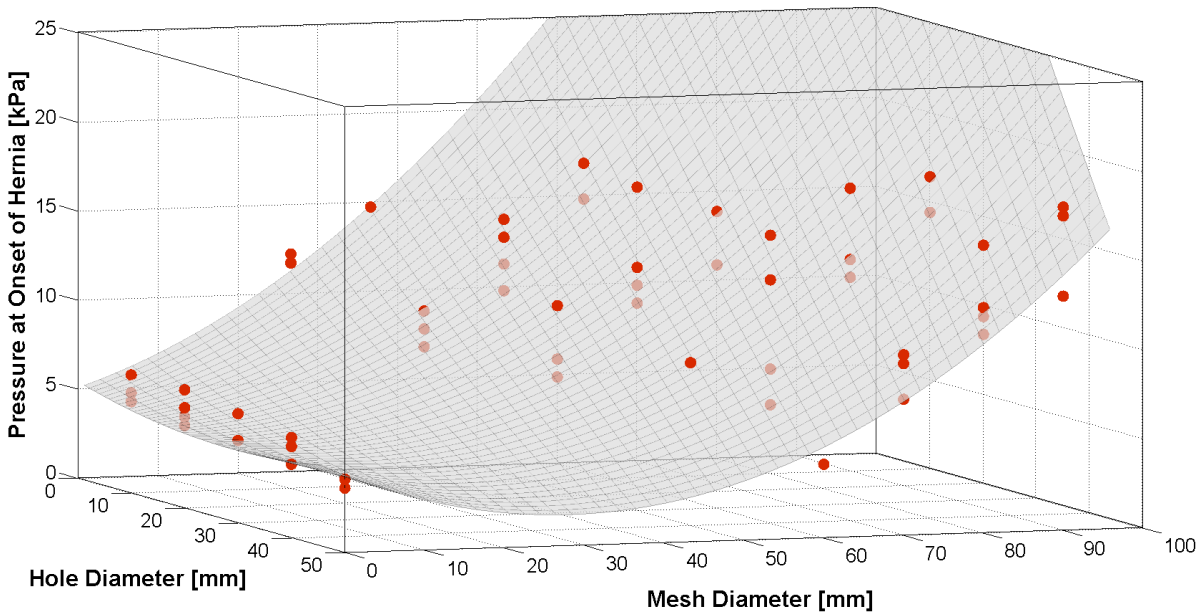

Figure 10.7 – Surface plot showing the relationship between hole diameter, mesh diameter and hernia onset pressure.

10.6. Discussion

The experiments generated a large amount of novel data on the relationship between mesh size and failure pressure for various hole diameters. The plots in Figures 10.5 to 10.7 show the relationship between hole size, mesh size and failure pressure. This relationship appears to be broadly quadratic, as would be expected with the pressure that causes the failure of the mesh acting over an area, which is related to the square of the diameter. Clearly, a defect cannot be closed with a mesh smaller than it, thus, to create the best fit quadratic curves, the pressure required to generate a hernia with no mesh can be considered constant for all mesh diameters less than the hole diameter (shown as dashed lines). Similarly, the friction force opposing mesh dislocation is related to the contact area, which is proportional to the square of the mesh diameter. Figure 10.5 shows that for each hole size from 20 to 50mm, the pressure required to generate a hernia increases approximately quadratically with the

size of the mesh used to block the hole. A baseline case was taken for each hole diameter where no mesh was used (plotted as a mesh diameter of zero). For a 10mm hole, the quadratic trend appears have the opposite curvature, but is likely that this is to do with the more limited data available for that hole size. To allow for adequate overlap for tacking, a 20mm diameter mesh was the smallest mesh it was possible to use for a 10mm hole. However, for larger holes, a greater range of mesh diameters were available, providing more data for the quadratic fit.

Similarly, in Figure 10.6, the relationship between hole diameter and hernia onset pressure is shown. Again, a quadratic relationship would be expected here, though this is not always possible to assess with the available data. For a quadratic fit, three distinct abscissae are required and these are only available for mesh sizes of 50 and 60mm which were used on three different hole diameters each. Each of the remaining mesh diameters were used on either just one hole diameter (10 and 90mm meshes) or on just two hole diameters (30, 40, 70 and 80mm meshes). In the cases with two distinct abscissae a linear fit is possible, for which the positive slope, in all cases, is consistent with the expected trend of a quadratic curve had enough data been available.

Further evidence for the expectation of a quadratic relationship between pressure, hole diameter and mesh diameter is Equation 10.9. This equation shows that the square of the required mesh diameter is dependent upon the pressure and the square of the hole diameter. The quadratic surface fit in Figure 10.7 and Equation 10.11 can be used to calculate a likely failure pressure for given hole and mesh diameters, and this is the first quantitative prediction of this relationship, and is a major finding of this study.

Figure 10.8 compares various recommendations on the mesh size required to close defects. The current standard of a 50mm overlap is shown alongside the Hollinsky model [20] of a mesh three times the diameter of the hole, and the mathematical and experimental results from the current study. Experimental data shows the maximum mesh size required in each case with error bars showing the range (maximum-minimum) of mesh sizes that were successful across all of the tests.

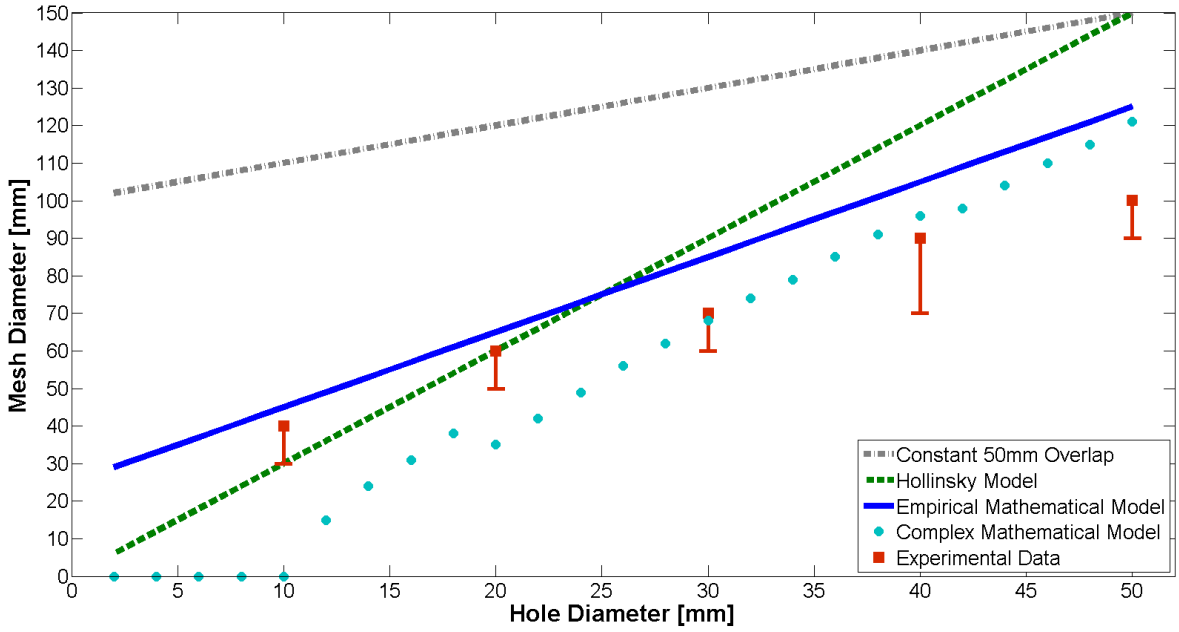

Figure 10.8 – Comparison of mesh size calculations including the empirical (Equation 10.10) and complex (Equation 10.9) mathematical models derived in Section 10.2.

As shown in Figure 10.8, the complex mathematical model (Equation 10.9) was found to under-predict the mesh size required for small holes due to the dominance of the tack pull-out force component and the fact that there is no consideration of the amount of underlying tissue to facilitate tack attachment.

For hole diameters of 30mm to 50mm there is a reasonable prediction by the model, with under-prediction of approximately 3% for holes of 30mm and over-prediction of approximately 15% for holes of 50mm. It is possible that the tacking was not optimum in some cases due to poor embedding of the tack in the abdominal wall. The mathematical assumption is also based on the abdominal wall being completely rigid when in fact it deforms with the simulated intra-abdominal pressure.

At very large hole diameters (>45mm) the mathematical model was found to over-predict the required mesh size. This may be due to assumptions relating to the number of tacks that must fail for the closure to fail. By modifying the mathematical model slightly, and revising some of the assumptions, a better fit to the experimental data can be achieved. Figure 10.9 shows the experimental data alongside the original (Equation 10.9) and modified mathematical models. To improve the model, the tack pull-out force was increased from 10N to 15N, which is closer to the mean values reported in the literature rather than the

minimum. Additionally, a logical switch was included to ensure adequate overlap for tacking. A 15mm overlap on all sides was considered adequate for tacking. If the mathematical model did not predict a mesh size that would allow a 15mm overlap, the mesh size was modified so that a 15mm overlap existed. Mesh sizes were over-ridden for all hole diameters up to 30mm. After this point, the mathematical formula predicted mesh sizes with adequate overlap. These modifications to the original assumptions and formula create a better fit to the experimental data, but could not have been made without the experimental data, highlighting the importance of confirming first principles analysis with experiments where possible.

Overall, it can be argued that the fit of the original complex mathematical model (Equation 10.9) is reasonable for a representation of a complex mesh, abdominal wall and tack interaction where there are deviations from the simplified assumptions and inter-specimen variability. The modifications to the model highlight the difficulty in accurately estimating parameters for engineering analysis of biomedical scenarios.

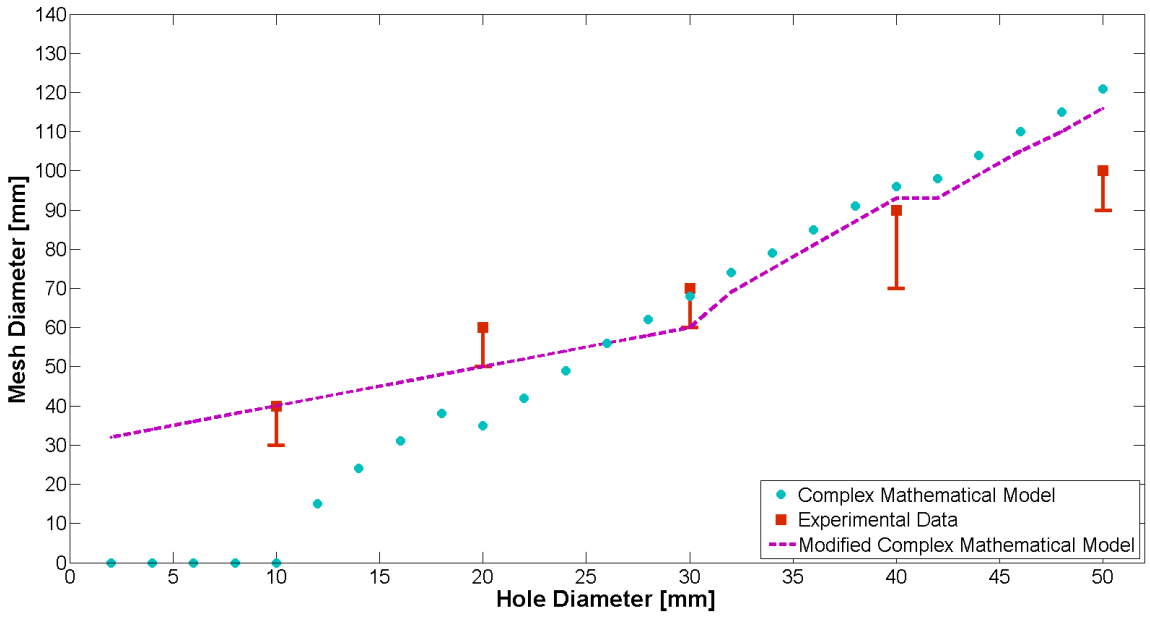

Figure 10.9 – Comparison of the complex mathematical model (Equation 10.9) and some modifications to the model based on the results of the experimental data.

The empirical mathematical model (Equation 10.10) was designed to fit the experimental data allowing simplicity of calculation of the required mesh size as well as incorporating some safety. Surgeons should use a mesh that is twice the diameter of the hole plus an

additional 25mm, and tack it around its circumference with tacks spaced 10mm apart. Equation 10.10 is presented again below (as Equation 10.12) with these parameters in place. This is a simple calculation to perform in the operating theatre and provides a mesh that is slightly bigger than was required in the experimental study (Figure 10.8).

$$mesh\ diameter[mm] = 2 \times hole\ diameter[mm] + 25mm \qquad \text{Eqn. 10.12}$$

The use of RPP instead of small intestine in the test rig set-up increases the factor of safety very slightly again. Chapter 9 found that RPP generated a hernia at a pressure approximately 10% less than the pressure required for the small intestine, though this was not found to be statistically significant. It is difficult to strike a balance between the safest and the most mechanically ideal mesh size. Safety and minimal risk of recurrence must take priority, but further study in humans or animals would be useful to relate the tendency of other complications to mesh size.

This study did not examine tack type, mesh type, tack spacing or the efficacy of other closure solutions such as staples or sutures – all of which could have a bearing on the mesh size required. Furthermore, non-circular hernia defects were not investigated, however it would seem sensible to use this approach with the major axis diameter for elliptical- or oblong-shaped defects where practical.

The current practice of using a 50mm overlap leads to low recurrence rates in many cases, which is desirable [13-18]. However, the practice is based solely on empirical evidence and has not been previously studied from a biomechanical perspective. For very small defects, it is clear that there is a large difference between the mesh size required in this study and the mesh size that would result if current practice is employed (Figure 10.8). This discrepancy improves for defects between 40 and 50mm, however, for mesh sizes above 75mm, the empirical mathematical model (Equation 10.12) predicts mesh sizes with overlaps larger than 50mm. This suggests that current practice may be under-estimating the mesh size required for large hernia defects, which may result in more hernia recurrences. Experimental data was not available to corroborate the extrapolation of the empirical mathematical model to 75mm defects, but given the linear relationship between pressure and area, it is reasonable to assume that the relationship will hold for large defect sizes.

Comparing to the model of Hollinsky et al. [20], who recommend using a mesh three times the diameter of the defect, there is less over-prediction of the experimental results by the current empirical mathematical model, particularly at large defect diameters. While this suggests the Hollinsky model is safer as larger mesh sizes will theoretically reduce the chance of hernia recurrence, excess mesh may lead to other complications including adhesions [127, 134] so a balance is necessary to select a suitable mesh to reduce recurrence and minimise other complications.

Again, for safety purposes, it is important to consider the maximum mesh size required in the experimental tests. The maximum mesh size will be the one that will work in all cases, whereas the mean or median will only succeed in a proportion of the cases. As such, the experimental data plotted in Figure 10.8 is the maximum mesh size required in each case with error bars showing the range over all of the tests. With a much larger study to develop a relationship for use in hernia repair, a statistical analysis could be conducted to find a 99.5 percentile mesh that would only experience failure in 0.5% of cases and incorporate any differences that might exist between mesh type and fixation method.

10.7. Conclusion

This study presents a new mathematical model for predicting the mesh size required to adequately close an abdominal defect. An equation has been derived that relates mesh size to intra-abdominal pressure, tack pull-out force and hole size and an empirical model was constructed to allow rapid use during surgery where a mesh two times the hole diameter, plus 25mm, tacked around its circumference with tacks every 10mm, would be sufficient to close the defect.

The mathematical model was verified experimentally using a physical surrogate model for the human abdomen and was found to accurately predict the mesh size required. Other formulae for mesh size calculation were found to over-predict the mesh size, most notably the current practice of using a 50mm overlap regardless of hole size. The close match between the mathematical model and the experimental results provides a degree of mutual validation for both techniques to predict the mesh size required to close a defect as both predictions were developed independently. Additionally, this gives confidence for the use of the rig in other investigations.

11. Discussion

Given the high incidence of trocar◊ site hernia◊ (TSH) after laparoscopic surgery, it is clear that there is a need for a more effective solution for post-operative closure of port◊-site defects. Some of the occurrences of TSH can be attributed to not closing the defect at all [31, 32] and thus any type of closure of these defects is likely to reduce the incidence somewhat. In obese◊ patients, however, it can be particularly difficult to close the defect. This is because access to the rectus sheath and *transversalis fascia*◊ is impeded by a thick layer of subcutaneous fat coupled with a small access hole of typically no more than 15mm in diameter. Thus an innovative, simple method of closing all of the trocar defects in all patients is necessary to effectively tackle this problem.

In order to design a device that can adequately close these defects using a method that is resilient enough to withstand intra-abdominal pressure loading without causing adverse complications for the patient requires a detailed understanding of the abdominal cavity and abdominal wall.

The loading environment has been investigated by many authors, as discussed in Section 3.3, however, it is clear that there is little consensus and incomplete data. It is widely accepted that the main loading environment of the abdominal wall is as a result of intra-abdominal pressure (IAP) and there have been some detailed studies investigating normal IAP in various situations. However, there is no fundamental mathematical and physical explanation for this IAP or for how it is generated. In Chapter 5, an explanation of the abdominal environment is presented and discussed and despite the fact that it contains broad assumptions for many aspects, it provides a clear starting point for a more detailed understanding of the abdominal cavity, IAP and loading in the abdominal wall. This has facilitated identification of the tissues implicated in the formation of a hernia, which was not clear at the outset. The word "fascia" is used frequently and interchangeably by many authors and clinicians and does not necessarily always refer to the *transversalis fascia*, which is often identified as the tissue implicated in hernia formation. The fundamental analysis of the abdominal wall has identified the rectus sheath, which is also referred to by some authors as a fascia, as the most important tissue implicated in TSH development. As shown

in Figure 5.2, the rectus sheath (and *linea alba* medially) connect the left and right pairs of abdominal wall muscles. When these muscles contract during an abdominal straining manoeuvre, the rectus sheath is loaded in tension. Using a simple pressure vessel formulation and Laplace's Law, the stress in this tissue was shown to be of the order of 1MPa during coughing.

Examining the loading condition in the abdominal wall provides a more detailed understanding of the tissues implicated in the herniation process, and the areas that must be targeted for accurate closure. While much of the evidence gained from these evaluations can be understood from discussions with surgeons and medical professionals, it is often useful to confirm them with fundamental analyses from an engineering point of view. A good design process does not simply accept the problem as presented by the patient or clinician, but rather investigates the root cause of the problem, examining the fundamental aspects, and subsequently generates an intervention that, in so far as possible, eliminates the problem close to its root cause.

To design solutions to these clinical problems, repeated testing of the proposed solutions is required, though this is commonly conducted in animal or even human trials. Such trials are expensive, limited in size and require detailed ethical applications and scrutiny. There is a need for a physical surrogate of the abdomen, capable of replicating intra-abdominal pressure and hernia formation to facilitate innovation in the abdominal surgery field. Currently there is no such model commercially available, and only limited descriptions of similar concepts in the literature [108]. A model is required that can use surrogate materials for the small intestine and the abdominal wall, or incorporate such tissues *ex vivo* and facilitate repetitive, trial-and-error testing of novel techniques and devices. Chapter 6 describes the concept and development of a surrogate abdomen that is evaluated in Chapter 9 and put to use in Chapter 10.

The fundamental understanding of the loading and pressure environment in the abdomen (Chapter 5) identified the key structures involved which resulted in an informed selection of materials to include in the surrogate abdomen model. Small intestine was identified as the key structure implicated in hernia formation, and thus selected as a key component for the rig. Extrusion testing of the tissue and possible surrogates identified reconstituted

powdered potato (RPP) as a suitable surrogate material to use in the rig for hernia formation (Chapter 7). RPP was found to extrude a similar amount, under a similar pressure, to small intestine but it is cheap to obtain, clean, repeatable and practical to use, making it a useful surrogate material.

The prevalence of TSH has inspired the development of many closure solutions for trocar defects, although anecdotal evidence reveals poor uptake of such devices. The evidence against tension repair for herniae, as discussed in Section 3.5, indicates a potential for a tension-free solution for closure of these port site defects and recently this has been further suggested in the literature [12]. Current practice is to either leave open or to suture closed trocar defects which potentially increases the risk of hernia development over a tension-free closure solution [95].

Currently, no commercially available surrogate model of the abdomen exists for examining wound closure in the laboratory. Schwab et al. [108] described and used a rig that is suitable for testing surgical meshes but, as discussed in Chapter 9, this rig has not been validated. A validated, reliable and repeatable physical surrogate model of the abdominal environment is essential for the cheap and successful design and assessment of devices for use in abdominal laparoscopic surgery.

A fundamental understanding of the abdominal environment, coupled with an operational mechanical surrogate of the abdomen, designed and developed based on the first principles analysis of porcine tissues, will allow a comprehensive design process for a novel closure solution in the future. Naturally, this solution will require subsequent live animal and even human trials in the long term, however it is believed that using a first principles approach will result in cheaper devices and avoid unnecessary trials on animals and humans.

11.1. Small Intestine

Selecting a suitable surrogate for the small intestine requires an understanding of its behaviour under the imposed loading environment. In hernia formation applications, the small intestine will be subject to extrusion, as it is squeezed through a defect under loading from intra-abdominal pressure. There is no available literature on the extrusion properties of the small intestine and no available surrogate that mimics the hernia formation

properties of small intestine. Chapter 7 describes a study of hernia extrusion properties and outlines the selection of a suitable surrogate material that replicates these properties. It was clear from initial testing that silicone and gelatine were wholly unsuitable materials, but that dough and Reconstituted Powdered Potatoes (RPP) were much more suitable.

Further repeated tests found that Reconstituted Powdered Potato (RPP) replicates the extrusion behaviour of the porcine small intestine under quasi-static extrusion conditions through a 13mm hole in a compliant silicone die. The RPP does not match the extrusion properties of the intestine exactly, but rather extrudes at a slightly lower force and extrudes slightly more than the small intestine (Figures 7.4 to 7.10), however these differences were not statistically significant (P=0.14-0.3). For the purposes of trial-and-error testing of closure devices, this small discrepancy between the two materials incorporates a small factor of safety – the RPP extrudes at a force of about 30% less than the small intestine. If a closure solution is capable of preventing extrusion of the RPP, it should be able to prevent extrusion of the small intestine. Furthermore, the extrusion of the RPP was found to be less variable than the intestine, with a similar amount extruding in each test. This makes the material more useful for frequent testing of techniques and devices where repeatability is required.

Dough was similarly found to replicate the amount of small intestine extruded, but the force required to extrude it was significantly higher, with P values ranging between 0.0001 and 0.002 for the various extrusion rates. Dough was further found to exhibit viscoelasticity, requiring a larger force to extrude the same amount at higher extrusion rates. RPP and small intestine did not show the same trait.

It was also found that there is a negligible difference between the extrusion force and the amount extruded for cleaned small intestine compared to non-cleaned small intestine, and the presence of mesenteries does not substantially affect the extrusion amount (Figure 7.3). It is useful to test techniques and devices with porcine small intestine, as well as surrogate materials to prove their efficacy, and this finding facilitates the use of cleaned small intestine for that purpose.

The RPP is a foodstuff and, as a result, it is perishable, which was one of the original problems with the small intestine. However, it has a longer lifespan than the small intestine does, and poses less of a hygiene risk than raw meat does. It is also substantially cheaper to

obtain (€4 per experiment compared to €40 for small intestine), it is cleaner than the small intestine and has more consistent properties across samples as there is little biological variation.

The use of RPP in subsequent validation tests of the surrogate abdomen rig provided a similar conclusion on the efficacy of RPP and the small factor of safety incorporated in its use. In a study of mesh size requirements for adequate wound closure (Chapter 10), RPP achieved the desired goals of repeatability, reliability and ease of use.

11.2. Rectus Sheath

A fundamental understanding of the structural properties of the porcine rectus sheath was developed through extensive uniaxial and biaxial tests in addition to computational modelling. The rectus sheath had not previously been identified as the key abdominal wall tissue implicated in abdominal wall hernia, but fundamental analysis of the IAP environment (Chapter 5) found that the rectus sheath is likely to be under tensile loading in a raised IAP situation due to the contraction of the abdominal wall muscles. Using a simplified pressure vessel assumption and Laplace's law with a pressure of 11kPa, it was calculated that the rectus sheath would be under a stress of 1.1MPa when a person coughs. The ultimate tensile strength of the tissue in the fibre direction was found experimentally to be 4.5MPa, indicating its ability to withstand this pressure.

Figures 8.7 to 8.10 show the horizontal and vertical stretch ratios for both the fibre and cross-fibre direction samples. There is noticeable variation in the stretch in each region due to the inhomogeneous nature of the biological tissue. Furthermore, the average stretch in each case was found to be less than the machine crosshead movement, indicating that a small amount of slippage occurred, despite best efforts to avoid this by using a torque wrench to close the grips.

The stress-stretch response presented in Figure 8.11 is the first detailed data on the fibre and cross-fibre response of the porcine rectus sheath under uniaxial tensile loading. In comparison to some other authors (Figure 8.19), the current study showed much less variability and reported more reasonable ultimate stretch values. Martins et al. [66] reported stretch values up to 2.6, which seem doubtful for a tendinous tissue. Good

agreement was observed between the current study and the results of Ben Abdelounis et al. [69], who tested a small number of human rectus sheath samples in the cross-fibre direction only. These authors used similar techniques to the current study, including graphical strain analysis. The agreement also gives confidence in the similarity between human and porcine rectus sheath.

ANOVA tests showed that the variation between samples was more significant than the variation between pig bellies, showing that there was no difference between pigs (P=0.18). Control charts also showed no time bias affecting the result as operator technique improved.

The equi-force biaxial tension results presented in Figure 8.14 are the first biaxial data on rectus sheath and show that the fibre direction is significantly stiffer than the cross-fibre direction, stretching 16% less for the same stress. In a small number of cases, the difference in stiffness between the two directions was so great that the tissue contracted slightly in the fibre direction (left-hand side of Figure 8.14) while stretching in the cross-fibre direction. An analysis based on linear elastic transverse isotropy using Equation 8.3 and Table 8.5 and presented in Figure 8.21 confirmed that a contraction in the stiffer direction is possible. This contraction occurs if there is sufficient difference between the stiffness of both directions, despite equi-force biaxial loading of the tissue. This can be interpreted by considering energy minimisation concepts: under biaxial loading, when significant anisotropy is present, stretch in the stiffer direction may be contractile to reach a state of overall minimum potential energy.

A phenomenon that caused tissue stretched in the fibre direction to bulge initially under load made it impossible to calculate the Poisson's ratio of the tissue. It is hypothesised that this bulging was caused by the behaviour of the fibres straightening initially and is explained graphically in Figure 8.22. Gripping of the tissue may cause some fibres to bend slightly but, under loading, these fibres straighten out, causing the tissue matrix to move with them. Only after these fibres have straightened can the tissue begin to contract in the unloaded direction as would be expected of a sample in uniaxial tension.

Computational modelling was conducted to investigate the effect of gripping on the stress at the centre of the element as some bulging of the tissue was noticed under the grips.

Figures 8.23 and 8.24 show that it has a minimal effect on the stress recorded at a central element in each sample with only a 5% deviation in maximum stress predicted in the fibre direction.

A simulation using the results from the uniaxial experiments in a biaxial set-up was run to investigate the ability of the computational model to predict the biaxial behaviour from the uniaxial data. The essential difference in stiffness between the two directions was captured, but the fit was not good, suggesting that a more complex model which would account for interactions between the two loading directions is required (Figure 8.17).

Development of a surrogate material, with the same structural properties as rectus sheath would be beneficial for use in conjunction with the surrogate small intestine in the surrogate abdomen rig and some initial attempts were made using silicon, cotton thread and rubber. There was substantial variation between each of the samples that were made and most were not suitable for tensile testing. It was therefore concluded that development of such a surrogate was beyond the scope of this project due to the complexities involved in material development and the limited equipment and expertise available.

Testing using the surrogate abdomen rig without a surrogate abdominal wall highlighted the benefits that would exist if a surrogate material was available. There was some variation in results attributed to the biological variation between porcine abdominal walls that could have been avoided had a surrogate material been used. Furthermore, porcine abdominal walls are expensive to obtain and dispose of and must be used under strict hygiene conditions.

Nonetheless, the data is very useful for abdominal wall closure solutions as it is the first detailed description of both the uniaxial and the biaxial properties of the rectus sheath, a tissue that is under significant stress as a result of intra-abdominal pressure (1.1MPa during coughing). An understanding of its loading regime, particularly in biaxial loading, can permit the development of meshes that better match the stiffness of the abdominal wall tissues which they are supporting, as well as informing the development of future closure solutions.

11.3. Surrogate Abdomen Rig

A mechanical rig has been designed and built to represent the abdomen (Figure 6.1). The rig can hold either real small intestine and a real abdominal wall, surrogate small intestine and a surrogate abdominal wall or a combination of both. The rig contains a balloon that generates a representation of intra-abdominal pressure.

The dimensions of the rig are smaller than the dimensions of a 50th percentile human abdomen. It was designed in this manner so that an abdominal wall from a three month old pig, sourced from the Trinity College Dublin Bio-Resources Department, could be used during testing. Nonetheless, the working area of the abdominal wall in the rig is significantly greater than the 13mm diameter of a large trocar and provided the trocar wound is central, it provides sufficient area for a mesh-based repair.

Experimental rigs to simulate the abdomen have been previously described by Schwab et al. [108] and Podwojewski et al. [149] and were used for investigations of mesh fixation and repair. Both rigs facilitate loading of the abdominal wall by direct air pressure, similar to the pneumoperitoneum established at the beginning of a laparoscopic procedure. While both experimental rigs perform well in their applications, it is not possible to use them in their current state to investigate hernia formation or to analyse devices and techniques in a representative model of the human abdomen. The surrogate abdomen developed in this study on the other hand facilitates trial-and-error testing of surgical innovations by replicating the intra-abdominal pressure environment and the formation of herniae.

In vivo, intra-abdominal pressure can be rapidly increased to 20kPa by the very quick action of the muscles. This application of an impulse pressure is not possible in the rig with the current compressed air system. The ramp time up to maximum pressure will be slightly longer than the *in vivo* case.

The rig was partially validated using data from a small observational study conducted in St. Vincent's University Hospital, Dublin. The study examined the intra-abdominal pressure developed by patients during an abdominal operation. However, due to safety restrictions imposed by the anaesthetists, it was not possible to observe the pressure at which hernia formation was initiated through a trocar site defect.

Figure 9.1 and Table 9.2 show the pressures recorded during this observational study and no hernia was observed at any of these pressures by the surgeons. During the abdominal straining manoeuvre (ASM), the defect was open and a high IAP was generated. When this pressure was replicated in the surrogate abdomen rig, no hernia was generated through a 10mm defect. Pressure was increased in the surrogate abdomen until a hernia was observed. Figure 9.4 shows a logistical regression between results from the perioperative tests (no hernia) and the laboratory tests (hernia formation) through a 10mm defect using RPP as surrogate intestines. Since there are no overlapping results between the sets of experiments, this regression effectively creates a step function approximately halfway between the highest no-hernia pressure and the lowest hernia pressure. For comparison purposes, a ramp function between these two data points is also included.

It is not possible to say with certainty what pressure will create a hernia in a 10mm defect, but the data shows that it is between 2.1kPa and 5kPa. Considering the IAPs recorded by Cobb et al. [41], the risk activities for developing a hernia in an unclosed 10mm defect include bending at the waist and sitting up in bed, both of which could frequently be done by patients post-operatively. It is also clear that activities such as climbing stairs and coughing are high risk.

The use of surrogate small intestine within the rig was also validated and yielded similar results to the laboratory study examining different possible surrogate materials. Figure 9.3 shows there is a natural factor of safety, with the RPP generating a hernia at a pressure approximately 10% less than the pressure required for small intestine. This provides some confidence that results of similar studies using biological materials would produce comparable results. Using RPP as a surrogate intestine material is suitable for investigations of wound closure techniques and was a valuable resource in the study examining mesh overlap (Chapter 10).

The rig is intended to function as a preliminary, pre-clinical evaluation environment for potential closure methods and any conclusions derived will need to be further verified in animal and clinical trials. However it is an ideal environment for large scale, randomised trials without many of the ethical concerns and costs of live trials.

There are a number of factors that are not possible to account for in the surrogate rig, which could have an effect on the results of technique or device testing. For example, in studies of mesh repair of defects, excessive movement, mesh migration and mesh shrinkage cannot be replicated, though these factors have been shown elsewhere to be important for mesh success [86-90, 94, 102, 136]. Furthermore, when investigating any type of implant, it is not currently possible to replicate ingrowth of the implant over time. An implant will naturally be most susceptible to dislocation in the early period before ingrowth begins, thus tests in the surrogate abdomen rig will replicate a worst case scenario. Nonetheless, the rig is limited to investigating these worst case scenarios in its current formulation.

11.4. Mesh Overlap

An investigation of the amount by which a mesh should overlap the defect it is repairing was conducted and presented in Chapter 10. Interestingly, there is limited literature on the relationship between defect size and mesh size, with surgeons using a constant overlap of 50mm regardless of defect size [13, 15-18, 118, 119]. This study compared a mathematical model of ideal mesh size (Equation 10.9), derived from a first principles approach, with an experimental study to identify the relationship between defect and mesh size.

The experiments created a large amount of novel data on mesh size and found that there is a quadratic relationship between mesh diameter, defect size and failure pressure (Figures 10.5 to 10.7 and Equation 10.11). Given the linear relationship between pressure, force and area, and the quadratic relationship between diameter and area, this is as expected. Figure 10.7 shows a three dimensional plot of this quadratic relationship and gives a best-fit quadratic surface to the data. This surface gives a prediction of whether a given mesh and defect diameter combination is likely to fail at a given pressure.

Figure 10.8 compares various recommendations for the required mesh size, including the current practice of a mesh overlap of 50mm. It is clear that for small defect sizes, current practice predicts a mesh much larger than was required in the experimental study. For hole diameters between 40 and 50mm, this discrepancy is not as large, however, for hole diameters above 75mm, current practice predicts a mesh smaller than is recommended by Equation 10.12. Thus, it is clear that current practice under-estimates the mesh size required for large abdominal wall defects, which could lead to an increased incidence of hernia

recurrence. A proposal by Hollinsky et al. [20] based on fundamental mathematical calculations is also plotted, although it can be seen to under-predict the mesh requirement for small defects and over-predict the requirement for large defects. Furthermore, the Hollinsky model was presented by the authors as a purely mathematical formulation with no experimental corroboration provided. The authors did not consider fixation of the mesh, but rather included just the friction between the mesh and the abdominal wall as the only force resisting mesh dislocation.

The empirical mathematical model (Equation 10.10) was developed by observing the approximately linear behaviour of the experimental data and fitting a first order polynomial to it. The constant of the polynomial was then modified to ensure it always predicted a mesh slightly larger than the maximum mesh size required in the experimental study (Figure 10.8). A mesh diameter two times the hole diameter, plus an additional 25mm, will sufficiently close a defect to withstand IAP up to 20kPa without wasting mesh or potentially increasing the likelihood of mesh complications. Furthermore, the use of RPP in the experiments adds an extra factor of safety as the RPP was found in Chapter 9 to extrude at a force approximately 10% less than the force required to extrude the small intestine in the surrogate abdomen rig.

The experimental and mathematical studies produced similar recommendations for the relationship between the size of the mesh and the defect. Naturally, there were scenarios which were difficult to incorporate initially into the mathematical model, such as the minimum amount of tissue required to anchor a tack, resulting in some discrepancies. These could subsequently be included as logic switches, providing a minimum overlap to allow mesh fixation or a mesh size predicted directly by the formula; whichever is larger. The results confirmed the efficacy of the rig as an environment in which to conduct preclinical investigations and to test and refine fundamental mathematical analyses of the abdominal environment.

In vivo, further factors would exist that cannot be replicated in the surrogate rig, including the ingrowth of the mesh or mesh migration. Mesh ingrowth would improve the fixation of the mesh and further lessen the chance of rupture, which cannot be replicated accurately in the rig. Furthermore, as discussed by Śmietański et al. [136], it is not known exactly how

a mesh moves and migrates within a closed abdomen, which may have a bearing on hernia recurrence rates. Again, this factor cannot be currently incorporated into the rig, which simply provides a binary result of failure or no failure for a given mesh size, defect size and pressure.

There is elegance to this simplicity, however, in that it eliminates confounding factors and allows an investigation to focus on the simple, well-understood parameters and to understand their influence. Armed with this understanding, and preclinical evidence of performance, animal trials can be conducted in an informed and more ethical manner to corroborate findings and investigate biological interactions.

12. Conclusions

The problem of trocar◊ site hernia◊ development following laparoscopic surgery is in need of an effective and simple solution. Simply designing a new device, or developing a new technique without a biomechanical understanding, may not solve the problem. Rather, a fundamental understanding of the abdominal environment and intra-abdominal pressure, along with a method to test closure solutions in a cheap and repeatable way, are essential first steps in finding a solution.

Intra-abdominal pressure (IAP) had not previously been studied in detail from a mechanical or biomedical engineering perspective. While it is not possible to understand the exact loading of the abdominal wall tissues during raised IAP, it is clear that the rectus sheath will be under tension when the abdominal wall muscles are contracted. Anecdotally, it appears that the majority of herniae occur when patients are straining in some way, which corroborates well with the implication of raised IAP in hernia formation.

Reconstituted Powdered Potato (RPP) has been identified as a suitable surrogate material for small intestine in extrusion loading, similar to the loading experienced during hernia formation. RPP was found to extrude slightly more than real small intestine at a lower force, incorporating a small factor of safety when examining herniae, whilst also being cheap, clean, repeatable and practical. RPP was also found to exhibit minimal viscoelasticity, similar to the intestines, with the properties remaining constant across three extrusion rates.

Structural properties for porcine rectus sheath have been identified through uniaxial and biaxial stress-stretch experiments. This new data added to and improved existing limited data on rectus sheath and also identified the similarity between human and porcine rectus sheath in the cross-fibre direction. The results also corroborated the fundamental study of IAP, proving that the rectus sheath was capable of withstanding the stress induced by raised IAP.

A rig to represent the human abdomen has been designed and built and can be used to test potential trocar site closure solutions or other abdominal surgery devices. The rig has been partially validated using data from a small observational study of human IAP in surgery

and produces repeatable results for the pressure required to initiate a hernia through a small defect.

The rig has been used to conduct a study of mesh overlap amounts required to close a defect in an abdominal wall. It was found that a mesh should be twice the hole diameter, plus an additional 25mm, to effectively close a defect. This study developed a clinical recommendation for the mesh size required to close an abdominal wall defect which could be tested in animal or human trials. It also proved the efficacy of the rig as a testing environment in which preliminary, preclinical trials and studies can be conducted to test new concepts or develop new ideas. The close match between the mathematical model and the experimental results provides a mutual validation for both techniques to predict the mesh size required to close a defect.

With more detailed understanding of IAP and rectus sheath behaviour along with a useful, easy-to-use surrogate model of the abdomen, this project lays a basis upon which further work can be conducted to attempt to reduce the incidence of trocar site hernia formation after laparoscopic surgery. Furthermore, the rig can be used for other trials of tack or suture efficacy, studies of mesh types, investigations of trocars and other studies in a simple, cheap and repeatable environment in order to reduce complications and improve abdominal surgery techniques and devices.

13. Further Work

Substantial further work can follow this project along a number of different paths. The abdominal rig that has been developed is a valuable testing resource for many future studies, some of which may not even be apparent today.

The most notable and substantial piece of further work would be the development of an innovative wound closure solution for trocar◊ site defects. As has been identified throughout this thesis, the incidence of trocar site hernia◊ formation is high and the current method of suturing defects is inadequate, particularly in obese◊ patients. There is a need for a novel closure solution, perhaps using a mesh-based, tension-free closure, as has been suggested recently [12]. The surrogate abdomen rig developed in this project would be an ideal facility for trial-and-error testing of concepts in advance of animal or human trials.

The surrogate abdomen rig requires a material that can be used in place of a porcine abdominal wall to represent the rectus sheath. As described in Chapter 8, the rectus sheath is a structurally complex material with anisotropic uniaxial and biaxial behaviour. Development of a surrogate material is a technically complex task that was beyond the scope of this project. Future work could see the production of a material to represent the rectus sheath that could easily be used within the surrogate abdomen rig which would permit cheap, repeatable testing in the laboratory. The structural properties and stress-stretch graphs provided in Chapter 8 should be sufficient to adequately validate a potential surrogate material. This material can be further validated in the surrogate abdomen rig by ensuring that extrusion of small intestine occurs at a similar pressure to the observations presented in Chapter 9.

Mesh repair of abdominal wall defects in humans should be evaluated in line with the findings of Chapter 10, as it has been found that a constant 50mm mesh overlap is a significant overestimation of the mesh size required. A trial, preliminarily in animals, where a mesh was sized to be twice the diameter of the defect it is repairing plus an additional 25mm should see significantly less mesh being used without an increase in hernia recurrence rates.

Finally, further studies using the surrogate abdomen rig would see it used to greater potential. These could include further mesh overlap work or mesh fixation studies examining tacks, sutures and staples. The rig is a unique model of the abdomen in which intra-abdominal pressure can be simulated and hernia formation can be investigated and it has many prospective uses.

References

1. Semm, K., *Endoscopic appendectomy.* Endoscopy, 1983. **15**(2): p. 59-64.

2. Fuller, J., Scott, W., Ashar, B. and Corrado, J., *Laparoscopic trocar injuries: a report from a US Food and Drug Administration (FDA) Center for Devices and Radiological Health (CDRH) Systematic Technology Assessment of Medical Products (STAMP) Committee*. 2005, FDA.

3. Yoo, J., *Laparoscopic colorectal surgery.* The Permanente Journal, 2008. **12**(1): p. 27-31.

4. Park, A.E., Roth, J.S. and Kavic, S.M., *Abdominal Wall Hernia.* Current Problems in Surgery, 2006. **43**(5): p. 326-375.

5. Kadar, N., Reich, H., Liu, C.Y., Manko, G.F. and Gimpelson, R., *Incisional hernias after major laparoscopic gynecologic procedures.* American Journal of Obstetrics and Gynecology, 1993. **168**(5): p. 1493-1495.

6. Bowrey, D.J., Blom, D., Crookes, P.F., Bremner, C.G., Johansson, J.L.M., Lord, R.V., Hagen, J.A., DeMeester, S.R., DeMeester, T.R. and Peters, J.H., *Risk factors and the prevalence of trocar site herniation after laparoscopic fundoplication.* Surgical Endoscopy, 2001. **15**(7): p. 663-666.

7. Tonouchi, H., Ohmori, Y., Kobayashi, M. and Kusunoki, M., *Trocar site hernia.* Archives of Surgery, 2004. **139**(11): p. 1248.

8. Velasco, J.M., Vallina, V.L., Bonomo, S.R. and Hieken, T.J., *Postlaparoscopic small bowel obstruction.* Surgical Endoscopy, 1998. **12**(8): p. 1043-1045.

9. Lafullarde, T., Van Hee, R. and Gys, T., *A safe and simple method for routine open access in laparoscopic procedures.* Surgical Endoscopy, 1999. **13**(8): p. 769-772.

10. Uslu, H.Y., Erkek, A.B., Cakmak, A., Kepenekci, I., Sozener, U., Kocaay, F.A., Turkcapar, A.G. and Kuterdem, E., *Trocar site hernia after laparoscopic cholecystectomy.* Journal of Laparoendoscopic & Advanced Surgical Techniques. Part A, 2007. **17**(5): p. 600-603.

11. Anthony, T., Bergen, P.C., Kim, L.T., Henderson, M., Fahey, T., Rege, R.V. and Turnage, R.H., *Factors Affecting Recurrence following Incisional Herniorrhaphy.* World Journal of Surgery, 2000. **24**(1): p. 95-101.

12. Armañanzas, L., Ruiz-Tovar, J., Arroyo, A., García-Peche, P., Armañanzas, E., Diez, M., Galindo, I. and Calpena, R., *Prophylactic Mesh vs Suture in the Closure of the Umbilical Trocar Site after Laparoscopic Cholecystectomy in High-Risk Patients for Incisional Hernia. A Randomized Clinical Trial.* Journal of the American College of Surgeons, 2014. **218**(5): p. 960-968.

13. Conze, J., Prescher, A., Klinge, U., Saklak, M. and Schumpelick, V., *Pitfalls in retromuscular mesh repair for incisional hernia: the importance of the "fatty triangle".* Hernia, 2004. **8**(3): p. 255-259.

14. Edwards, C., Geiger, T., Bartow, K., Ramaswamy, A., Fearing, N., Thaler, K. and Ramshaw, B., *Laparoscopic transperitoneal repair of flank hernias: a retrospective review of 27 patients.* Surgical Endoscopy, 2009. **23**(12): p. 2692-2696.

15. Phillips, M.S., Krpata, D.M., Blatnik, J.A. and Rosen, M.J., *Retromuscular preperitoneal repair of flank hernias.* Journal of Gastrointestinal Surgery, 2012. **16**(8): p. 1548-1553.

16. Ponsky, T.A., Nam, A., Orkin, B.A. and Lin, P.P., *Open, intraperitoneal, ventral hernia repair: lessons learned from laparoscopy.* Archives of Surgery, 2006. **141**(3): p. 304-306.

17. Schumpelick, V., Klinge, U., Junge, K. and Stumpf, M., *Incisional abdominal hernia: the open mesh repair.* Langenbeck's Archives of Surgery, 2004. **389**(1): p. 1-5.

18. Sharma, A., Dey, A., Khullar, R., Soni, V., Baijal, M. and Chowbey, P.K., *Laparoscopic repair of suprapubic hernias: transabdominal partial extraperitoneal (TAPE) technique.* Surgical Endoscopy, 2011. **25**(7): p. 2147-2152.

19. Binnebosel, M., Rosch, R., Junge, K., Flanagan, T.C., Schwab, R., Schumpelick, V. and Klinge, U., *Biomechanical analyses of overlap and mesh dislocation in an incisional hernia model in vitro.* Surgery, 2007. **142**(3): p. 365-371.

20. Hollinsky, C. and Hollinsky, K.H., *Static calculations for mesh fixation by intraabdominal pressure in laparoscopic extraperitoneal herniorrhaphy.* Surgical Laparoscopy Endoscopy & Percutaneous Techniques, 1999. **9**(2): p. 106-109.

21. National Cancer Institute. *Anatomical Terminology*. 2008 [cited 2014; Available from: http://training.seer.cancer.gov/anatomy/body/terminology.html.

22. Antranik. *Muscles of the Abdominal Wall*. 2011 [cited 2014; Available from: http://antranik.org/muscles-of-the-abdominal-wall/.

23. Schleip, R., Jäger, H. and Klingler, W., *What is 'fascia'? A review of different nomenclatures.* Journal of Bodywork and Movement Therapies, 2012. **16**(4): p. 496-502.

24. Netter, F.H., *Atlas of human anatomy*. 2006: Saunders/Elsevier.

25. Standring, S., *Gray's anatomy*. 2008: Churchill Livingstone, Elsevier.

26. Marcovitch, H., *Black's Medical Dictionary*. 2010: A & C Black Publishers.

27. Jenkins, J.T. and O'Dwyer, P.J., *Inguinal hernias.* British Medical Journal, 2008. **336**(7638): p. 269-272.

28. Simons, M.P., Aufenacker, T., Bay-Nielsen, M., Bouillot, J.L., Campanelli, G., Conze, J., Lange, D., Fortelny, R., Heikkinen, T., Kingsnorth, A., Kukleta, J., Morales-Conde, S., Nordin, P., Schumpelick, V., Smedberg, S., Smietanski, M., Weber, G. and

Miserez, M., *European Hernia Society guidelines on the treatment of inguinal hernia in adult patients.* Hernia, 2009. **13**(4): p. 343-403.

29. Bucknall, T.E., Cox, P.J. and Ellis, H., *Burst abdomen and incisional hernia: a prospective study of 1129 major laparotomies.* British Medical Journal, 1982. **284**(6320): p. 931-933.

30. Mudge, M. and Hughes, L.E., *Incisional hernia: A 10 year prospective study of incidence and attitudes.* British Journal of Surgery, 1985. **72**(1): p. 70-71.

31. Sanz-López, R., Martínez-Ramos, C., Núñez-Peña, J.R., Ruiz de Gopegui, M., Pastor-Sirera, L. and Tamames-Escobar, S., *Incisional hernias after laparoscopic vs open cholecystectomy.* Surgical Endoscopy, 1999. **13**(9): p. 922-924.

32. Comajuncosas, J., Vallverdu, H., Orbeal, R. and Pares, D., *[Trocar site incisional hernia in laparoscopic surgery].* Cirugia Espanola, 2011. **89**(2): p. 72-76.

33. Waldhaussen, J., *Incisional hernia in a 5-mm trocar site following pediatric laparoscopy.* Journal of Laparoendoscopic Surgery, 1996. **6**: p. S89.

34. Nassar, A.M., Ashkar, K.A., Rashed, A.A. and Abdulmoneum, M.G., *Laparoscopic cholecystectomy and the umbilicus.* British Journal of Surgery, 1997. **84**(5): p. 630-633.

35. Sørensen L., Hemmingsen U. B., Kirkeby L. T., Kallehave F. and L., J., *Smoking is a risk factor for incisional hernia.* Archives of Surgery, 2005. **140**(2): p. 119-123.

36. Sugerman, H.J., Kellum Jr, J.M., Reines, H.D., DeMaria, E.J., Newsome, H.H. and Lowry, J.W., *Greater risk of incisional hernia with morbidly obese than steroid-dependent patients and low recurrence with prefascial polypropylene mesh.* The American Journal of Surgery, 1996. **171**(1): p. 80-84.

37. Immè, A. and Cardì, F., *Incisional hernia at the trocar site in laparoscopic surgery.* Chirurgia Italiana, 2006. **58**(5): p. 605-609.

38. Lambert, D., Marceau, S. and Forse, R., *Intra-abdominal Pressure in the Morbidly Obese.* Obesity Surgery, 2005. **15**(9): p. 1225-1232.

39. Sanchez, N.C., Tenofsky, P.L., Dort, J.M., Shen, L.Y., Helmer, S.D. and Smith, R.S., *What is Normal Intra-Abdominal Pressure?* American Surgeon, 2001. **67**(3): p. 243.

40. Campbell, E. and Green, J., *The variations in intra-abdominal pressure and the activity of the abdominal muscles during breathing; a study in man.* The Journal of Physiology, 1953. **122**(2): p. 282.

41. Cobb, W.S., Burns, J.M., Kercher, K.W., Matthews, B.D., James Norton, H. and Todd Heniford, B., *Normal Intraabdominal Pressure in Healthy Adults.* Journal of Surgical Research, 2005. **129**(2): p. 231-235.

42. Malbrain, M., Chiumello, D., Pelosi, P., Wilmer, A., Brienza, N., Malcangi, V., Bihari, D., Innes, R., Cohen, J., Singer, P., Japiassu, A., Kurtop, E., De Keulenaer, B., Daelemans, R., Del Turco, M., Cosimini, P., Ranieri, M., Jacquet, L., Laterre, P.-F.

and Gattinoni, L., *Prevalence of intra-abdominal hypertension in critically ill patients: a multicentre epidemiological study.* Intensive Care Medicine, 2004. **30**(5): p. 822-829.

43. Talasz, H., Kofler, M. and Lechleitner, M., *Misconception of the Valsalva maneuver.* International Urogynecology Journal, 2011. **22**(9): p. 1197-1198.

44. Leith, D.E., Butler, J.P., Sneddon, S.L. and Brain, J.D., *Cough.* Comprehensive Physiology, 1968.

45. Rosen, M. and Ponsky, J., *Minimally invasive surgery.* Endoscopy, 2001. **33**: p. 358-366.

46. Boldo, E., de Lucia, G.P., Aracil, J.P., Martin, F., Escrig, J., Martinez, D., Miralles, J.M. and Armelles, A. *Trocar site hernia after laparoscopic ventral hernia repair* in *16th World Congress of the International Association of Surgeons and Gastroenterologists*. 2006. Madrid: Springer.

47. Hasson, H.M., *A modified instrument and method for laparoscopy.* American Journal of Obstetrics and Gynecology, 1971. **110**(6): p. 886-887.

48. Taura, P., Lopez, A., Lacy, A.M., Anglada, T., Beltran, J., Fernandez-Cruz, L., Targarona, E., Garcia-Valdecasas, J.C. and Marin, J.L., *Prolonged pneumoperitoneum at 15 mmHg causes lactic acidosis.* Surgical Endoscopy, 1998. **12**(3): p. 198-201.

49. Sugerman, H., Windsor, A., Bessos, M. and Wolfe, L., *Intra-abdominal pressure, sagittal abdominal diameter and obesity comorbidity.* Journal of Internal Medicine, 1997. **241**(1): p. 71-79.

50. Marras, W.S. and Mirka, G.A., *Intra-abdominal pressure during trunk extension motions.* Clinical Biomechanics, 1996. **11**(5): p. 267-274.

51. Malbrain, M., *Different techniques to measure intra-abdominal pressure (IAP): time for a critical re-appraisal.* Intensive Care Medicine, 2004. **30**(3): p. 357-371.

52. Iqbal, A., Haider, M., Stadlhuber, R., Karu, A., Corkill, S. and Filipi, C., *A study of intragastric and intravesicular pressure changes during rest, coughing, weight lifting, retching, and vomiting.* Surgical Endoscopy, 2008. **22**(12): p. 2571-2575.

53. Daggfeldt, K. and Thorstensson, A., *The role of intra-abdominal pressure in spinal unloading.* Journal of Biomechanics, 1997. **30**(11-12): p. 1149-1155.

54. Malbrain, M., *Abdominal pressure in the critically ill: measurement and clinical relevance.* Intensive Care Medicine, 1999. **25**(12): p. 1453-1458.

55. de Vries, D.R., van Herwaarden, M.A., Smout, A.J.P.M. and Samsom, M., *Gastroesophageal Pressure Gradients in Gastroesophageal Reflux Disease: Relations With Hiatal Hernia, Body Mass Index, and Esophageal Acid Exposure.* American Journal of Gastroenterology, 2008. **103**(6): p. 1349-1354.

56. Devereux, G., *Definition, epidemiology, and risk factors.* British Medical Journal, 2006. **332**(7550): p. 1142-1144.

57. Song, C., Alijani, A., Frank, T., Hanna, G. and Cuschieri, A., *Elasticity of the living abdominal wall in laparoscopic surgery.* Journal of Biomechanics, 2006. **39**(3): p. 587-591.

58. Kureshi, A., Vaiude, P., Nazhat, S.N., Petrie, A. and Brown, R.A., *Matrix mechanical properties of transversalis fascia in inguinal herniation as a model for tissue expansion.* Journal of Biomechanics, 2008. **41**(16): p. 3462-3468.

59. Kirilova, M., Stoytchev, S., Pashkouleva, D. and Kavardzhikov, V., *Experimental study of the mechanical properties of human abdominal fascia.* Medical Engineering & Physics, 2011. **33**(1): p. 1-6.

60. Hernández, B., Peña, E., Pascual, G., Rodríguez, M., Calvo, B., Doblaré, M. and Bellón, J.M., *Mechanical and histological characterization of the abdominal muscle. A previous step to modelling hernia surgery.* Journal of the Mechanical Behavior of Biomedical Materials, 2011. **4**(3): p. 392-404.

61. Minns, R.J. and Tinckler, L.F., *Structural and mechanical aspects of prosthetic herniorrhaphy.* Journal of Biomechanics, 1976. **9**(7): p. 435-438.

62. Korenkov, M., Beckers, A., Koebke, J., Lefering, R., Tiling, T. and Troidl, H., *Biomechanical and morphological types of the linea alba and its possible role in the pathogenesis of midline incisional hernia.* European Journal of Surgery, 2001. **167**(12): p. 909-914.

63. Hollinsky, C. and Sandberg, S., *Measurement of the tensile strength of the ventral abdominal wall in comparison with scar tissue.* Clinical Biomechanics, 2007. **22**(1): p. 88-92.

64. Förstemann, T., Trzewik, J., Holste, J., Batke, B., Konerding, M.A., Wolloscheck, T. and Hartung, C., *Forces and deformations of the abdominal wall—A mechanical and geometrical approach to the linea alba.* Journal of Biomechanics, 2011. **44**(4): p. 600-606.

65. Gräβel, D., Prescher, A., Fitzek, S., Keyserlingk, D.G.v. and Axer, H., *Anisotropy of human linea alba: A biomechanical study.* Journal of Surgical Research, 2005. **124**(1): p. 118-125.

66. Martins, P., Peña, E., Jorge, R.M.N., Santos, A., Santos, L., Mascarenhas, T. and Calvo, B., *Mechanical characterization and constitutive modelling of the damage process in rectus sheath.* Journal of the Mechanical Behavior of Biomedical Materials, 2012. **8**(0): p. 111-122.

67. Takaza, M., Moerman, K.M., Gindre, J., Lyons, G. and Simms, C.K., *The anisotropic mechanical behaviour of passive skeletal muscle tissue subjected to large tensile strain.* Journal of the Mechanical Behavior of Biomedical Materials, 2013. **17**(0): p. 209-220.

68. Rath, A.M., Zhang, J. and Chevrel, J.P., *The sheath of the rectus abdominis muscle: an anatomical and biomechanical study.* Hernia, 1997. **1**(3): p. 139-142.

69. Ben Abdelounis, H., Nicolle, S., Otténio, M., Beillas, P. and Mitton, D., *Effect of two loading rates on the elasticity of the human anterior rectus sheath.* Journal of the Mechanical Behavior of Biomedical Materials, 2013. **20**(0): p. 1-5.

70. Nilsson, T., *Biomechanical studies of rabbit abdominal wall. Part I.—The mechanical properties of specimens from different anatomical positions.* Journal of Biomechanics, 1982. **15**(2): p. 123-129.

71. Song, C., Alijani, A., Frank, T., Hanna, G. and Cuschieri, A., *Mechanical properties of the human abdominal wall measured in vivo during insufflation for laparoscopic surgery.* Surgical Endoscopy, 2006. **20**(6): p. 987-990.

72. Bellini, C., Glass, P., Sitti, M. and Di Martino, E.S., *Biaxial mechanical modeling of the small intestine.* Journal of the Mechanical Behavior of Biomedical Materials, 2011. **4**(8): p. 1727-1740.

73. Gregersen, H. and Kassab, G., *Biomechanics of the gastrointestinal tract.* Neurogastroenterology & Motility, 1996. **8**(4): p. 277-297.

74. Egorov, V.I., Schastlivtsev, I.V., Prut, E.V., Baranov, A.O. and Turusov, R.A., *Mechanical properties of the human gastrointestinal tract.* Journal of Biomechanics, 2002. **35**(10): p. 1417-1425.

75. Dou, Y., Fan, Y., Zhao, J. and Gregersen, H., *Longitudinal residual strain and stress-strain relationship in rat small intestine.* Biomedical Engineering Online, 2006. **5**(1): p. 37.

76. Rutkow, I.M., *Demographic and socioeconomic aspects of hernia repair in the United States in 2003.* The Surgical Clinics of North America, 2003. **83**(5): p. 1045-1051, v-vi.

77. Luijendijk, R.W., Hop, W.C.J., van den Tol, M.P., de Lange, D.C.D., Braaksma, M.M.J., IJzermans, J.N.M., Boelhouwer, R.U., de Vries, B.C., Salu, M.K.M., Wereldsma, J.C.J., Bruijninckx, C.M.A. and Jeekel, J., *A Comparison of Suture Repair with Mesh Repair for Incisional Hernia.* New England Journal of Medicine, 2000. **343**(6): p. 392-398.

78. Helgstrand, F., Rosenberg, J., Kehlet, H. and Bisgaard, T., *Low risk of trocar site hernia repair 12 years after primary laparoscopic surgery.* Surgical Endoscopy, 2011. **25**(11): p. 3678-3682.

79. Birdi, I., Hunt, T.M., Veitch, P.S., Armon, M., Jervis, P. and Barr, C., *Laparoscopic cholecystectomy in Leicester: an audit of 555 patients.* Annals of The Royal College of Surgeons of England, 1994. **76**(6): p. 390.

80. Azurin, D.J., Go, L.S., Arroyo, L.R. and Kirkland, M.L., *Trocar site herniation following laparoscopic cholecystectomy and the significance of an incidental preexisting umbilical hernia.* The American Surgeon, 1995. **61**(8): p. 718-720.

81. Mayol, J., Garcia-Aguilar, J., Ortiz-Oshiro, E., De-Diego Carmona, J.A. and Fernandez-Represa, J.A., *Risks of the Minimal Access Approach for Laparoscopic Surgery: Multivariate Analysis of Morbidity Related to Umbilical Trocar Insertion.* World Journal of Surgery, 1997. **21**(5): p. 529-533.

82. Coda, A., Bossotti, M., Ferri, F., Mattio, R., Ramellini, G., Poma, A., Quaglino, F., Filippa, C. and Bona, A., *Incisional Hernia and Fascial Defect Following Laparoscopic Surgery.* Surgical Laparoscopy Endoscopy & Percutaneous Techniques, 2000. **10**(1): p. 34-38.

83. Duca, S., Bãlã, O., Al-Hajjar, N., Iancu, C., Puia, I.C., Munteanu, D. and Graur, F., *Laparoscopic cholecystectomy: incidents and complications. A retrospective analysis of 9542 consecutive laparoscopic operations.* HPB, 2003. **5**(3): p. 152-158.

84. Montz, F.J., Holschneider, C.H. and Munro, M., *Incisional Hernia Following Laparoscopy: A Survey of the American Association of Gynecologic Laparoscopists.* The Journal of the American Association of Gynecologic Laparoscopists, 1994. **1**(4, Part 2): p. S23-24.

85. Matthews, B.D., Heniford, B.T. and Sing, R.F., *Preperitoneal Richter hernia after a laparoscopic gastric bypass.* Surgical Laparoscopy Endoscopy & Percutaneous Techniques, 2001. **11**(1): p. 47.

86. Ferrone, R., Scarone, P. and Natalini, G., *Late complication of open inguinal hernia repair: Small bowel obstruction caused by intraperitoneal mesh migration.* Hernia, 2003. **7**(3): p. 161-162.

87. Nowak, D.D., Chin, A.C., Singer, M.A. and Helton, W.S., *Large scrotal hernia: A complicated case of mesh migration, ascites, and bowel strangulation.* Hernia, 2005. **9**(1): p. 96-99.

88. Ott, V., Groebli, Y. and Schneider, R., *Late intestinal fistula formation after incisional hernia using intraperitoneal mesh.* Hernia, 2005. **9**(1): p. 103-104.

89. LeBlanc, K. and Whitaker, J., *Management of chronic postoperative pain following incisional hernia repair with Composix mesh: a report of two cases.* Hernia, 2002. **6**(4): p. 194-197.

90. Rettenmaier, M.A., Heinemann, S., Truong, H., Micha, J.P., Brown, J.V., III and Goldstein, B.H., *Marlex mesh mimicking an adnexal malignancy.* Hernia, 2009. **13**(2): p. 221-223.

91. Chand, M., On, J., Bevan, K., Mostafid, H. and Venkatsubramaniam, A.K., *Mesh erosion following laparoscopic incisional hernia repair.* Hernia, 2012. **16**(2): p. 223-226.

92. Goswami, R., Babor, M. and Ojo, A., *Mesh erosion into caecum following laparoscopic repair of inguinal hernia (TAPP): a case report and literature review.* Journal of Laparoendoscopic & Advanced Surgical Techniques. Part A, 2007. **17**(5): p. 669-672.

93. Riaz, A.A., Ismail, M., Barsam, A. and Bunce, C.J., *Mesh erosion into the bladder: A late complication of incisional hernia repair. A case report and review of the literature.* Hernia, 2004. **8**(2): p. 158-159.

94. Borchert, D., Kumar, B., Dennis, R. and Alberts, J., *Mesh migration following obturator hernia repair presenting as a bezoar inducing small intestinal obstruction.* Hernia, 2008. **12**(1): p. 83-85.

95. Burger, J.W., Luijendijk, R.W., Hop, W.C., Halm, J.A., Verdaasdonk, E.G. and Jeekel, J., *Long-term follow-up of a randomized controlled trial of suture versus mesh repair of incisional hernia.* Annals of Surgery, 2004. **240**(4): p. 578-583; discussion 583-575.

96. Usher, F.C., Hill, J.R. and Ochsner, J.L., *Hernia repair with Marlex mesh. A comparison of techniques.* Surgery, 1959. **46**: p. 718-724.

97. Pavlidis, T.E., Atmatzidis, K.S., Lazaridis, C.N., Papaziogas, B.T., Makris, J.G. and Papaziogas, T.B., *Comparison between modern mesh and conventional non-mesh methods of inguinal hernia repair.* Minerva Chirurgica, 2002. **57**(1): p. 7-12.

98. Sauerland, S., Schmedt, C.-G., Lein, S., Leibl, B. and Bittner, R., *Primary incisional hernia repair with or without polypropylene mesh: a report on 384 patients with 5-year follow-up.* Langenbeck's Archives of Surgery, 2005. **390**(5): p. 408-412.

99. Israelsson, L.A., Jönsson, L. and Wimo, A., *Cost analysis of incisional hernia repair by suture or mesh.* Hernia, 2003. **7**(3): p. 114-117.

100. Hollinsky, C. and Göbl, S., *Bursting strength evaluation after different types of mesh fixation in laparoscopic herniorrhaphy.* Surgical Endoscopy, 1999. **13**(10): p. 958-961.

101. Schmidt, S.C. and Langrehr, J.M., *Autologous fibrin sealant (Vivostat) for mesh fixation in laparoscopic transabdominal preperitoneal hernia repair.* Endoscopy, 2006. **38**(8): p. 841-844.

102. Beldi, G., Wagner, M., Bruegger, L., Kurmann, A. and Candinas, D., *Mesh shrinkage and pain in laparoscopic ventral hernia repair: a randomized clinical trial comparing suture versus tack mesh fixation.* Surgical Endoscopy, 2011. **25**(3): p. 749-755.

103. Descottes, B. and Bagot d'Arc, M., *Fibrin sealant in inguinal hernioplasty: an observational multicentre study in 1,201 patients.* Hernia, 2009. **13**(5): p. 505-510.

104. Byrd, J.F., Agee, N., Swan, R.Z., Lau, K.N., Heath, J.J., McKillop, I.H., Sindram, D., Martinie, J.B. and Iannitti, D.A., *Evaluation of absorbable and permanent mesh fixation devices: adhesion formation and mechanical strength.* Hernia, 2011. **15**(5): p. 553-558.

105. Lovisetto, F., Zonta, S., Rota, E., Mazzilli, M., Bardone, M., Bottero, L., Faillace, G. and Longoni, M., *Use of Human Fibrin Glue (Tissucol) Versus Staples for Mesh Fixation in Laparoscopic Transabdominal Preperitoneal Hernioplasty: A Prospective, Randomized Study.* Annals of Surgery, 2007. **245**(2): p. 222-231.

106. Olmi, S., Cesana, G., Sagutti, L., Pagano, C., Vittoria, G. and Croce, E., *Laparoscopic incisional hernia repair with fibrin glue in select patients.* JSLS, Journal of the Society of Laparoendoscopic Surgeons, 2010. **14**(2): p. 240-245.

107. Boldo, E., Armelles, A., Perez de Lucia, G., Martin, F., Aracil, J.P., Miralles, J.M., Martinez, D. and Escrig, J., *Pain after laparascopic bilateral hernioplasty : Early results of a prospective randomized double-blind study comparing fibrin versus staples.* Surgical Endoscopy, 2008. **22**(5): p. 1206-1209.

108. Schwab, R., Schumacher, O., Junge, K., Binnebösel, M., Klinge, U., Becker, H. and Schumpelick, V., *Biomechanical analyses of mesh fixation in TAPP and TEP hernia repair.* Surgical Endoscopy, 2008. **22**(3): p. 731-738.

109. Khaleal, F. and Berney, C., *The role of fibrin glue in decreasing chronic pain in laparoscopic totally extraperitoneal (TEP) inguinal hernia repair: a single surgeon's experience.* ANZ Journal of Surgery, 2011. **81**(3): p. 154-158.

110. Nguyen, S.Q., Divino, C.M., Buch, K.E., Schnur, J., Weber, K.J., Katz, L.B., Reiner, M.A., Aldoroty, R.A. and Herron, D.M., *Postoperative pain after laparoscopic ventral hernia repair: a prospective comparison of sutures versus tacks.* JSLS, Journal of the Society of Laparoendoscopic Surgeons, 2008. **12**(2): p. 113-116.

111. Bansal, V., Misra, M., Kumar, S., Keerthi Rao, Y., Singhal, P., Goswami, A., Guleria, S., Arora, M.K. and Chabra, A., *A prospective randomized study comparing suture mesh fixation versus tacker mesh fixation for laparoscopic repair of incisional and ventral hernias.* Surgical Endoscopy, 2011. **25**(5): p. 1431-1438.

112. Eriksen, J.R., Poornoroozy, P., Jørgensen, L.N., Jacobsen, B., Friis-Andersen, H.U. and Rosenberg, J., *Pain, quality of life and recovery after laparoscopic ventral hernia repair.* Hernia, 2009. **13**(1): p. 13-21.

113. Lepere, M., Benchetrit, S., Bertrand, J.C., Chalbet, J.Y., Combier, J.P., Detruit, B., Herbault, G., Jarsaillon, P., Lagoutte, J., Levard, H. and Rignier, P., *Laparoscopic resorbable mesh fixation. Assessment of an innovative disposable instrument delivering resorbable fixation devices: I-ClipTM. Final results of a prospective multicentre clinical trial.* Hernia, 2008. **12**(2): p. 177-183.

114. Sajid, M.S., Ladwa, N., Kalra, L., Hutson, K., Sains, P. and Baig, M.K., *A meta-analysis examining the use of tacker fixation versus no-fixation of mesh in laparoscopic inguinal hernia repair.* International Journal of Surgery, 2012. **10**(5): p. 224-231.

115. Tam, K.-W., Liang, H.-H. and Chai, C.-Y., *Outcomes of Staple Fixation of Mesh Versus Nonfixation in Laparoscopic Total Extraperitoneal Inguinal Repair: A Meta-Analysis of Randomized Controlled Trials.* World Journal of Surgery, 2010. **34**(12): p. 3065-3074.

116. Bell, R.C.W. and Price, J.G., *Laparoscopic inguinal hernia repair using an anatomically contoured three-dimensional mesh.* Surgical Endoscopy And Other Interventional Techniques, 2003. **17**(11): p. 1784-1788.

117. Schwab, R., Schumacher, O., Junge, K., Binnebosel, M., Klinge, U., Becker, H.P. and Schumpelick, V., *Biomechanical analyses of mesh fixation in TAPP and TEP hernia repair.* Surgical Endoscopy, 2008. **22**(3): p. 731-738.

118. Schumpelick, V., Klinge, U., Rosch, R. and Junge, K., *Light weight meshes in incisional hernia repair.* Journal of Minimal Access Surgery, 2006. **2**(3): p. 117-123.

119. Shah, R.H., Sharma, A., Khullar, R., Soni, V., Baijal, M. and Chowbey, P.K., *Laparoscopic repair of incarcerated ventral abdominal wall hernias.* Hernia, 2008. **12**(5): p. 457-463.

120. Amato, G., Romano, G., Goetze, T., Salamone, G., Agrusa, A., Gulotta, G. and Paolucci, V., *New mesh shape and improved implantation procedure to simplify and standardize open ventral hernia repair: a preliminary report.* Hernia, 2011. **15**(6): p. 659-665.

121. LeBlanc, K.A., *The critical technical aspects of laparoscopic repair of ventral and incisional hernias.* American Surgeon, 2001. **67**(8): p. 809-812.

122. LeBlanc, K.A., Whitaker, J.M., Bellanger, D.E. and Rhynes, V.K., *Laparoscopic incisional and ventral hernioplasty: lessons learned from 200 patients.* Hernia, 2003. **7**(3): p. 118-124.

123. Tsimoyiannis, E.C., Tsimogiannis, K.E., Pappas-Gogos, G., Nikas, K., Karfis, E. and Sioziou, H., *Seroma and recurrence in laparoscopic ventral hernioplasty.* JSLS, Journal of the Society of Laparoendoscopic Surgeons, 2008. **12**(1): p. 51-57.

124. Bay-Nielsen, M., Nordin, P., Nilsson, E. and Kehlet, H., *Operative findings in recurrent hernia after a Lichtenstein procedure.* The American Journal of Surgery, 2001. **182**(2): p. 134-136.

125. Carbonell, A.M., Cobb, W.S. and Chen, S.M., *Posterior components separation during retromuscular hernia repair.* Hernia, 2008. **12**(4): p. 359-362.

126. Stumpf, M., Conze, J., Prescher, A., Junge, K., Krones, C.J., Klinge, U. and Schumpelick, V., *The lateral incisional hernia: anatomical considerations for a standardized retromuscular sublay repair.* Hernia, 2009. **13**(3): p. 293-297.

127. Jenkins, E., Yom, V., Melman, L., Brunt, L.M., Eagon, J.C., Frisella, M. and Matthews, B., *Prospective evaluation of adhesion characteristics to intraperitoneal mesh and adhesiolysis-related complications during laparoscopic re-exploration after prior ventral hernia repair.* Surgical Endoscopy, 2010. **24**(12): p. 3002-3007.

128. Kiudelis, M., Jonciauskiene, J., Deduchovas, O., Radziunas, A., Mickevicius, A., Janciauskas, D., Petrovas, S., Endzinas, Z. and Pundzius, J., *Effects of different kinds of meshes on postoperative adhesion formation in the New Zealand White rabbit.* Hernia, 2007. **11**(1): p. 19-23.

129. Amid, P.K., Shulman, A.G., Lichtenstein, I.L., Sostrin, S., Young, J. and Hakakha, M., *Experimental evaluation of a new composite mesh with the selective property of*

incorporation to the abdominal wall without adhering to the intestines. Journal of Biomedical Materials Research, 1994. **28**(3): p. 373-375.

130. Borrazzo, E.C., Belmont, M.F., Boffa, D. and Fowler, D.L., *Effect of prosthetic material on adhesion formation after laparoscopic ventral hernia repair in a porcine model.* Hernia, 2004. **8**(2): p. 108-112.

131. Chelala, E., Debardemaeker, Y., Elias, B., Charara, F., Dessily, M. and Allé, J.L., *Eighty-five redo surgeries after 733 laparoscopic treatments for ventral and incisional hernia: adhesion and recurrence analysis.* Hernia, 2010. **14**(2): p. 123-129.

132. Gukas, I.D. and Massouh, F., *Serious life-threatening complication 5 years after laparoscopic totally extraperitoneal hernia repair: case report and discussion of the literature.* Hernia, 2011. **15**(4): p. 459-462.

133. Foschi, D., Corsi, F., Cellerino, P., Trabucchi, A. and Trabucchi, E., *Late rejection of the mesh after laparoscopic hernia repair.* Surgical Endoscopy, 1998. **12**(5): p. 455-457.

134. Agrawal, A. and Avill, R., *Mesh migration following repair of inguinal hernia: a case report and review of literature.* Hernia, 2006. **10**(1): p. 79-82.

135. Lo, D.J., Bilimoria, K.Y. and Pugh, C.M., *Bowel complications after prolene hernia system (PHS) repair: a case report and review of the literature.* Hernia, 2008. **12**(4): p. 437-440.

136. Śmietański, M., Bury, K., Tomaszewska, A., Lubowiecka, I. and Szymczak, C., *Biomechanics of the front abdominal wall as a potential factor leading to recurrence with laparoscopic ventral hernia repair.* Surgical Endoscopy, 2012. **26**(5): p. 1461-1467.

137. Hofbauer, C., Andersen, P.V., Juul, P. and Qvist, N., *Late mesh rejection as a complication to transabdominal preperitoneal laparoscopic hernia repair.* Surgical Endoscopy, 1998. **12**(9): p. 1164-1165.

138. Taylor, S.G. and O'Dwyer, P.J., *Chronic groin sepsis following tension-free inguinal hernioplasty.* British Journal of Surgery, 1999. **86**(4): p. 562-565.

139. Hubbell, D.S., Dwornik, J.J., Alway, S.E., Eliason, R. and Norenberg, R.E., *Teaching gross anatomy using living tissue.* Clinical Anatomy, 2002. **15**(2): p. 157-159.

140. Swindle, M.M. and Smith, A.C., *Comparative anatomy and physiology of the pig.* Scandinavian Journal of Laboratory Animal Science, 1998. **25**(Suppl 1): p. 11-21.

141. Bedell, G.N., Marshall, R., DuBois, A.B. and Harris, J.H., *Measurement of the volume of gas in the gastrointestinal tract. Values in normal subjects and ambulatory patients.* The Journal of Clinical Investigation, 1956. **35**(3): p. 336-345.

142. Duez, A., Cotte, E., Glehen, O., Cotton, F. and Bakrin, N., *Appraisal of peritoneal cavity's capacity in order to assess the pharmacology of liquid chemotherapy solution in hyperthermic intraperitoneal chemotherapy.* Surgical and Radiologic Anatomy, 2009. **31**(8): p. 573-578.

143. Talasz, H., Kremser, C., Kofler, M., Kalchschmid, E., Lechleitner, M. and Rudisch, A., *Phase-locked parallel movement of diaphragm and pelvic floor during breathing and coughing—a dynamic MRI investigation in healthy females.* International Urogynecology Journal, 2011. **22**(1): p. 61-68.

144. Reber, A., Nylund, U. and Hedenstierna, G., *Position and shape of the diaphragm: implications for atelectasis formation.* Anaesthesia, 1998. **53**(11): p. 1054-1061.

145. Egan, D.F., Wilkins, R.L., Stoller, J.K. and Kacmarek, R.M., *Egan's Fundamentals of Respiratory Care*. 2009: Mosby.

146. Kshirsagar, A.V., Carpenter, M., Bang, H., Wyatt, S.B. and Colindres, R.E., *Blood pressure usually considered normal is associated with an elevated risk of cardiovascular disease.* The American Journal of Medicine, 2006. **119**(2): p. 133-141.

147. Sandler, G., Leishman, S., Branson, H., Buchan, C. and Holland, A.J.A., *Body wall thickness in adults and children—Relevance to penetrating trauma.* Injury, 2010. **41**(5): p. 506-509.

148. Yarwood, J. and Berrill, A., *Nerve blocks of the anterior abdominal wall.* Continuing Education in Anaesthesia, Critical Care & Pain, 2010. **10**(6): p. 182-186.

149. Podwojewski, F., Otténio, M., Beillas, P., Guérin, G., Turquier, F. and Mitton, D., *Mechanical response of animal abdominal walls in vitro: Evaluation of the influence of a hernia defect and a repair with a mesh implanted intraperitoneally.* Journal of Biomechanics, 2013. **46**(3): p. 561-566.

150. Early, M. and Kelly, D.J., *The role of vessel geometry and material properties on the mechanics of stenting in the coronary and peripheral arteries.* Proceedings of the Institution of Mechanical Engineers, Part H: Journal of Engineering in Medicine, 2010. **224**(3): p. 465-476.

151. Rogers, C., Tseng, D.Y., Squire, J.C. and Edelman, E.R., *Balloon-artery interactions during stent placement - A finite element analysis approach to pressure, compliance, and stent design as contributors to vascular injury.* Circulation research, 1999. **84**(4): p. 378-383.

152. Müller-Hülsbeck, S., Jahnke, T., Liess, C., Glass, C., Grimm, J. and Heller, M., *Comparison of various cerebral protection devices used for carotid artery stent placement: an in vitro experiment.* Journal of Vascular and Interventional Radiology, 2003. **14**(5): p. 613-620.

153. Zhang, J., Yoganandan, N., Pintar, F.A., Guan, Y. and Gennarelli, T.A., *Experimental model for civilian ballistic brain injury biomechanics quantification.* Journal of Biomechanics, 2007. **40**(10): p. 2341-2346.

154. Prendergast, P.J., Lally, C., Daly, S., Reid, A.J., Lee, T.C., Quinn, D. and Dolan, F., *Analysis of prolapse in cardiovascular stents: a constitutive equation for vascular tissue and finite-element modelling.* Journal of Biomechanical Engineering, 2003. **125**(5): p. 692-699.

155. Eberl, C. *Digital Image Correlation and Tracking*. 2010 [cited 2013; Available from: http://www.mathworks.com/matlabcentral/fileexchange.

156. Maas, S.A., Ellis, B.J., Ateshian, G.A. and Weiss, J.A., *FEBio: finite elements for biomechanics.* Journal of Biomechanical Engineering, 2012. **134**(1): p. 011005.

157. Maas, S. and Weiss, J., *FeBio Theory Manual*. Vol. 1.5. 2013.

158. Takaza, M., Moerman, K.M. and Simms, C.K., *Passive skeletal muscle response to impact loading: Experimental testing and inverse modelling.* Journal of the Mechanical Behavior of Biomedical Materials, 2013. **27**(0): p. 214-225.

159. Gaidukov, K.M., Raibuzhis, E.N., Hussain, A., Teterin, A.Y., Smetkin, A.A., Kuzkov, V.V., Malbrain, M.L. and Kirov, M.Y., *Effect of intra-abdominal pressure on respiratory function in patients undergoing ventral hernia repair.* World journal of Critical Care Medicine, 2013. **2**(2): p. 9-16.

160. Nguyen, M.T., Berger, R.L., Hicks, S.C., Davila, J.A., Li, L.T., Kao, L.S. and Liang, M.K., *Comparison of Outcomes of Synthetic Mesh vs Suture Repair of Elective Primary Ventral Herniorrhaphy: A Systematic Review and Meta-analysis.* JAMA Surgery, 2014.

161. Hollinsky, C., Sandberg, S., Koch, T. and Seidler, S., *Biomechanical properties of lightweight versus heavyweight meshes for laparoscopic inguinal hernia repair and their impact on recurrence rates.* Surgical Endoscopy, 2008. **22**(12): p. 2679-2685.

162. Hollinsky, C., Kolbe, T., Walter, I., Joachim, A., Sandberg, S., Koch, T., Rülicke, T. and Tuchmann, A., *Tensile strength and adhesion formation of mesh fixation systems used in laparoscopic incisional hernia repair.* Surgical Endoscopy, 2010. **24**(6): p. 1318-1324.

163. van't Riet, M., de Vos van Steenwijk, P.J., Kleinrensink, G.J., Steyerberg, E.W. and Bonjer, H.J., *Tensile strength of mesh fixation methods in laparoscopic incisional hernia repair.* Surgical Endoscopy And Other Interventional Techniques, 2002. **16**(12): p. 1713-1716.